GOETHE UNIVERSITÄT FRANKFURT AM MAIN

Paul-Ehrlich-Institut

Influence of Hepatitis B Virus on Insulin Receptor Signaling and Liver Regeneration

Dissertation

zur Erlangung des Doktorgrades

der Naturwissenschaften (*Dr. phil. nat.*)

vorgelegt beim Fachbereich

Biochemie, Chemie und Pharmazie

der Johann Wolfgang Goethe-Universität

in Frankfurt am Main

von

Sebastian Robert Barthel

aus Frankfurt am Main

Frankfurt (2015)

(D30)

Im Fachbereich Biochemie, Chemie, Pharmazie (14) der

Johann Wolfgang Goethe-Universität als Dissertation angenommen.

Dekan:	Prof. Dr. Michael Karas
Gutachter:	Prof. Dr. Robert Tampé
	Prof. Dr. Eberhard Hildt
Datum der Disputation:	25. August 2016

“Das ist das Leben – ein zum großen Teil von mir noch nicht ausgeführtes Experiment.”

— Henry David Thoreau *(1817 – 1862)*

The research work documented in the present thesis was conducted from October 1st 2012 through September 30th 2015 at the Paul-Ehrlich-Institut (PEI) in Langen under supervision of **Professor Dr. Eberhard Hildt** (PEI) and **Professor Dr. Robert Tampé** (Goethe-Universität, Frankfurt am Main).

Table of Contents

Abbreviations

ALT	Alanine transaminase
AP-1	Activator protein 1
APS	Ammonium persulfate
ARE	Antioxidant response element
AST	Aspartate transaminase
AuAg	Australia antigen
Bad	Bcl-2-associated death promoter
Bcl-2	B-cell lymphoma 2
BrdU	5-bromo-2'-deoxyuridine
BSA	Bovine serum albumine
bZIP	Basic leucine zipper
cAMP	Cyclic adenosine monophosphate
caNrf2	Constitutively active mutant of Nrf2
Cbl	Cas-Br-M ecotropic retroviral transforming sequence homology
cccDNA	Covalently closed circular DNA
CCl_4	Carbon tetrachloride
CD	Cluster of differentation
cDNA	Complementary DNA
CLSM	Confocal laser scanning microscopy
cm	Centimeter
c-Raf	Rapidly accelerated fibrosarcoma
CREB	cAMP response element binding protein
CRTC2	CREB-regulated transcription coactivator-2
CTL	Cytotoxic T lymphocyte
Cy3	Cyanin-3
DAPI	4',6-diamidino-2-phenylindole
ddH_2O	Double-distilled water
DEPC	Diethylpyrocarbonate
DMEM	Dulbecco's Modified Eagle Medium
DNA	Deoxyribonucleic acid
dNTP	Deoxynucleoside triphosphate
DR	Direct repeat
E. coli	Escherichia coli
ECL	Enhanced chemiluminescence
ECM	Extracellular matrix
EDTA	Ethylenediaminetetraacetic acid
EGF(R)	Epidermal growth factor (receptor)
EGTA	Ethylene glycol tetraacetic acid
ELISA	Enzyme-linked immunosorbent assay
EM	Electron microscope
ER	Endoplasmic reticulum
ESCRT	Endosomal sorting complexes required for transport
et al.	Et alii
FACS	Fluorescence-activated cell sorting
FCS	Fetal calf serum
Fig.	Figure
Figs.	Figures
FITC	Fluorescein isothiocyanate
FOXO1	Forkhead box protein O1
g	Gram
Gab1	Grb2-associated binder-1
galT	Galactosyltransferase
GAPDH	Glyceraldehyde 3-phosphate dehydrogenase
GCK	Glucokinase
GCLC	Glutamate-cysteine ligase catalytic subunit
GFP	Green fluorescent protein
GLUT4	Glucose transporter 4
Grb2	Growth factor receptor-bound protein 2
GSK3β	Glycogen synthase kinase 3β
GST	Glutathione S-transferase
h	Hour
HBc, HBcAg	Hepatitis B core antigen

HBe, HBeAg	Hepatitis B early antigen
HBs, HBsAg	Hepatitis B surface antigen
HBV	Hepatitis B virus
HBx	Hepatitis B X protein
HCC	Hepatocellular carcinoma
HCV	Hepatitis C virus
HE	Hematoxylin and eosin
HEPES	4-(2-hydroxyethyl)-1-piperazineethanesulfonic acid
HGF	Hepatocyte growth factor
HIV	Human immunodeficiency virus
HRP	Horseradish peroxidase
HSC	Hepatic stellate cell
IDE	Insulin-degrading enzyme
i.p.	Intraperitoneally
IF	Immunofluorescence
IFN	Interferon
IGF	Insulin-like growth factor
IGF-IR	Insulin-like growth factor I receptor
IgG	Immunoglobulin G
IgM	Immunoglobulin M
IHC	Immunohistochemistry
IL	Interleukin
INSR	Insulin receptor gene
IR	Insulin receptor
IRS	Insulin receptor substrate
IU	International unit
JNK	Jun N-terminal kinase
kb	Kilobases
kDa	Kilodalton
Keap1	Kelch-like ECH-associated protein 1
L	Liter
LB	Lysogeny broth
LHBs	Large hepatitis B surface protein
M	Molar
mA	Milliampere
MAPK	Mitogen-activated protein kinase
mg	Milligram
MHBs	Middle hepatitis B surface protein
MHBs^t	Truncated middle hepatitis B surface protein
min	Minute
mL	Milliliter
mm	Millimeter
mRNA	Messenger RNA
mTORC	Mammalian target of rapamycin complex
MVB	Multivesicular body
NF-κB	Nuclear factor kappa-light-chain-enhancer of activated B-cells
NKT cell	Natural killer T cell
NLS	Nuclear localization sequence
nm	Nanometer
nM	Nanomolar
NQO1	NAD(P)H quinone oxidoreductase 1
Nrf2	Nuclear factor (erythroid-derived 2)-like-2 factor
NTCP	Sodium-taurocholate co-transporting polypeptide
OD	Optical density
ORF	Open reading frame
PAGE	Polyacrylamide gel electrophoresis
PBS	Phosphate buffered saline
PBST	Phosphate buffered saline-Triton X
PCR	Polymerase chain reaction
PDE	Phosphodiesterase

PDI	Protein disulfide isomerase
PDK	Phosphoinositide-dependent protein kinase
PEG	Polyethylen glycol
PEI	Polyethyleneimine
PGC-1	Peroxisome proliferator-activated receptor gamma coactivator 1
pgRNA	Pregenomic RNA
PH	Pleckstrin homology domain
PHx	Partial hepatectomy
PI3K	Phosphoinositid-3-kinase
PIP2	Phosphatidylinositol-(4,5)-bisphosphate
PIP3	Phosphatidylinositol-(3,4,5)-trisphosphate
PKB	Protein kinase B
PKC	Protein kinase C
PM	Plasma membrane
PMH	Primary mouse hepatocyte
PMSF	Phenylmethylsulfonyl fluoride
PP1	Protein phosphatase 1
PTB	Phosphotyrosine binding-domain
PTFE	Polytetrafluoroethylene
PTP	Protein tyrosine phosphatase
PVDF	Polyvinylidene fluoride
qRT-PCR	Quantitative real time PCR
rcDNA	Relaxed circular DNA
Rheb	Ras homolog enriched in brain
RIPA	Radio immunoprecipitation
RNA	Ribonucleic acid
ROS	Reactive oxygen species
RPL27	60S ribosomal protein L27
rpm	Revolutions per minute
RT	Reverse transcriptase
RT	Room temperature
RTK	Receptor tyrosine kinase
S6K1	p70 S6 kinase 1
SDS	Sodium dodecyl sulfate
SEM	Standard error of the mean
SHBs	Small hepatitis B surface protein
Shc	Src-homology-2-containing protein
sMaf	Small Maf
SNARE	Soluble N-ethylmaleimide-sensitive factor receptor
SOCS	Suppressor of cytokine signalling
SOS	Son-of-sevenless
SREBP-1c	Sterol regulatory element-binding protein-1c
STAT	Signal transducer and activator of transcription
Tab.	Table
TAE	Tris-acetate-EDTA
tBHQ	tert-Butylhydroquinone
TBS	Tris buffered saline
TBST	Tris buffered saline-Tween 20
tdnNrf2	Transdominant negative mutant of Nrf2
TdT	Terminal deoxynucleotidyl transferase
TEMED	Tetramethylethylenediamine
TGF	Transforming growth factor
TLM	Translocation motif
TNF	Tumor necrosis factor
TSC	Tuberous sclerosis complex
TUNEL	TdT dUTP nick end labeling
UDP	Uridine diphosphate
(d)UTP	(Deoxy) Uridine triphosphate
UV	Ultraviolet
V	Volt
v/v	Volume/volume
w/v	Weight/volume

WB	Western blot	**γ-GCSc**	Gamma-glutamylcysteine synthetase catalytic subunit
WHO	World Health Organization	**µg**	Microgram
WT	Wild type	**µL**	Microliter
α-SMA	Alpha-smooth muscle actin	**µM**	Micromolar

"The beginning of health is to know the disease."

— Spanish proverb

1 Introduction

1.1 Hepatitis B virus infection

1.1.1 Disease

Hepatitis is an inflammation of the liver (from the Greek *hêpar* meaning liver, and *itis* meaning inflammation) as a result of liver cell (hepatocyte) destruction (Arndt et al., 2013). Besides several causative factors, i.e. mechanical damage, radiation, toxins, alcohol, drugs, bacteria and parasites, viral infections are the most common cause of hepatitis (WHO, 2015a). Hepatitis viruses are grouped into five main types, A, B, C, D and E with hepatitis B virus (HBV) infection being the most frequent viral hepatitis worldwide (WHO, 2015a). The clinical course of HBV infection can be inapparent, acute or chronic. Typical symptoms of acute infection comprise fever, fatigue, nausea and vomiting, muscle or joint pain and icterus (Hepatitis B Foundation, 2014). Acute infection is mostly self-limiting but is able to cause acute liver failure. However, infection can progress to a chronic manifestation in 5–10 % of infected adults (Rehermann et al., 2005). The rate of chronification is even increased up to 90 % in newborns after vertical mother-to-child-transmission (WHO, 2015a; Rehermann et al., 2005). Once established, chronic HBV infection is the leading cause for lethal liver pathologies such as liver cirrhosis and hepatocellular carcinoma (HCC) (Lupberger et al., 2007).

1.1.2 Epidemiology

With an estimate of 240 million chronically infected individuals worldwide, HBV infection remains a major public health concern and one of the most common and serious infectious diseases (WHO, 2015a). In addition, more than 780.000 people die every year from HBV-associated complications (WHO, 2015a; Lozano et al., 2012). The World Health Organization (WHO) has estimated that about 2 billion individuals of today's world population have been infected by HBV. However, global prevalence of HBV infection differs markedly throughout different regions of the world (**Fig. 1.1**). South East Asia, China, Saudi Arabia, Sub-Saharan Africa, the Amazonas Basin and Greenland belong to the highly endemic areas where at least 8 % of the population are chronically infected and 70–95 % of the population show serological signs of past or present HBV infection (Hou et al., 2005). In these regions, vertical mother-to-child transmission is the most common mode of transmission and the rate of chronic liver disease is high (Hwang et al., 2011). Intermediate prevalence is found in Alaska, parts of Middle and South America, North Africa, Eastern and Southern Europe, the Middle East, Russia, India and Japan. Here, 2–7 % of the population are chronic HBV carriers and acute disease in adolescents and adults is common (Hou et al., 2005). Areas of low endemicity are North America, Southeastern South America, Northern and Western Europe, Australia and New Zealand where 0,5–2 % are chronically infected (Hwang et al., 2011).

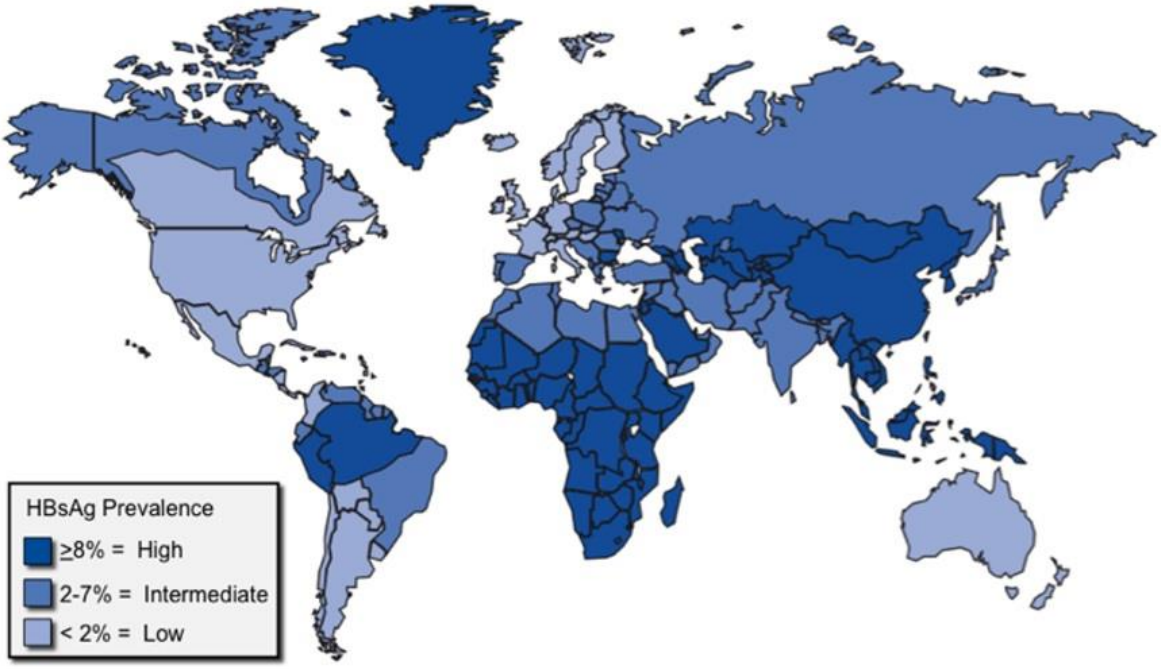

Fig. 1.1: Global epidemiology of HBV infection. The world map shows high HBV prevalence (≥ 8 %) in South East Asia, China, Saudi Arabia, Sub-Saharan Africa, the Amazonas Basin and Greenland. Intermediate prevalence (2–7 %) of HBV infection is found in Alaska, parts of Middle and South America, North Africa, Eastern and Southern Europe, the Middle East, Russia, India and Japan. Regions of low endemicity (< 2 %) are North America, Southeastern South America, Northern and Western Europe, Australia and New Zealand (taken from Hwang et al., 2011).

1.1.3 Transmission

A prophylactic vaccine against hepatitis B is available since 1980 (Stevens et al., 1980; Szmuness et al., 1980). Nevertheless, the most common sources of HBV infection in unvaccinated individuals are infected body fluids such as blood, semen or saliva (Scott et al., 1980). Remarkably, HBV is 100-fold more likely to be transmitted compared to HIV (Thio, 2009; Ranjbar et al., 2011). HBV spreads by parenteral (direct blood-to-blood contact), perinatal (mother-to-child) or percutaneous/mucosal transmission (WHO, 2015a). Perinatal transmission from an infected mother to her child at birth is most prevalent in highly endemic areas

(Hwang et al., 2011). Percutaneous and mucosal transmission requires lesions in the skin or the mucosa, so the virus can enter the blood stream and cause infection (Jilg and Gerlich, 2014). Once HBV has reached the blood stream, its primary target cells are hepatocytes of the liver where the virus can replicate (Guidotti et al., 2006). Several groups can be delineated who are at high risk of HBV infection. Those include healthcare workers and emergency personnel, men who have unprotected sex with men, sexually promiscuous individuals as well as individuals who inject drugs or get tattoos and body piercings with infected needles (Hepatitis B Foundation, 2014). HBV can persist outside of the human body in desiccated blood or other fluids for about 7 days and retains its infectivity during this time (WHO, 2015a). However, the virus is not able to cause infection after enteral uptake of contaminated food or water, by shaking hands or touching contaminated surfaces (Hepatitis B Foundation, 2014).

1.1.4 Pathogenesis

1.1.4.1 Acute HBV infection

The majority of HBV infections (65–80 %) is self-limiting without treatment and shows an inapparent clinical course with merely a slight increase in alanine transaminase (ALT) in the blood (Chang et al., 2007; Tugendheim, 2015). However, acute infection occurs in 20–35 % of all HBV infections after an incubation period of 4–12 weeks and is characterized by the detection of the hepatitis B surface antigen (HBsAg) and the hepatitis B early antigen (HBeAg) as well as HBV-specific DNA in the blood (Mauss et al., 2015; Tugendheim, 2015) (**Fig. 1.2**). This acute phase of infection can last from 2 weeks up to 3 months in

which symptoms become apparent and ALT levels increase. During this phase, antibodies against the hepatitis B core antigen (HBcAg) (IgG and IgM) and HBeAg are generated and the titer of HBV antigens and HBV DNA decreases. In the following post-acute phase ranging from 3–6 months, HBs-specific antibodies are produced and anti-HBc IgM antibodies slowly disappear from the blood. High titers of anti-HBc, anti-HBe and anti-HBs antibodies ensure life-long protection when acute infection has been cleared after 6 months at the latest (Liang, 2009). On the contrary, 0.5–1 % of HBV infections may have a fulminant outcome leading to liver failure and death within few days of infection (Tugendheim, 2015). HBV preferentially targets the parenchymal hepatocytes of the liver to execute its replication cycle (Guidotti et al., 2006). Importantly, HBV itself is not cytopathogenic, but liver pathogenesis and viral clearance are considered to be mainly mediated by adaptive immune responses of the host (Rehermann et al., 2005; Chisari et al., 2010). After infection, HBV does not induce an innate immune response (e.g. induction of the type I interferons IFN-α/β) in infected cells and hence initially remains unrecognized by the immune system (Wieland et al., 2004; Wieland et al., 2005; Chisari et al., 2010). Until detection by the adaptive immune system several weeks later, HBV can replicate non-cytopathically and spread through the liver (Chisari et al., 2010; Oh et al., 2015). Ultimate viral clearance in acute infection is primarily accomplished by cytotoxic $CD8^+$ T lymphocytes (CTL) (Thimme et al., 2003). However, an early $CD4^+$ T cell response is required to induce HBV-specific $CD8^+$ T cells (Chisari et al., 2010). The T cell-dependent antibody response specific to the HBV surface proteins further helps to clear HBV from the circulation by complexing free viral particles and preventing them from

attachment to hepatocytes (Chisari et al., 2010). The killing of HBV-infected hepatocytes by the cytopathic activity of $CD8^+$ T cells is responsible for acute hepatic inflammation and coincides with the increase in ALT levels in the acute phase of infection (Webster et al., 2000; Chang et al., 2007). Nevertheless, secretion of interferon gamma (IFN-γ) and tumor necrosis factor α (TNF-α) contribute to viral clearance in a non-cytopathic manner by inhibition of HBV expression and replication in hepatocytes (Guidotti et al., 2006; Chisari et al., 2010).

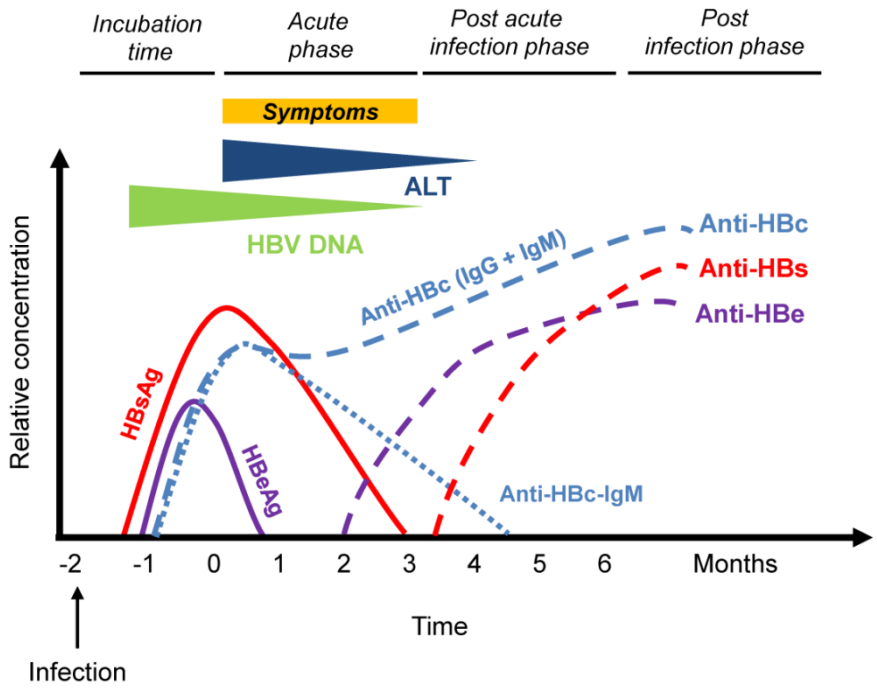

Fig. 1.2: Serological course of acute HBV infection. The graph shows the relative concentrations of viral markers that can be detected in the blood during the course of an acute HBV infection. During the incubation period after infection, HBV DNA, HBsAg and HBeAg start to appear in the blood but decrease in the course of the acute phase while symptoms become apparent and elevated ALT levels are detected. Within the acute phase, anti-HBc antibodies are generated (IgM and IgG). While anti-HBc IgM antibodies have disappeared from the blood after 4−5 months, anti-HBc IgG antibodies are permanently detectable. In addition, anti-HBe and anti-

◄ HBs are generated at the end of the acute phase and together with anti-HBc antibodies contribute to life-long protection when HBV has been finally cleared after 6 months (adapted from and modified according to www.tugendheim.de/images/impfen/hep_b/hbv_labor_grafic_gr.png).

1.1.4.2 Chronic HBV infection

Chronic HBV infection is the major etiological cause of fatal liver diseases such as cirrhosis and HCC (Beasley, 1988; Perz et al., 2006). Chronic infection is characterized by persistence of HBsAg and HBeAg as well as HBV DNA in the blood for more than six months after infection (**Fig. 1.3**). In addition, seroconversion of anti-HBs and anti-HBe antibodies does not occur and merely antibodies against HBc are detectable. However, a large group of chronically infected individuals, designated as “inactive” (formerly “healthy”) carriers, is positive for HBsAg but characterized by absence of HBeAg, presence of anti-HBe, low levels of HBV DNA, normal range of ALT levels and absence of significant hepatitis (Sharma et al., 2005; Tong et al., 2013). These patients have a favorable clinical prognosis but are still at risk to develop liver disease due to possible viral reactivation (Tong et al., 2013). Vertical transmission from HBV-infected mothers to neonates contributes to the majority of chronic infections (Glebe et al., 2014). Viral persistence can thereby be attributed to the immature immune system of neonates (You et al., 2014). In addition, HBeAg in the peripheral blood is able to cross the placenta and has immune modulatory effects which result in immune tolerance against HBV (Rehermann et al., 2005; Guidotti et al., 2006). In up to 10 % of adult individuals that have been horizontally infected with HBV, infection can persist and become chronic (Rehermann et al., 2005). Men have an increased

risk to become chronic carriers compared to women (London et al., 1977; Drew et al., 1978). Persistence of HBV in adults is multifactorial and depends on viral and host factors as well as the host's genetic background that determines the immune response against HBV (Rehermann et al., 2005; You et al., 2014). Further determinants that facilitate viral persistence are viral inhibition of antigen presentation and downregulation of viral gene expression, so that HBV-infected hepatocytes remain undetected by T cells (Rehermann et al., 2005). Yet, since HBV acts as a 'stealth virus' to evade innate immune responses, the adaptive immune response is of fundamental importance for viral clearance (Chisari et al., 2010; Wieland et al., 2004). Development of persistent infection is thus associated with an inefficient induction of HBV-specific $CD8^+$ T cells by $CD4^+$ T cell priming early in the infection which are unable to eradicate HBV-infected hepatocytes and to ultimately clear HBV infection (Chisari et al., 2010). Moreover, persistent presence of HBV antigens and viral DNA eventually induces progressive exhaustion and deletion of HBV-specific T cells, while immunosuppressive regulatory T cells increase (Rehermann, 2013). It is therefore thought that non-specific inflammatory immune responses by immune cells other than HBV-specific T cells (e.g. macrophages, neutrophils and NK cells) cause liver damage while being unable to clear HBV-infected hepatocytes (Rehermann, 2013). The chronic inflammatory milieu in the liver and the inefficient immune response to HBV perpetuate continuous cycles of hepatocyte death and liver regeneration that ultimately lead to chronic liver damage and foster the development of liver disease (Chisari et al., 2010). Liver regeneration is a physiological and essential response of the liver to injury where hepatocytes start to proliferate and compensate for the

loss of functional liver tissue (Taub, 2004; Fausto, 2004) (see 1.3). In addition, liver repair also involves fibrogenic processes by non-parenchymal cells such as activated hepatic stellate cells (HSC) and myofibroblasts which maintain tissue integrity (Ramadori et al., 2004; Pellicoro et al., 2014). These cells sequester and deposit extracellular matrix (ECM) components as a natural reparative response of wound-healing (Pellicoro et al., 2014). However, recurrent immune-mediated liver damage in chronic HBV infection can result in a deregulated fibrotic response and in an excessive and abnormal intrahepatic ECM deposition leading to liver fibrosis (Guidotti et al., 2006). In this regard, progressive replacement of functional hepatocytes by non-functional fibrotic scar tissue over decades results in the establishment of liver cirrhosis and ultimately in the failure of liver function. Taken together, chronic HBV infection is characterized by viral persistence and an inefficient immune response towards HBV that sustains long-term immune-mediated liver damage and facilitates the development of lethal liver disease such as cirrhosis and HCC.

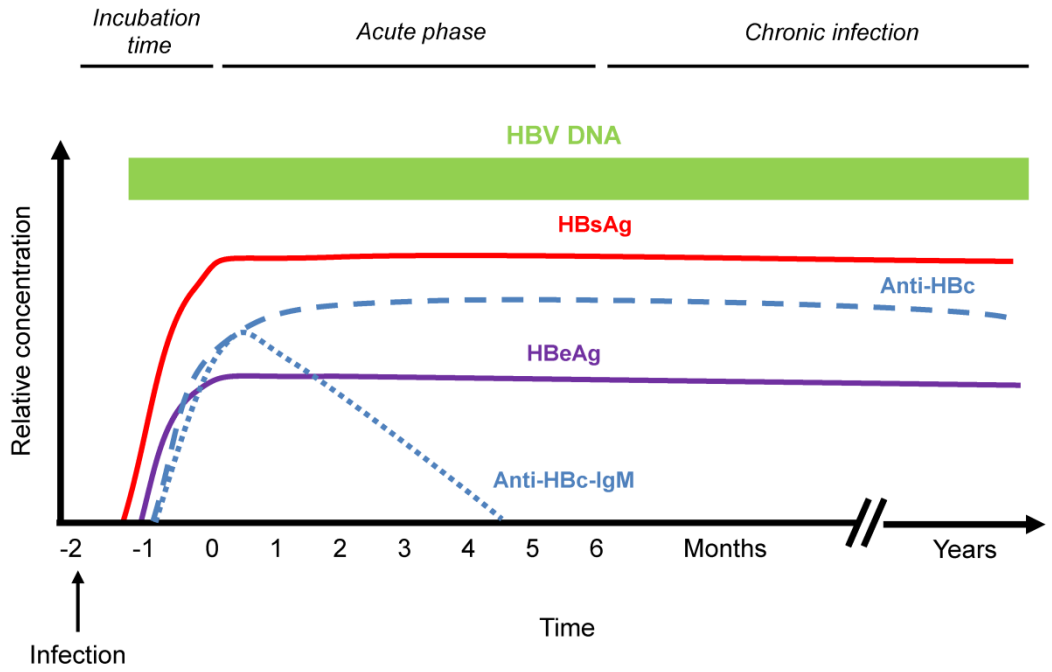

◄ **Fig. 1.3: Serological course of chronic HBV infection.** The graph shows the relative concentrations of viral markers that can be detected in the blood during the course of a chronic HBV infection. In contrast to acute HBV infection, HBV DNA, HBsAg and HBeAg are permanently detectable even after the acute phase of 6 months. ALT levels are moderately elevated (not shown). Moreover, only anti-HBc antibodies are generated, while anti-HBe and anti-HBs antibodies are completely absent. Seroconversion to anti-HBe antibodies may occur, and viral DNA may temporarily be reduced (not shown) (adapted from and modified according to Hoffmann, 2013).

1.1.4.3 HBV-associated HCC

HCC ranks among the five most frequent cancers worldwide and is the second most common cause of cancer death after lung cancer (WHO, 2015b). It is estimated that more than 50 % of HCC cases worldwide and 70–80 % of HCC cases in highly endemic areas are related to chronic HBV infection (Nguyen et al., 2009). Although non-cirrhotic hepatitis B can progress to HCC, the formation of liver cirrhosis upon chronic hepatitis B increases the risk to develop HCC by a factor of 100 (Mahoney et al., 1999). As a consequence of the long-term interplay between hepatic degeneration, regeneration and permanent inflammation, chromosomal alterations can accumulate that lead to malignant mutations in the host genome and promote the development of HCC (Guidotti et al., 2006; Lupberger et al., 2007). Additionally, almost all HBV-associated HCCs have been observed to harbor chromosomally integrated HBV DNA (Brechot et al., 1980; Lupberger et al., 2007). It is hypothesized that the integration of HBV DNA into cell cycle-relevant genes (e.g. c-myc, cyclin A) *per se* is able to cause insertional mutagenesis and malignant cell transformation (*cis-hypothesis*) (Lupberger et al., 2007; Rivière et al., 2014). However, HBV DNA integrates encode HBV-specific

gene products that exert tumor promoter-like functions and can further enhance the malignant transformation of HBV-infected hepatocytes (Lupberger et al., 2007). Most of the integrates harbor the open reading frames for the HBV regulatory proteins, HBx and preS2 (Schlüter et al., 1994; Lupberger et al., 2007). HBx is known to act as a transcriptional transactivator and has been ascribed a contribution to hepatocarcinogenesis (Wollersheim et al., 1988; Kim et al., 1991; Slagle et al., 1996; Terradillos et al., 1997; Madden et al., 2001; Bouchard et al., 2004). HBx affects expression of genes involved in cell cycle control, proliferation and apoptosis and interferes with the DNA repair machinery and mitogenic signaling cascades, such as c-Raf1 signaling (Benn et al., 1994; Hafner et al., 2003; Lupberger et al., 2007). C-terminally truncated HBV surface proteins ($MHBs^t$), so-called preS2 activators, also arise from integrate transcription and can permanently activate the growth-promoting mitogen-activated protein kinase (MAPK) pathway and induce increased cell proliferation (Hildt et al., 2002). Taken together, HBV-associated hepatocarcinogenesis represents a multifactorial process involving direct and indirect mechanisms which contribute to malignant cell transformation.

1.1.5 Prevention and treatment

HBV infection is effectively prevented by prophylactic passive or active immunization. Passive immunization is highly indicated as post-exposure prophylaxis for newborns of infected mothers immediately after birth as well as non-immune individuals after having suffered an injury and contact with HBV-contaminated fluids or material (Jilg and Gerlich, 2014). Protection is achieved by

application of neutralizing anti-HBs antibodies that should be administered within 2–12 hours after exposure (Cornberg et al., 2011). Active immunization involves a recombinant vaccine which contains the small HBV surface antigen (SHBs) of subgenotype A2 produced in yeast cells (Gerlich, 2013). Invented in 1986, it was the first recombinant vaccine available worldwide that superseded the plasma-derived HBV vaccine that had been used since the early 1980s (Gerlich, 2013). The vaccine is administered three times and successful vaccination is confirmed by an anti-HBs titer of > 100 IU/l one month after completion of the vaccination cycle (Jilg and Gerlich, 2014). Vaccination is supposed to deliver protection for at least 10 years or more. Nevertheless, an estimated 5–15 % of persons may not respond to vaccination (Hepatitis B Foundation, 2009). Several reasons for HBsAg nonresponse have been widely discussed, including defects in the generation of primary HBsAg-specific T cells or B cell repertoires (Goncalves et al., 2004). Antiviral treatment of acute hepatitis B is not indicated due to its high rate of spontaneous healing and clearance of HBsAg (Mauss et al., 2015). In contrast, for the treatment of chronic hepatitis B, two classes of drugs exist. The first class comprises standard interferon α-2b (IFN α-2b) or pegylated interferon α-2a (PEG-IFN α-2a) which act as immune modulators that inhibit virus production and activate the immune response (Jilg and Gerlich, 2014; Mauss et al., 2015). The second class involves the five nucleoside and nucleotide analogs lamivudine, telbivudine, entecavir, adefovir and tenofovir which have been approved as reverse transcriptase inhibitors for the treatment of chronic hepatitis B (Mauss et al., 2015). These inhibitors block viral replication by inhibiting reverse transcription of the pregenomic RNA (pgRNA) into HBV DNA by HBV polymerase (Jilg and

Gerlich, 2014). The major goal of antiviral treatment is long-term suppression of viral replication in order to prevent the establishment of liver cirrhosis and HCC (Halegoua-De Marzio et al., 2014). Treatment success is thereby reflected by a decrease or even loss of HBsAg, HBeAg and HBV DNA in the blood as well as a preferable seroconversion to anti-HBs and anti-HBe antibodies (Halegoua-De Marzio et al., 2014). Moreover, it has been reported that application of nucleos(t)ide analogs is able to revert liver fibrosis and even cirrhosis in chronic HBV patients (Schiff et al., 2011). Nevertheless, there are several caveats that have to be taken into consideration regarding HBV therapy. Nucleos(t)ide analogs are prone to the development of resistance due to viral mutations during long-term treatment (Fung et al., 2011; Mauss et al., 2015). Resistance may therefore lead to a loss of therapeutic potency. In spite of their good safety profile, severe adverse effects for nucleos(t)ide analogs such as myopathy and nephrotoxicity have been reported (Khungar et al., 2010). In addition, the primary obstacle in chronic HBV therapy is the persistent presence of covalently circular closed DNA (cccDNA) in the nucleus of infected hepatocytes that serves as a template for the HBV genome (Mauss et al., 2015). Even after antiviral treatment, the cccDNA remains within the nucleus and can cause HBV reactivation (Yang et al., 2014). Another caveat is the integration of HBV DNA into the host genome of infected cells that creates a reservoir for subviral HBV genomes that can be transcribed from the integrate (Lupberger et al., 2007). Although there is evidence that inhibition of HBV replication can reduce HBV cccDNA (Werle–Lapostolle et al., 2004; Wursthorn et al., 2006), antiviral treatment is still considered to be non-curative and complete eradication of HBV is impossible (Rehermann et al., 1996).

1.2 Hepatitis B virus (HBV)

1.2.1 History

In 1963, Baruch S. Blumberg, an American physician, discovered a previously unknown antigen in the serum of an Australian aborigine (Blumberg et al., 1965; Gerlich, 2013). The discovery initially led to the name Australia antigen (AuAg). During the late 1960s, the Australia antigen was further identified to be the major cause of “serum hepatitis” (London et al., 1969; Blumberg, 2002). However, by that time it was still unclear what the AuAg exactly was. This changed fundamentally when in 1970 David S. Dane discovered virus-like particles with 42 nm in size while inspecting AuAg immune complexes using electron microscopy (EM). Owing to this discovery, the HBV viral particle was called “Dane particle” (Dane et al., 1970). Thereafter, the AuAg was finally recognized as the surface antigen of the HBV envelope and was named HBsAg (Hepatitis B surface antigen). Eventually, in 1976, Blumberg was awarded the Noble Prize in Physiology or Medicine, together with D.C. Gajdusek – "*for their discoveries concerning new mechanisms for the origin and dissemination of infectious diseases*" (Blumberg, 2002).

1.2.2 Taxonomy

The human hepatitis B virus is classified as a member of the *Hepadnaviridae* family. This family is subdivided into two genera, the mammalian *Orthohepadnaviridae* and the avian *Avihepadnaviridae*. The genus of *Orthohepadnaviridae* comprises the human (HBV), the chimpanzee (ChHBV), the

gibbon (GiHBV), the orangutan (OuHBV), the gorilla (GoHBV) and the wooly monkey hepatitis B virus (WMHBV) as well as the woodchuck hepatitis virus (WHV), the ground squirrel hepatitis virus (GSHV) and the arctic squirrel (ASHV) (Schaefer, 2007). Strikingly, recent studies have identified a new species of *Orthohepadnaviruses* in bats that is antigenically related to HBV and may have been an ancestral source of primate hepadnaviruses (Drexler et al., 2013; He et al., 2013). Typical representatives of the *Avihepadnaviridae* are the duck hepatitis B virus (DHBV), the heron hepatitis B virus (HHBV) and the snow goose hepatitis B virus (SGHBV) (Schaefer, 2007; Guo et al., 2005). All members of the *Hepadnaviridae* family are hepatotropic, highly host-specific and can cause acute or chronic infection (Jilg and Gerlich, 2014). The genetic variability of human HBV has resulted in 8 different genotypes ranging from A to H with a distinct geographic distribution as illustrated in **Fig. 1.4** (Kramvis et al., 2005). Two putative new genotypes have been identified in Vietnam, Laos and Japan and were provisionally assigned to genotype I and J (Tran et al., 2008; Tatematsu et al., 2009; Sunbul 2014). HBV genotypes differ in their pathogenic severity and the propensity to develop chronic infection and HCC (Suk-Fong Lok, 2015; Sunbul, 2014; Pujol et al., 2009). In addition, nine serological subtypes are known based on amino acid substitutions in the S-domain of the surface proteins (Pujol et al., 2009).

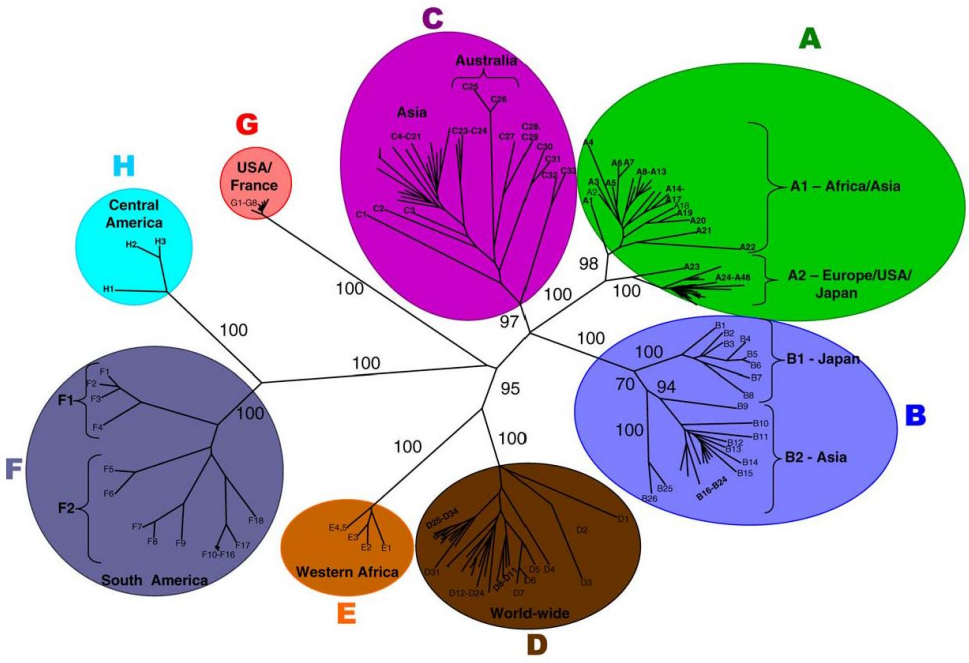

Fig. 1.4: Geographic distribution of HBV genotypes. The illustration shows a phylogenetic tree of 175 full genome sequences of HBV corresponding to the eight genotypes (A–H) and their geographic restriction (taken from Kramvis et al., 2005).

1.2.3 Molecular virology

1.2.3.1 Morphology and structure

Hepadnaviridae are the smallest DNA-containing, enveloped animal viruses that are known (Cheng et al., 2014). Three distinct morphological forms of viral particles can be observed in the serum of HBV-infected patients when examined under the EM (Mauss et al., 2015) (**Fig. 1.5**). The infectious Dane particle is a double-shelled, spherical particle with a diameter of 42−45 nm containing a single copy of the viral DNA genome covalently linked to the viral polymerase (Schädler et al., 2009) (**Fig. 1.5**, 1). It consists of an icosahedral nucleocapsid with a diameter of 28 nm that harbors the viral DNA and is surrounded by a lipid bilayer in which three types of viral surface proteins are embedded to form the viral

envelope (Schädler et al., 2009) (**Fig. 1.6**). The viral envelope comprises about 400 molecules of the HBV surface proteins (HBsAg), which are the small (SHBs), the middle (preS2, MHBs) and the large (preS1, LHBs) surface protein, in a ratio of 4:1:1 (S:M:L) (Siegler et al., 2013; Jilg and Gerlich, 2014). Including the preS domains, the outer hydrodynamic diameter of this particle is 52 nm (Gerlich, 2013; Jilg and Gerlich, 2014). The viral capsid is formed by 120 copies of HBV core protein dimers in T4 symmetry (Schädler et al., 2009). Besides infectious viral particles, there is a vast excess of non-infectious subviral particles that do not contain viral DNA and are exclusively composed of viral surface proteins and host-derived lipids (Bruns et al., 1998). These subviral particles appear as spheres and filaments. Spheres are 17−25 nm in diameter (**Fig. 1.5**, 3), whereas filaments form tubular structures with variable length and a diameter of about 20 nm (**Fig. 1.5**, 2) (Gerlich, 2013). Function and relevance of these subviral particles are highly debated. It is supposed that due to their high amounts in the blood of infected individuals subviral particles bind neutralizing antibodies directed against HBsAg in order to enable infectious viral particles to reach susceptible cells for infection (Ganem, 1991). It has also been observed that subviral particles are able to enhance intracellular viral replication and gene expression dependent on multiplicity of infection and the ratio between viral and subviral particles (Bruns et al., 1998). In addition, subviral particles might contribute to immune tolerance that fosters persistent infection (Gerlich et al., 2005; Mauss et al., 2015).

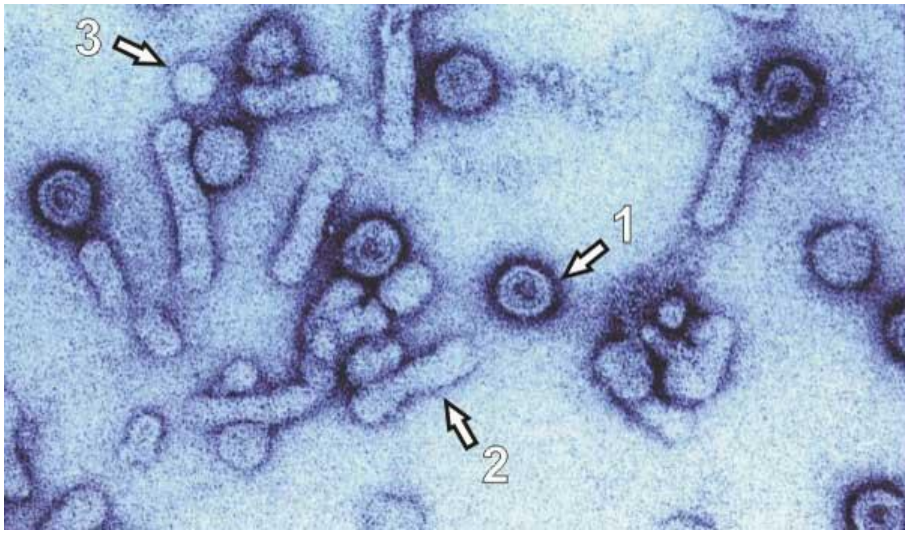

Fig. 1.5: Viral and subviral HBV particles. EM image represents infectious Dane particles (**1**) as well as non-infectious filaments (**2**) and spheres (**3**) (EM picture by H.-W. Zentgraf, Heidelberg).

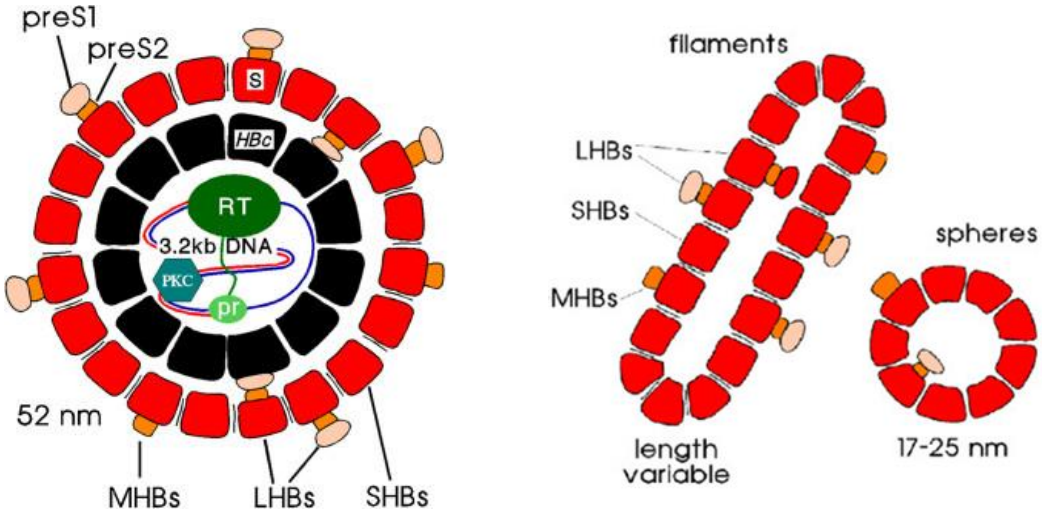

Fig. 1.6: Schematic representation of viral and subviral HBV particles. Infectious viral particles (left) contain the viral DNA surrounded by the nucleocapsid which is formed by the core protein (HBc). The nucleocapsid is surrounded by the viral envelope that is formed by a host-derived lipid bilayer (not shown) in which three types of viral surface proteins are embedded. The small surface protein (SHBs) consists of the S domain. The middle surface protein (MHBs) consists of the S and the preS2 domain. The large surface protein (LHBs) consists of the S, the preS1 and the preS2

◄ domain. Subviral particles (right) are devoid of viral DNA and are composed solely of the viral surface proteins. Filaments (middle) are of variable length while spheres (right) are 17−25 nm in size (adapted from Gerlich, 2013).

1.2.3.2 Genome organization

The genome of HBV consists of a relaxed circular, partially double-stranded DNA molecule encircled by the viral capsid (Nassal, 2008). It comprises a complete negative coding strand with a length of about 3.200 nucleotides and an incomplete positive non-coding strand with variable length at the 3' end (Lutwick et al., 1977; Summers, 1988) (**Fig. 1.7**). The 5' end of the negative strand is covalently linked to the viral polymerase *via* a phosphotyrosine bond (Bartenschlager et al., 1988; Mauss et al., 2015). The 5' end of the positive strand features a small covalently bound RNA oligonucleotide which serves as a primer for the synthesis of the positive strand (Beck et al., 2007; Mauss et al., 2015). The complete negative strand harbors four open reading frames (ORF) which partially overlap. These four ORFs encode the viral polymerase (P), the core (HBcAg) and the precore protein (HBeAg), the regulatory X protein (HBx) and the three surface proteins SHBs, MHBs and LHBs (HBsAg) (Schädler et al., 2009). Once a cell has been infected by HBV, the genome is released and transported to the nucleus where the incomplete positive strand is completed by the cellular DNA repair machinery. This yields the plasmid-like cccDNA which remains stable in the nucleus of infected hepatocytes (Jilg and Gerlich, 2014). The cccDNA serves as a template for the pgRNA and the subgenomic viral RNA transcripts which are all transcribed by host RNA polymerase II and are capped and polyadenylated (Beck et al., 2007;

Schädler et al., 2009). Translation of the 3.5 kb mRNA generates the core and the precore protein as well as the viral polymerase. The translation product of the 2.4 mRNA is the large surface protein (LHBs), whereas translation of the 2.1 kb mRNA delivers the middle and small surface proteins (MHBs and SHBs). The 0.7 kb mRNA is translated into the X protein (HBx) (Seeger et al., 2000; Nassal 2008).

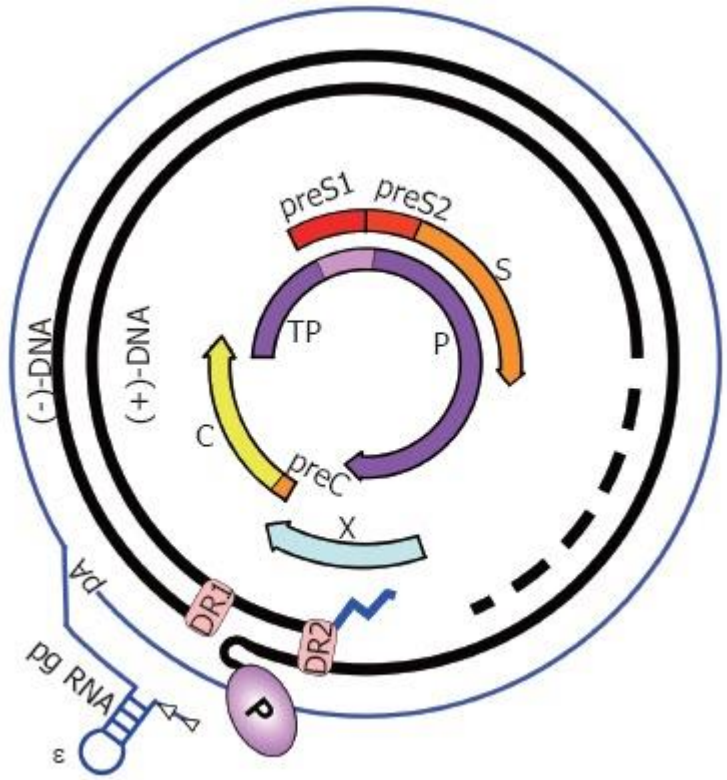

Fig. 1.7: HBV genome organization. The HBV genome consists of a partially double-stranded DNA molecule (black thick lines). The complete negative coding strand ((-)-DNA) has a length of about 3.200 nucleotides, whereas the positive non-coding strand ((+)-DNA) is variable in length (dashed black thick lines). The negative strand is covalently linked to the viral polymerase (P). The positive strand harbors a small RNA oligonucleotide at its 5' end (blue zigzag line). There are two direct repeats (DR1, DR2) which are important for replication. The four partially overlapping open reading frames on the negative strand encode the polymerase (P) together with the terminal protein domain (TP), the core (C) and the precore (preC) protein as well as the preS1, preS2 and the S domain of the small, middle and large surface proteins. The pregenomic RNA (pgRNA, outer

◄ blue circle) arises from transcription of the cccDNA after an infection has been established. pgRNA is an RNA intermediate essential for viral replication and other subgenomic RNAs. It possesses a polyA-tail (pA) and an RNA hairpin structure (ε) (adapted from Beck et al., 2007).

1.2.3.3 Viral life cycle

The primary target cells of HBV are the parenchymal hepatocytes of the liver (Guidotti et al., 2006). After entering the bloodstream by penetrating skin lesions or the mucosa, the virus is transported to the liver through the *fenestrae* of the sinusoidal endothelial cells into the space of Disse and by this gains access to hepatocytes (Jilg and Gerlich, 2014). Before employing a hepatocyte-specific receptor, viral particles initially bind energy-independently and unspecifically to hepatocytes by attachment to carbohydrate side chains of hepatocyte-associated heparin sulfate proteoglycans on the plasma membrane (Schulze et al., 2007; Leistner et al., 2008). The sodium-taurocholate co-transporting polypeptide (NTCP) is expressed and enriched at the sinusoidal membrane of differentiated hepatocytes and serves as a liver-specific receptor for the entry of HBV into hepatocytes (Ananthanarayanan et al., 1994; Yan et al., 2012). *Via* its preS1 domain of the LHBs, HBV binds with high affinity to NTCP (Yan et al., 2012). However, the cellular factor α-taxilin was also described to play an essential role in the HBV entry process (Hoffmann, 2013). Although the precise mechanism of viral entry has not been elucidated yet, internalization of the viral particles is accomplished by receptor-mediated endocytosis (Offensperger et al., 1991; Stoeckl et al., 2006). Once localized in the endosome, the low pH triggers a structural change in the preS2 domain of the surface proteins that leads to

exposure of a translocation motif (TLM) (Stoeckl et al., 2006). The TLM is conserved in all *hepadnaviridae* and represents a membrane-permeable peptide formed by a labile amphipathic helix which mediates the fusion of the viral particle with the endosomal membrane and release of the nucleocapsid from the endosomal compartment into the cytoplasm (Oess et al., 2000; Schädler et al., 2009). Presence of the TLM was shown to be essential for infectivity, although there is another report claiming that the TLM is dispensable for productive infection (Lepère et al., 2007). In the cytoplasm, the nucleocapsid is directly transported to the nucleus *via* the microtubule system (Brandenburg et al., 2005; Döhner et al., 2005; Rabe et al., 2006). With the help of two nuclear localization sequences (NLS) in the C-terminal domain of the core protein, the viral genome is actively delivered *via* the nuclear pore complex into the nucleoplasm after the capsid has been disassembled in the nuclear basket (Eckhardt et al., 1991; Kann et al., 1999; Schmitz et al., 2010). Within the nucleus, the relaxed circular viral DNA (rcDNA) is converted into the episomal cccDNA and associates with histones to form an episomal minichromosome in the nucleus of infected hepatocytes (Bock et al., 1994; Bock et al., 2001; Schädler et al., 2009). The cccDNA serves as a template for the synthesis of the pgRNA which is indispensable for viral replication and transcription of the subgenomic mRNAs (2.4, 2.1 and 0.7 kb mRNA) (Raney et al., 1992; Schädler et al., 2009). After export into the cytoplasm, the 3.5 kb pgRNA itself is translated into the viral polymerase, the core and the precore protein. On the other hand, the pgRNA represents the template for reverse transcription of the pgRNA into DNA (Schädler et al., 2009). The ε signal on the pgRNA (**Fig. 1.7**) functions as an encapsidation signal and binds the viral

polymerase so the pgRNA-polymerase complex can be packed in the lumen of assembling capsids. In addition, the ε-polymerase interaction induces reverse transcription within the immature core particles yielding first single-stranded and then partially double-stranded DNA (Bruss, 2007; Schädler et al., 2009). Subsequently, mature nucleocapsids can take two routes: they can interact with the viral surface proteins which are simultaneously translated at the membrane of the endoplasmic reticulum (ER) and are then released as infectious virions, or they can be re-transported to the nucleus where they again release their cargo DNA to contribute to nuclear cccDNA accumulation (Schädler et al., 2009). Interaction and envelopment of the viral capsids with surface proteins requires an interaction of the core protein with the LHBs at the cytosolic face of the ER. By budding of the nucleocapsids into the ER, they are coated with the surface proteins and are then translocated to the Golgi apparatus where further processing of the surface proteins occurs (Devarajan et al., 2014). The final release of the mature HBV virions is facilitated by the ESCRT (*endosomal sorting complex required for transport*)-dependent export machinery (Kian Chua et al., 2006; Lambert et al., 2007; Watanabe et al., 2007; Hoffmann et al., 2013). The HBV life cycle is schematically illustrated in **Fig. 1.8**.

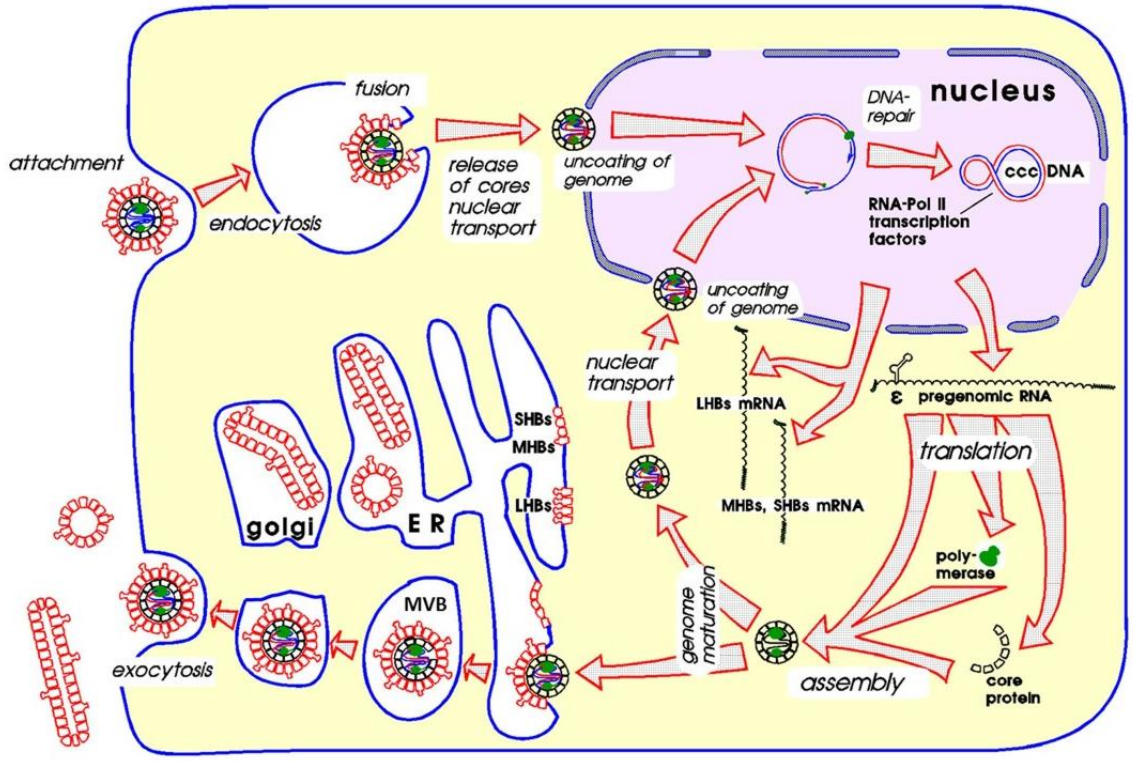

Fig. 1.8: The HBV life cycle. Viral entry is initiated after binding of HBV to the hepatocyte-specific receptor NTCP. Subsequently, viral particles are taken up by receptor-mediated endocytosis into the cell. Within the endosomes, fusion of the viral envelope with the endosomal membrane results in the release of the nucleocapsid into the cytoplasm. The nucleocapsid is transported to the nucleus where the viral genome is released into the nucleoplasm. Within the nucleus, the partially double-stranded DNA is repaired and converted into episomal cccDNA by the cellular DNA repair machinery. The cccDNA is transcribed into the pgRNA and the subgenomic RNAs which are transported into the cytoplasm for translation. Translation of the pgRNA yields the viral polymerase, the core and the precore protein, while translation of the 2.4 and the 2.1 kb mRNA at the ER produces the viral surface proteins (SHBs, MHBs, LHBs). A complex of the pgRNA and the viral polymerase are incorporated into assembling capsids to form immature core particles. The pgRNA within the particles serves as a template for reverse transcription of the pgRNA into (-)ssDNA and then the relaxed circular DNA which marks the maturation of the virions. Mature HBV virions can then either be recycled back to the nucleus or are enveloped by the surface proteins at the ER and are secreted from the cell by the cellular export machinery (taken from Gerlich, 2013).

1.3 Liver regeneration

The liver is a vital organ with crucial functions in metabolic homeostasis, detoxification of toxins and xenobiotics, protein synthesis as well as production, storage and secretion of nutrients (Beyer et al., 2008b). Since it is frequently exposed to toxins and noxious compounds that can cause liver damage and tissue loss, the liver retains the remarkable capability to fully regenerate (Fausto, 2000; Taub, 2004). Under normal physiological conditions, hepatocytes are in a quiescent state and rarely divide. Following an injury, hepatocytes can re-enter the cell cycle and proliferate until the original liver mass is restored (Taub, 2004). A variety of growth factors and cytokines are involved in the control of liver regeneration (Taub, 2004; Böhm et al., 2010). These include the hepatocyte growth factor (HGF), the epidermal growth factor (EGF), the transforming growth factors (TGFs), insulin and glucagon, the tumor necrosis factor (TNF) α and interleukin (IL)-6 (Taub, 2004). The regeneration process can be divided into three phases: priming, proliferation and cessation (Diehl, 2002; Beyer et al., 2008b). In the priming phase, the pro-inflammatory cytokines TNFα and IL-6 play an important role (Fausto, 2000; Beyer et al., 2008a). They activate the transcription factors nuclear factor κB (NF-κB), activator protein 1 (AP-1) and signal transducer and activator of transcription 3 (STAT3) which mediate the transition from the G_0 to the G_1 state of the cell cycle (Cressman et al., 1995; FitzGerald et al., 1995; Heim et al., 1997). In the second phase, growth factors assist hepatocytes to enter the S phase where DNA synthesis and proliferation take place (Taub, 2004; Beyer et al., 2008a). Upon completion of liver repair, hepatocyte proliferation is inhibited by TGF-β and activin signaling and hepatocytes return to quiescence (Oe et al., 2004;

Beyer et al., 2008a). However, chronic liver injury, e.g. as a result of long-term alcohol or drug abuse as well as chronic viral hepatitis can exhaust the regenerative capacity of the liver and promote the development of liver disease such as fibrosis and cirrhosis (Diehl, 2002; Beyer et al., 2008a). To experimentally investigate liver regeneration there are several methods that can be utilized, such as partial hepatectomy (PHx) (Mitchell et al., 2008), carbon tetrachloride (CCl_4) (Iredale, 2007) treatment or induction of autoimmune hepatitis (Hintermann et al., 2012).

1.4 Nrf2

Reactive oxygen species (ROS) that are generated during the normal course of cellular metabolism or from exogenous sources can cause oxidative stress and cellular damage (Aleksunes et al., 2007). One of the major cellular defense mechanisms against oxidative stress is the transcriptional upregulation of a variety of genes that encode cytoprotective and ROS-detoxifying enzymes (Lau et al., 2008; Niture et al., 2014). These include glutathione S-transferases (GSTs), NAD(P)H quinone oxidoreductase 1 (NQO1) and glutamate-cysteine ligase catalytic subunit (GCLC) (Jaiswal 2004; Kobayashi et al., 2005). The corresponding genes that encode these enzymes harbor an antioxidant response element (ARE) in their promoter region (*TGACnnnGC*) (Wasserman et al., 1997). ARE-dependent gene expression is controlled by the cap ‘n’ collar basic leucine zipper (bZIP) transcription factor nuclear factor (erythroid-derived 2)-like-2 factor (Nrf2) (Aleksunes et al., 2007). Under normoxic conditions, Nrf2 resides in its inactive state bound to the Kelch-like ECH-associated protein 1 (Keap1) in the

cytoplasm and is targeted for proteasomal degradation (McMahon et al., 2003; Kobayashi et al., 2004; Köhler et al., 2014). The presence of ROS or electrophiles results in the dissociation of Nrf2 and Keap1, enabling Nrf2 to translocate to the nucleus. In combination with small Maf proteins (sMaf), Nrf2 forms a heterodimer to bind to ARE sequences and to activate ARE-dependent gene expression (Itoh et al., 1997; Lau et al., 2008) (**Fig. 1.9**). Since one of its major functions is the detoxification of xenobiotics, toxins and other chemicals, the liver is continuously exposed to ROS which are inevitably generated in the course of detoxification (Chan et al., 2001; Aleksunes et al., 2007). Hence, proper functionality of the Nrf2 pathway is indispensable for hepatic performance and protection. Nrf2 was even demonstrated to protect the liver from toxin-induced injury and fibrosis (Xu et al., 2008). Abolishment of Nrf2 functionality results in hepatotoxicity and increased sensitivity to hepatocarcinogenesis (Enomoto et al., 2001; Ramos-Gomez et al., 2001). Importantly, Nrf2 also plays an essential role in the regulation of liver regeneration (Beyer et al., 2008a; Beyer et al., 2008b; Dayoub et al., 2013; Köhler et al., 2014). After liver injury induced by partial hepatectomy, Nrf2 knock-out mice show impaired liver regeneration. This impairment is a consequence of increased ROS levels in the liver due to the lack of Nrf2. Increased ROS thereby cause inhibition of insulin/IGF-I receptor signaling which is necessary for hepatocyte survival and proliferation (Beyer et al., 2008a; Beyer et al., 2008b). Interestingly, HBV was observed to induce activation of Nrf2 and increased expression of Nrf2/ARE-regulated genes (Schädler et al., 2010). This activation is triggered by the HBV-regulatory proteins HBx and LHBs *via* the MAPK pathway and results in a better protection against oxidative damage (Schädler et al., 2010).

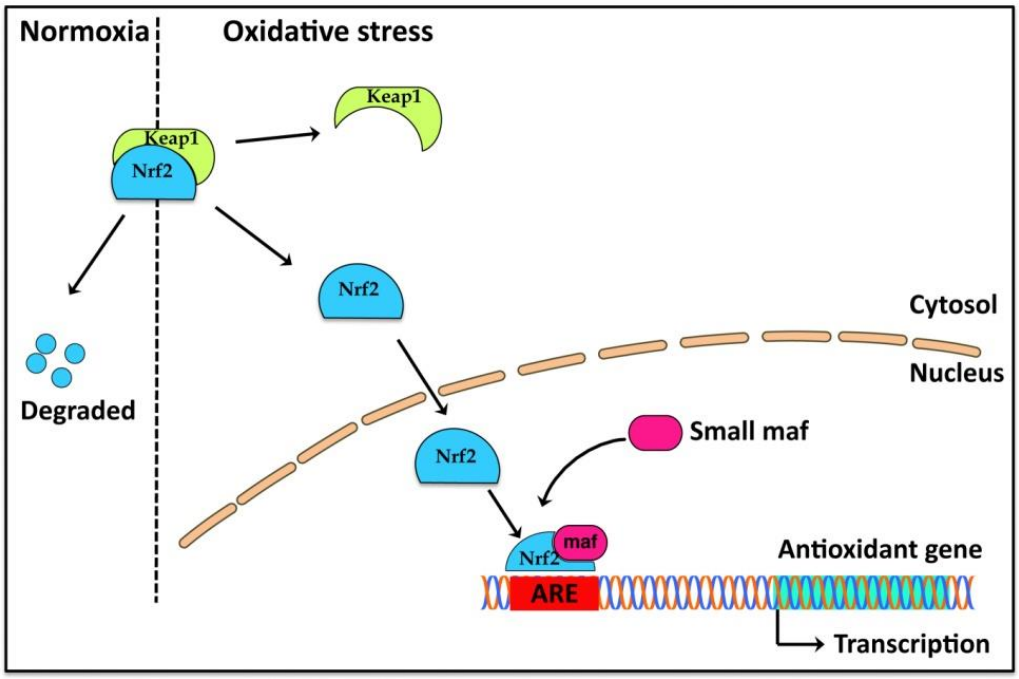

Fig. 1.9: Antioxidant gene expression *via* the Nrf2/ARE pathway. Under normoxic conditions, Nrf2 is bound to Keap1 in the cytoplasm and is targeted for proteasomal degradation. Upon oxidative stress, Nrf2 dissociates from Keap1 and translocates to the nucleus where it forms a heterodimer with a small Maf protein (sMaf). The Nrf2:sMaf complex then binds to ARE sequences on the target gene and initiates gene transcription of the antioxidant gene. A lack of Nrf2 causes increased oxidative stress and is known to impair of liver regeneration (taken from Bhatia et al., 2013).

1.5 Insulin receptor signaling

1.5.1 Insulin and its physiological functions

Insulin is an important anabolic peptide hormone, primarily regulating glucose and lipid metabolism and homeostasis (Saltiel et al., 2001). Moreover, insulin together with insulin-like growth factors (IGFs) is involved in numerous cellular processes such as the regulation of cellular growth, development and differentiation as well as proliferation and survival (Siddle, 2011; Singh et al., 2014). Insulin and IGF-I

are known to activate pro-mitogenic and anti-apoptotic signaling pathways, including the MAPK pathway and the phosphoinositide 3-kinase (PI3K)/protein kinase B (Akt) pathway (Beyer et al., 2008a; Siddle, 2011) and are thus also considered to be involved in the development and progression of cancer (LeRoith et al., 2003; Malaguarnera et al., 2014). As a response to increasing blood glucose levels, insulin is expressed and secreted from the β-cells located in the islets of Langerhans of the pancreas (Nielsen et al., 1985; Xu et al., 1998; Singh et al., 2014). The primary translation product of insulin mRNA is the inactive preproinsulin (Steiner et al., 2009). A signal peptidase in the ER cleaves off a signal peptide at the N-terminus of the preproinsulin to yield proinsulin. After proper folding and formation of three intrachain disulfide bonds, proinsulin is transported from the ER to the Golgi apparatus where the C-peptide is cleaved off to yield the mature insulin peptide (Fu et al., 2012). Mature and active insulin peptide consists of the two polypeptide chains A and B that are linked by two disulfide bonds, with the A chain possessing an additional intramolecular disulfide bond (Steiner et al., 2009). Insulin binds to classical insulin-responsive cells such as hepatocytes, adipocytes and skeletal muscle cells that express high levels of the insulin receptor (Xu et al., 1998; Singh et al., 2014). Binding of insulin to its cognate receptor induces translocation of glucose transporter 4 (GLUT4) from intracellular vesicles to the plasma membrane and results in glucose uptake into the cell (Suzuki et al., 1980). By this mechanism, insulin is able to reduce and regulate blood glucose levels (Saltiel et al., 2001). Furthermore, insulin stimulates glycogen synthesis by activation of the glycogen synthase (Saltiel et al., 2001). This activation of glycogen synthase by insulin occurs on the one hand *via*

allosteric regulation by elevated levels of glucose-6-phosphate after glucose transport and on the other hand by promoting the dephosphorylation of glycogen synthase through activation of protein phosphatase 1 (PP1) and Akt-dependent inactivation of glycogen synthase kinase 3β (GSK3β) (Brady et al., 1997; McManus et al., 2005; Bouskila et al., 2010). Insulin blocks gluconeogenesis and glycogenolysis in the liver by inhibiting transcription of the phosphoenolpyruvate carboxylase, fructose-1,6-bisphosphatase and glucose-6-phosphatase (Pilkis et al., 1992; Sutherland et al., 1996; Saltiel et al., 2001). *Vice versa*, insulin increases transcription of glycolytic and lipogenic enzymes such as glucokinase and pyruvate kinase, fatty acid synthase and acetyl-CoA carboxylase (Saltiel et al., 2001). In doing so, insulin promotes synthesis of lipids and inhibits their degradation (Saltiel et al., 2001). More than 150 genes are known to be regulated by insulin (O'Brien et al., 2001). Important transcription factors mediating insulin-dependent gene expression are forkhead box protein O1 (FOXO1), peroxisome proliferator-activated receptor gamma coactivator 1 (PGC-1) as well as steroid regulatory element-binding protein (SREBP)-1c (Foretz et al., 1999; Nakae et al., 1999; Shimomura et al., 1999; Yoon et al., 2001). Importantly, an impairment of insulin-stimulated glucose transport, glucose utilization and glycogen synthesis is associated with insulin resistance and the pathogenesis of type 2 diabetes (Shulman, 2000; Bouskila et al., 2010).

1.5.2 The insulin receptor

The insulin receptor (IR) is a transmembrane receptor that belongs to the family of receptor tyrosine kinases (RTK) (Patti et al., 1998). It is encoded by a single 22-exon gene (*INSR*) localized on chromosome 19 (Belfiore et al., 2009). *INSR* mRNA encodes for a protein of 1370 amino acids which is posttranslationally cleaved by furin into α- and β-subunits (Belfiore et al., 2009). The α-subunit contains 723 amino acids, with a molecular mass of 130 kDa. The β-subunit contains 620 amino acids, with a molecular mass of 95 kDa. Both subunits are glycosylated (Belfiore et al., 2009). The IR exists in two isoforms (IR-A and IR-B) due to exclusion (IR-A) or inclusion (IR-B) of exon 11 by alternative splicing during *INSR* transcription (Seino et al., 1989). Inclusion of exon 11 adds a 12-amino acid segment at the C-terminal end of the α-subunit (Belfiore et al., 2009). The two isoforms mainly differ in their binding affinity for IGF-II and their tissue-specific expression (Belfiore et al., 2009). The fully assembled and functional insulin receptor represents a heterotetramer composed of two extracellular α-subunits and two transmembrane β-subunits which are linked by disulfide bonds (Lawrence et al., 2007) (**Fig. 1.10**). The β-subunits contain the tyrosine kinase domains flanked by two regulatory regions that contain phosphotyrosine binding sites for signaling molecules (Belfiore et al., 2009; Hubbard, 2013). Besides the major insulin-responsive tissues liver, adipose tissue and skeletal muscle, the insulin receptor is also expressed in the brain, heart, kidney, pulmonary alveoli, pancreatic acini, placenta vascular endothelium, monocytes, granulocytes, erythrocytes, and fibroblasts (Kaplan, 1984; Belfiore et al., 2009). Besides insulin, also IGF-I and IGF-II act as functional ligands that bind and activate the insulin

receptor (Belfiore et al., 2009). Once insulin and its related ligands have executed their function, the insulin receptor in complex with its ligand is internalized, primarily by clathrin-mediated endocytosis (Carpentier, 1994; Goh et al., 2013). Within the endosome, the acidic pH triggers dissociation of the ligand from the receptor and degradation of insulin is initiated by the insulin-degrading enzyme (IDE) (Duckworth et al., 1998). While insulin molecules are further degraded by acidic proteinases in late endosomes, the insulin receptor is recycled back to the plasma membrane to be reused (Fehlmann et al., 1982; Carpentier et al., 1985; Authier et al., 1994; Carpentier, 1994). Strikingly, in liver cells the insulin receptor has also been reported to translocate to the nucleus to regulate cell proliferation and liver regeneration (Amaya et al., 2014).

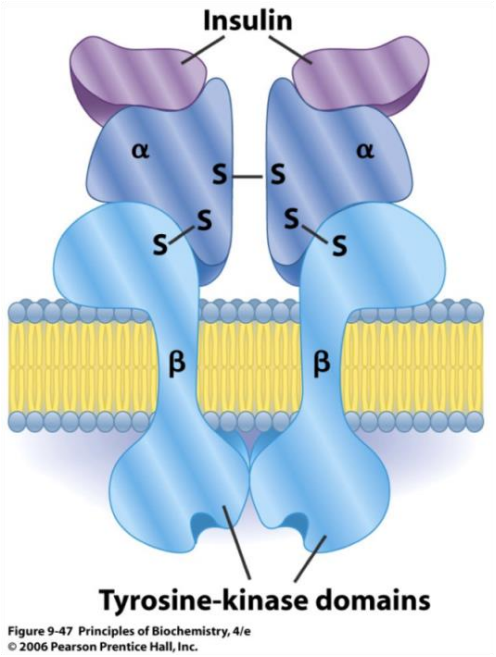

Fig. 1.10: Structure of the insulin receptor. The insulin receptor is a heterotetramer composed of two extracellular α-subunits which bind insulin and two transmembrane β-subunits which harbor the tyrosine kinase domains. The α-subunits are linked to each other by a disulfide bond. The β-subunits are linked to the α-subunits also by disulfide bonds (taken from Nelson et al., 2004).

1.5.3 The insulin receptor signaling pathway

Binding of insulin to the α-subunit of the insulin receptor induces a conformational change in the receptor molecule, which brings the two β-subunits into close opposition leading to activation of the tyrosine kinase activity in the cytoplasmic tail of the β-subunit (Belfiore et al., 2009). Activation of the tyrosine kinase activity subsequently leads to autophosphorylation of multiple tyrosine residues in the β-subunit and to receptor activation (Kasuga et al., 1982a; Kasuga et al., 1982b). Tyrosine phosphorylation of the receptor enables recruitment and cytoplasmic binding of several intracellular substrates, including insulin-receptor substrates 1 to 6 (IRS-1 to IRS-6) which bind to the activated receptor *via* their phosphotyrosine binding-domain (PTB) (He et al., 1995; Wolf et al., 1995; Taniguchi et al., 2006). IRS-1 and IRS-2 are the two major substrates which are responsible for most of the metabolic effects of insulin (Kadowaki et al., 2012). Other intracellular substrates that bind to the phosphorylated insulin receptor are Grb2-associated binder-1 (Gab1), Cas-Br-M ecotropic retroviral transforming sequence homologue (Cbl) and Src-homology-2-containing protein (Shc) (Taniguchi et al., 2006). After they have been phosphorylated by the insulin receptor, these substrates (e.g. IRS-1) function as docking platforms for other intracellular effector molecules harboring Src homology 2 (SH2) domains that specifically bind to specific phosphotyrosine residues (Sun et al., 1993; Taniguchi et al., 2006; Belfiore et al., 2009). Two important representatives of these effector molecules are PI3K and growth factor receptor-bound protein 2 (Grb2) (Taniguchi et al., 2006). Grb2, for example, associates with son-of-sevenless (SOS) to activate the Ras-MAPK pathway, one important signaling pathway within the insulin receptor signaling cascade which

triggers mitogenesis and cellular growth (Virkamäki et al., 1999; Sasaoka et al., 2000). On the other hand, activation of the p110 catalytic subunit of PI3K in concert with its regulatory subunit p85 results in phosphorylation of phosphatidylinositol-(4,5)-bisphosphate (PIP2) in the plasma membrane to phosphatidylinositol-(3,4,5)-trisphosphate (PIP3) (Taniguchi et al., 2006). The PI3K pathway is another signaling pathway which is of major importance for the insulin receptor signaling cascade. PIP3 serves as a lipid second messenger and can recruit and activate pleckstrin homology domain (PH)-containing proteins such as 3-phosphoinositide-dependent protein kinase-1 and -2 (PDK-1/2) (Taniguchi et al., 2006; Guo, 2014). PDK-1 and PDK-2 are then in turn responsible for the activation of PKB/Akt by inducing its phosphorylation (Guo, 2014). Once activated, PKB/Akt fulfills a central role in the insulin receptor signaling pathway by phosphorylating numerous downstream targets. For example, it phosphorylates and inhibits GSK3β to activate glycogen synthase (Cross et al., 1995). Moreover, the activating phosphorylation of the Rab-GTPase activating protein AS160 by PKB/Akt results in GLUT4 translocation and glucose uptake in myocytes and adipocytes (Mîinea et al., 2005; Kadowaki et al., 2012; Guo, 2014). PKB/Akt also mediates phosphorylation of the B-cell lymphoma-2 (Bcl-2) family member Bcl-2-associated death promoter (Bad) for inhibition of apoptosis as well as the cAMP response element binding protein (CREB)-regulated transcription coactivator-2 (CRTC2) and FOXO1 for inactivation of gene expression involved in gluconeogenesis (Kadowaki et al., 2012; Guo, 2014). In addition, Akt-mediated phosphorylation of phosphodiesterase 3B (PDE3B) inhibits lipolysis (Kadowaki et al., 2012). Tuberous sclerosis complex 1/2 (TSC1/2) as well underlies

phosphorylation by PKB/Akt. Phosphorylation suppresses its GTPase-activating protein activity, leading to activation of the mammalian target of rapamycin complex 1 (mTORC1) activator Ras homolog enriched in brain (Rheb), which ultimately results in increased cell proliferation through phosphorylation of S6K1 (p70 S6 kinase 1) and stimulation of protein synthesis (Kadowaki et al., 2012). S6K1 activation can also occur *via* activated PDK-1. In addition, PDK-1 activates the protein kinase C (PKC) λ/ζ which in turn stimulates the activation of SREBP-1c and results in the induction of lipogenic gene expression (Sajan et al., 2009; Kadowaki et al., 2012). **Fig. 1.11** summarizes the important features of the insulin receptor signaling pathway.

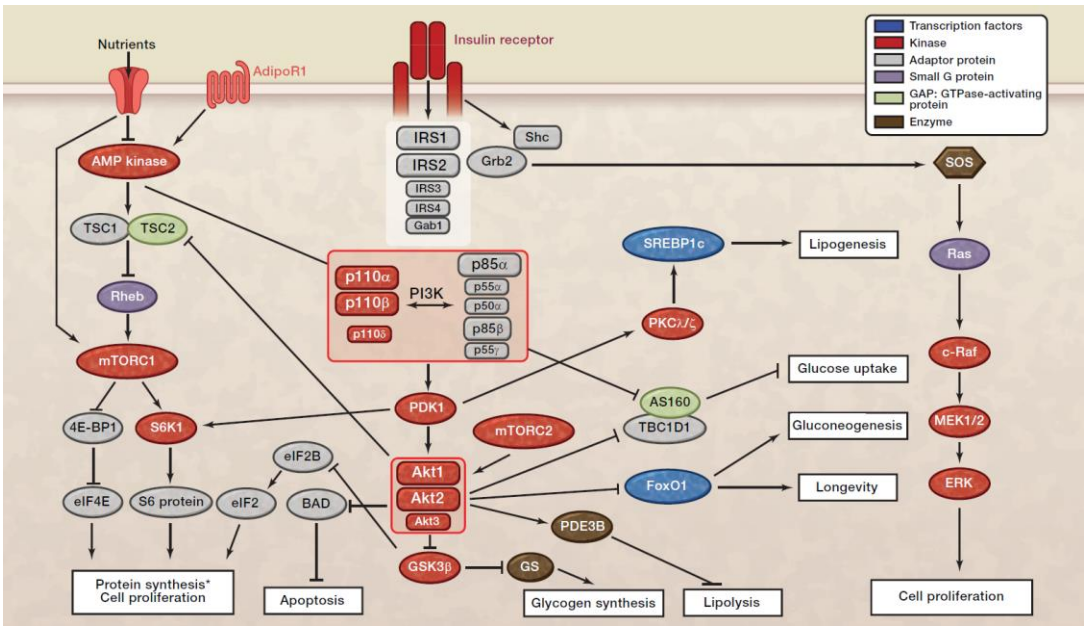

Fig. 1.11: Insulin receptor signaling pathway. Binding of insulin to the insulin receptor induces its own phosphorylation, leading to recruitment of several adaptor molecules such as insulin receptor substrates (IRS) and Shc. These adaptor molecules then recruit further effector molecules, e.g. Grb2 or PI3K. Two major signaling pathways are triggered by insulin binding, the Ras-MAPK and the PI3K pathway. Both pathways are primarily responsible for the execution of insulin-mediated metabolic and mitogenic effects (taken from Kadowaki et al., 2012).

A critical pathway such as insulin receptor signaling needs to be tightly regulated. One important measure that serves for attenuation of insulin receptor signaling is the inhibitory phosphorylation of the insulin receptor as well as the insulin receptor substrates (IRS) on specific serine residues which decreases activating tyrosine phosphorylation (Hotamisligil et al., 1996; Saltiel et al., 2001; Pirola et al., 2004). Serine phosphorylation of IRS-1/2, for example, is accomplished by Jun N-terminal kinase (JNK) or IκB kinase-β (IKKβ) (Gao et al., 2002; Hirosumi et al., 2002). Furthermore, insulin receptor signaling is inhibited by protein tyrosine phosphatases (PTPases), among others PTP1B, which dephosphorylate the receptor and its associated substrates (Seely et al., 1996; Salmeen et al., 2000, Saltiel et al., 2001). In addition, there is a variety of other modulators that negatively regulate insulin receptor activity and signaling (Du et al., 2014). Low concentrations of ROS, such as superoxide and H_2O_2 are naturally generated by insulin stimulation, and play a role in facilitating normal signal transduction by insulin (Goldstein et al., 2005). Moreover, H_2O_2 is widely accepted as a crucial signaling molecule (Forman, 2010; Besse-Patin et al., 2014). Nevertheless, it is well established that sustained oxidative stress by high concentrations of ROS is associated with the development of insulin resistance and diabetes (Urakawa et al., 2003; Furukawa et al., 2004; Anderson et al., 2009). Stress-sensitive serine/threonine kinases such as JNK cause inhibitory serine phosphorylation of IRS-1/2 and promote ROS-induced insulin resistance (Boura-Halfon et al., 2009; Besse-Patin et al., 2014). This has already been described for the hepatitis C virus (HCV). HCV promotes insulin resistance and impairs insulin receptor downstream signaling by inducing serine phosphorylation of IRS-1 (Banerjee et

al., 2008; Parvaiz et al., 2015). Furthermore, HCV was observed to impair induction of ROS-detoxifying Nrf2-regulated genes, thereby facilitating oxidative stress and ROS-induced insulin resistance (Carvajal-Yepes et al., 2011). Taken together, **Fig. 1.12** depicts the importance of Nrf2 for the detoxification of ROS, thereby inhibiting JNK activity and increasing insulin sensitivity.

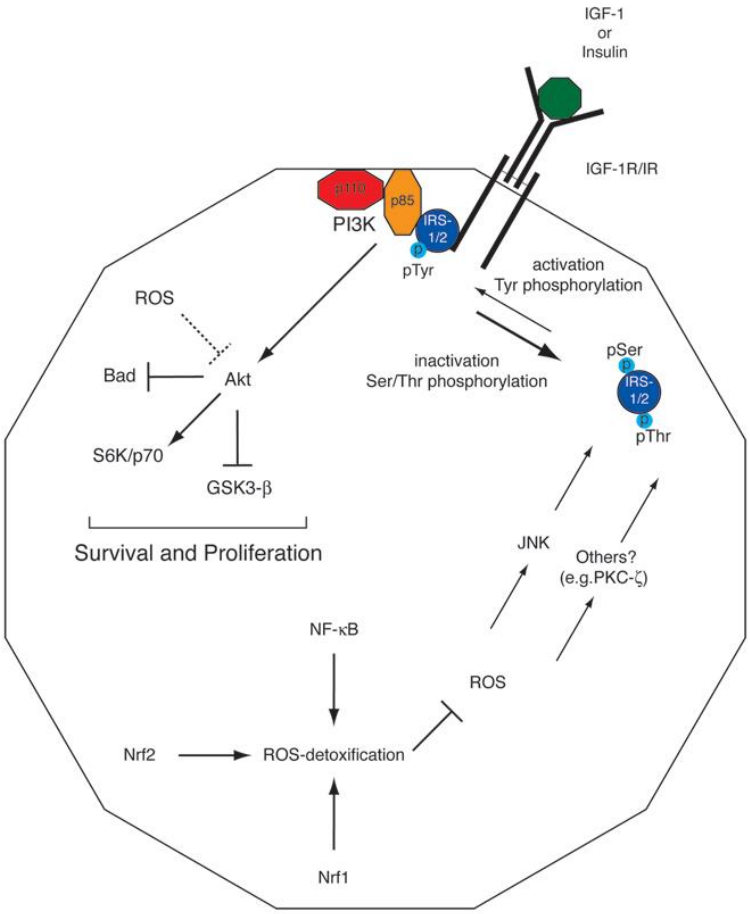

Fig. 1.12: Importance of Nrf2 for insulin receptor signaling. Nrf2 activity induces expression of ROS-detoxifying enzymes to reduce intracellular ROS concentrations. Otherwise, increased levels of ROS can induce stress-sensitive kinases such as JNK and PKC-ζ which catalyze inactivating serine/threonine phosphorylation of IRS-1/2 and cause their dissociation from the insulin receptor. Consequently, inactivated IRS-1/2 are not available for tyrosine phosphorylation and transmission of the insulin signal, thereby inactivating insulin receptor signaling (taken from Beyer et al., 2008a).

2 Thesis objectives

2.1 Previous results

It was recently found that stably HBV-expressing cells *in vitro* possess increased amounts of insulin receptor protein in contrast to HBV-negative control cells. These results were further confirmed in transiently HBV-expressing cells as well as *in vivo* in liver sections derived from HBV transgenic mice and patients suffering from chronic HBV infection (unpublished results by T. Heinrich). Contrarily to the elevated amounts of insulin receptor protein in HBV-expressing cells, it was also observed that stably HBV-expressing cells fail to respond to insulin stimulation and show impaired glucose uptake from the cell culture supernatant. In addition, HBV transgenic mice reveal increased serum glucose levels compared to HBV-negative wild type mice (unpublished results by T. Heinrich).

2.2 Aims of the study

The fundamental mechanisms of HBV-associated liver pathogenesis still remain elusive. Liver pathologies in chronic HBV infection such as cirrhosis and HCC are mainly the result of immune-mediated liver damage which is not fully compensated by liver regeneration. For the control of liver regeneration, insulin-dependent signaling cascades as well as the cytoprotective and redox-sensitive transcription factor Nrf2 play a pivotal role. A deficiency in Nrf2 results in elevated levels of ROS that impair insulin receptor signaling and liver regeneration. HBV was observed to activate Nrf2 and expression of Nrf2-regulated genes. This argues

against an inhibitory effect of HBV on insulin receptor signaling due to elevated ROS levels. Nevertheless, chronic HBV infection is obviously associated with impaired liver regeneration and development of fatal liver diseases. Considering the relevance of Nrf2 for liver regeneration and insulin receptor signaling, this appears contradictory. Moreover, the previous results described above suggest that HBV interferes with insulin receptor expression and the insulin receptor signaling pathway, which mediates glucose uptake. Hence, this thesis aimed to investigate the influence of HBV on liver regeneration in depth with respect to insulin receptor signaling in order to obtain a better understanding of the underlying mechanisms of HBV-associated pathogenesis. Thereby, the scope of the present study can be divided into two sections:

(1) The ***in vitro*** **studies** should focus on the clarification of how HBV upregulates insulin receptor expression and interferes with insulin receptor signaling.

(2) The ***in vivo*** **studies** should focus on the influence of HBV on hepatocyte proliferation and liver regeneration in wild type and HBV transgenic mice after short- and long-term liver damage artificially induced by CCl_4 treatment.

3 Materials

3.1 Cells

3.1.1 Prokaryotic cells

Strain	Genotype	Source
E. coli TOP10	F-mcrA Δ(mrr-hsdRMS-mcrBC) φ80lacZΔM15 ΔlacX74 nupG recA1 araD139 Δ(ara-leu)7697 galE15 galK16 rpsL(Str^R) endA1 λ^-	Invitrogen, Karlsruhe

3.1.2 Mammalian cells

Strain	Description	Source
HuH7.5	Human hepatoma cell line derived from HuH7 cells	Blight et al., 2002
HepG2	Human hepatoma-derived cell line	Knowles et al., 1980
HepAD38	Human hepatoma cell line derived from HepG2 cell line containing a stably integrated 1.2-fold HBV genome (Serotype ayw, genotype D)	Ladner et al., 1997
HepG2.2.15	Human hepatoma cell line derived from HepG2 cell line containing a stably integrated 2.15-fold HBV genome (Serotype ayw, genotype D)	Sells et al., 1987
Primary mouse hepatocytes (PMHs)	Isolated from mouse liver by retrograde liver perfusion	--

3.2 Mice

All wild type and HBV transgenic mice used were on a C57Bl/6 background and originated from the central animal facility of the Paul-Ehrlich-Institut. Mice used for experiments were 5−8 months of age. The transgene in HBV transgenic mice consists of 1.3 copies of the complete HBV genome as described (Guidotti et al., 1995). Presence of the HBV transgene and HBV expression in HBV transgenic mice was kindly determined by Andrea Henkes by HBsAg ELISA (Siemens, Erlangen) from blood samples and PCR using sequence-specific primers (see 3.4). All animal experiments were performed in accordance with institutional policies and had been approved by the local veterinary authorities of Darmstadt, Germany.

3.3 Plasmids

Plasmid	Description	Source
pUC19(-)	Control vector, Ampicillin resistance	Invitrogen, Karlsruhe
peGFP-N1	Coding for *enhanced green fluorescent protein (eGFP)*, Kanamycin resistance	Clontech, Saint-Germain-en-Laye, FR
ptdnNrf2	Coding for a transdominant negative mutant of Nrf2	auf dem Keller. et al., 2006
pcaNrf2	Coding for a constitutively active mutant of Nrf2	auf dem Keller. et al., 2006
pmCherry-Txlna	Coding for α-taxilin N-terminally fused to mCherry	Dr. D. Ploen
pmCherry	Coding for mCherry	Dr. D. Ploen

3.4 Oligonucleotides

All oligonucleotides were synthesized by Biomers.net, Ulm.

Internal Number	Name	Sequence (5'->3')
42	GAPDH_fwd	*gacccttcattgacctcaac*
43	GAPDH_rev	*tggactgtggtcatgagtcc*
60	GCLC_fwd	*cccatggaggtgcaattaac*
61	GCLC_rev	*tgcgataaactccctcatcc*
405	HBV_3.5kb_fwd	*ctccaagctgtgccttggg*
406	HBV_3.5kb_rev	*cccacccaggtagctagag*
584a	Insulin receptor_fwd	*gtggtgatggagctgatgg*
585b	Insulin receptor_rev	*accatgcagtttctcgctg*
775	GLUT4_fwd	*cctacgtcttccttctatttg*
776	GLUT4_rev	*ctcatctggccctaaatactc*
811	GCK_fwd	*tggaccaagggcttcaaggc*
812	GCK_rev	*catgtagcaggcattgcagcc*
835	RPL27_fwd	*aaagctgtcatcgtgaagaac*
836	RPL27_rev	*gctgctactttgcgggggtag*

3.5 Molecular weight markers

3.5.1 DNA markers

Name	Manufacturer
GeneRuler™ 100 bp DNA Ladder	Fermentas, St. Leon-Rot
GeneRuler™ 1 kb DNA Ladder	Fermentas, St. Leon-Rot

3.5.2 Protein markers

Name	Manufacturer
PageRuler™ Prestained Protein Ladder	Fermentas, St. Leon-Rot
PageRuler™ Plus Prestained Protein Ladder	Fermentas, St. Leon-Rot

3.6 Antibodies

3.6.1 Primary antibodies

Antibody	Host species	Clonality	Dilution (WB / IF / IHC)	Manufacturer
anti-β-actin	mouse	monoclonal	1:10000 / -- / --	Sigma-Aldrich, Seelze
anti-IRβ (C-19)	rabbit	polyclonal	1:300 / 1:80 / --	Santa Cruz Biotech, US
anti-NQO1 (A-180)	mouse	monoclonal	1:300 / -- / --	Santa Cruz Biotech, US
anti-NQO1	rabbit	polyclonal	-- / -- / 1:80	Abnova, Heidelberg
anti-γ-GCSc (H-300)	rabbit	polyclonal	1:300 / -- / --	Santa Cruz Biotech, US
anti-LHBs (Ma18/07)	mouse	monoclonal	1:600 / -- / --	Dr. D. Glebe, Uni Gießen
anti-PDI	mouse	monoclonal	1:250 / -- / --	BD Biosciences, Heidelberg
anti-Na/K-ATPase (M7-PB-E9)	mouse	monoclonal	1:500 / -- / --	Life Technologies, Karlsuhe
anti-SHBs	goat	polyclonal	-- / -- / 1:100	Abcam, UK

Antibody	Host species	Clonality	Dilution (WB / IF / IHC)	Manufacturer
anti-phospho-IR*β* (Tyr 1162/1163)	rabbit	polyclonal	1:300 / -- / --	Santa Cruz Biotech, US
anti-IGF-RI	rabbit	polyclonal	1:300 / -- / --	Cell Signaling, US
anti-BrdU [IIB5]	mouse	monoclonal	-- / -- / 1:100	Abcam, UK
anti-GAPDH (FL-335)	rabbit	polyclonal	1:300 / -- / --	Santa Cruz Biotech, US
anti-smooth muscle actin (SMA)	mouse	monoclonal	-- / -- / 1:100	eBioscience, Frankfurt/Main

3.6.1 Secondary antibodies

Antibody	Host species	Clonality	Dilution (WB / IF / IHC)	Manufacturer
anti-mouse-HRP	donkey	polyclonal	1:2000 / -- / --	GE Healthcare, Freiburg
anti-rabbit-HRP	donkey	polyclonal	1:2000 / 1:80 / --	GE Healthcare, Freiburg
anti-mouse-Cy3	donkey	polyclonal	-- / -- / 1:400	Jackson ImmunoResearch, UK
anti-mouse IRDye® 680LT	donkey	polyclonal	1:5000 / -- / --	LI-COR, Bad Homburg
anti-rabbit IRDye® 680LT	donkey	polyclonal	1:5000 / -- / --	LI-COR, Bad Homburg

Antibody	Host species	Clonality	Dilution (WB / IF / IHC)	Manufacturer
anti-mouse IRDye® 800CW	donkey	polyclonal	1:5000 / -- / --	LI-COR, Bad Homburg
anti-rabbit IRDye® 800CW	donkey	polyclonal	1:5000 / -- / --	LI-COR, Bad Homburg

3.7 Enzymes

Enzyme	Manufacturer
Accutase	Merck Millipore, Schwalbach
Collagenase	Sigma-Aldrich, Seelze
DNase I	Promega, Mannheim
Revert Aid™ H Minus M-MuLV RT	Fermentas, St.-Leon Rot

3.8 Inhibitors

Inhibitor	Concentration / Dilution	Manufacturer
Aprotinin	10 µg/µL	AppliChem, Darmstadt
Leupeptin	25 µg/µL	AppliChem, Darmstadt
Pepstatin	2 µg/mL	AppliChem, Darmstadt
Phosphatase Inhibitor Cocktail II	1:1000	Sigma-Aldrich, Seelze
PMSF	1 mM	AppliChem, Darmstadt

3.9 Reagents for cell culture

Reagent	Manufacturer
DMEM (with 4,5 g/L glucose)	PAA, Linz, AT
FCS	PAA, Linz, AT
FITC-insulin	Sigma-Aldrich, Seelze
L-glutamine	PAA, Linz, AT
Hydrocortison	Sigma-Aldrich, Seelze
Insulin	Roche, Mannheim
PBS without Ca^{2+} and Mg^{2+}	PEI, Langen
Pencillin/Streptomycin	PAA, Linz, AT
Trypsin/EDTA	PAA, Linz, AT
Williams Medium E	PAA, Linz, AT

3.10 Chemicals

All chemicals were purchased from Carl-Roth (Karlsruhe) with the following exceptions.

Chemical	Manufacturer
Ampicillin	Sigma-Aldrich, Seelze
Bradford reagent	Sigma-Aldrich, Seelze
Bromodeoxyuridine (BrdU)	AppliChem, Darmstadt
Bromophenol blue	Sigma-Aldrich, Seelze
BSA fraction V	PAA, Linz, AT
CCl_4	Merck, Darmstadt
Collagen	Collaborative Biomedical Products, US

Chemical	Manufacturer
DAPI	Merck, Darmstadt
Direct 80, dye content 25 %	Sigma-Aldrich, Seelze
dNTP mix (10 mM)	Fermentas, St. Leon-Rot
EDTA	Serva, Heidelberg
EGTA	Serva, Heidelberg
Entellan	Merck, Darmstadt
Ethidiumbromide	AppliChem, Darmstadt
Fixable Viability Dye eFluor® 450	eBioscience, Frankfurt/Main
GenAgarose LE	Genaxxon, Biberach
Glycerol	Gerbu Biotechnik, Heidelberg
Iodixanol	Fresenius Kabi, Bad Homurg
Luminata Western HRP Substrate	Merck Millipore, Schwalbach
β-Mercaptoethanol	Sigma-Aldrich, Seelze
Mowiol	Sigma-Aldrich, Seelze
N-Acetylglucosamine	Sigma-Aldrich, Seelze
Olive oil	Aldi-Süd, Mülheim a. d. Ruhr
peqGold TriFast	PeqLab, Erlangen
Phenol Red	Sigma-Aldrich, Seelze
Picric Acid	Sigma-Aldrich, Seelze
Polyethyleneimine (PEI)	Polysciences, Eppelheim
Random hexamer primer 0,2 µg/µL	Fermentas, St. Leon-Rot
SuperSignal West Pico Chemiluminescent Substrate	Thermo Scientific, Karlsruhe
tBHQ	Sigma-Aldrich, Seelze
TEMED	Merck, Darmstadt

Chemical	Manufacturer
Triton X-100	Fluka, Deisenhofen
Tween 20	Genaxxon, Biberach
UDP-Galactose	Merck Millipore, Schwalbach
Xylene cyanol	Sigma-Aldrich, Seelze

3.11 Commercial buffers

Buffer	Manufacturer
10x Cell lysis buffer	Cell Signaling, US
10x DNaseI buffer (with $MgCl_2$)	Promega, Mannheim
5x M-MuLV Reverse transcriptase buffer	Fermentas, St. Leon-Rot

3.12 Buffers and solutions

Buffer	Composition
Anode buffer I	20 % (v/v) Ethanol 300 mM Tris base
Anode buffer II	20 % (v/v) Ethanol 25 mM Tris base
Borate buffer	0.1 M Boric acid ad pH 8,5

Buffer	Composition
Citrate buffer	10 mM Sodium citrate ad pH 6
Collagenase/$CaCl_2$ solution	160.8 mM NaCl 3.15 mM KCl 0.7 mM Na_2HPO_4 0.33 mM HEPES 0.3 mg/mL collagenase 5 mM $CaCl_2$ pH 7.5
DNA loading dye (6x)	10 mM Tris-HCl pH 7.6 0.03 % Bromophenol blue 0.03 % Xylene cyanol 60 % Glycerol 60 mM EDTA
EGTA solution	160.8 mM NaCl 3.15 mM KCl 0.7 mM Na_2HPO_4 0.33 mM HEPES 0.5 mM EGTA pH 7.5
FACS buffer	2 % (w/v) BSA 20 mM EDTA

Buffer	Composition
Homogenization buffer	0.25 M Sucrose 1 mM EDTA 10 mM HEPES-NaOH ad pH 7.4
Lysogeny broth medium (LB)	1 % Trypton (w/v) 0.5 % Yeast extract (w/v) 1 % Sodium chloride (w/v)
Mounting medium (Mowiol)	10 % Mowiol (w/v) 25 % Glycerol (w/v) 100 mM Tris-HCl pH 8.5
Phosphate buffered saline (PBS) (10x)	80.0 g NaCl 2.0 g KCl 14.4 g Na_2HPO_4 2.4 g KH_2PO_4 ad 1 L ddH_2O ad pH 7.4
Phosphate buffered saline (PBS) + Triton X-100 (PBST)	1x PBS pH 7.4 0.3 % (v/v) Triton X-100
PMH medium	Williams medium E (without glutamine) 100 nM hydrocortisone 10 % (v/v) FCS 2 mM glutamine 0.1 U/mL penicillin 100 µg/mL streptomycin

Buffer	Composition
Radioimmunoprecipitation assay buffer (RIPA)	50 mM Tris-HCl pH 7.2 150 mM NaCl 0.1 % SDS (w/v) 1 % Sodium desoxycholat (w/v) 1 % Triton X-100
SDS Running buffer (10x)	0.25 M Tris 2 M Glycin 1 % (w/v) SDS ad pH 8.3
SDS Sample buffer (4x)	4 % (w/v) SDS 125 mM Tris-HCl pH 6.8 10 % (v/v) Glycerol 10 % (v/v) β-Mercaptoethanol 0.02 % (w/v) Bromphenol blue
Separation gel buffer	1.5 M Tris-HCl 0.4 % (w/v) SDS ad pH 8.8
Stacking gel buffer	0.5 M Tris-HCl 0.4 % (w/v) SDS ad pH 6.7
TAE buffer (50x)	2 M Tris base 1 M NaAc 50 mM EDTA ad pH 8

Buffer	Composition
Tris buffered saline (TBS) + Tween 20 (TBST) (10x)	200 mM Tris-HCl pH 7.8 1.5 M Sodium chloride 0.5 % Tween 20

3.13 Kits

Kit	Manufacturer
DeadEnd™ Fluorometric TUNEL system	Promega, Mannheim
Maxima SYBR Green qPCR Kit	Fermentas, St. Leon-Rot
QIAGEN Plasmid Maxi Kit	Qiagen, Hilden
IR [pYpY1162/1163] Human ELISA Kit	Life Technologies, Karlsruhe
PathScan Total IRβ Sandwich ELISA Kit	Cell Signaling, US

3.14 Devices

3.14.1 Electrophoresis

Product	Manufacturer
Electrophoresis power supply EPS301	GE Healthcare, Freiburg
Horizontal electrophoresis system HE33	GE Healthcare, Freiburg
SE250 Series electrophoresis unit	GE Healthcare, Freiburg
Semidry blotting chambers TE77	GE Healthcare, Freiburg
Semidry blotting chambers TE77 PWD	GE Healthcare, Freiburg
Semiphor TE70 semi-dry transfer unit blotter	GE Healthcare, Freiburg
Standard power pack P25	Biometra, Göttingen

Product	Manufacturer
Triple Wide Mini vertical electrophoresis system, CE	VWR, Darmstadt

3.14.2 Microscopy

Product	Manufacturer
Confocal Laser Scanning Microscope 510	Zeiss, Jena
Leitz DM RBE Microscope	Leica, Wetzlar
Infinity 2 Microscope Camera	Lumenera, Canada
PL Fluotar Objective 10x / 0.3	Leica, Wetzlar
PL Fluotar Objective 20x / 0.5	Leica, Wetzlar
PL Fluotar Objective 40x / 0.7	Leica, Wetzlar
Axiovert 40 CFL	Zeiss, Jena
A-Plan Objective 10x / 0.25 Ph1	Zeiss, Jena
NeoFluar Objective 20x /	Zeiss, Jena
NeoFluar Objective 40x /	Zeiss, Jena
NeoFluar Objective 100x /	Zeiss, Jena

3.14.3 Flow cytometry

Cytometer	Manufacturer
BD Accuri C6 flow cytometer	BD Biosciences, Heidelberg
LSRII SORP flow cytometer	BD Biosciences, Heidelberg

3.14.4 Imaging

Imaging Device	Manufacturer
AGFA Curix60 Film Developer	AGFA, Köln
C-DiGit Chemiluminescence Western Blot Scanner	LI-COR, Bad Homburg
INTAS Imaging System	INTAS, Göttingen
Odyssey Infrared Imaging System	LI-COR, Bad Homburg

3.14.5 PCR cycler

Product	Manufacturer
LightCycler® 1.5 Instrument	Roche, Mannheim
LightCycler® 480 Instrument II	Roche, Mannheim

3.14.6 Centrifuges

Product	Manufacturer
Avanti J26 XPI	Beckman Coulter, Krefeld
Hereaus Fresco 17 centrifuge	Thermo Scientific, Karlsruhe
Microcentrifuge	Carl-Roth, Karlsruhe
Multifuge 1 S-R	Heraeus, Osterode
Optima™ L-80 XP Ultracentrifuge	Beckman Coulter, Krefeld
Optima™ L-70 Ultracentrifuge	Beckman Coulter, Krefeld
RC 5C Plus	Sorvall, Langenselbold
Varifuge RF	Heraeus, Osterode

3.14.7 Other devices

Device	Manufacturer
Dako Pen	Dako, Denmark
Glass homogenizer	B. Braun, Melsungen
Incubator Innova 44	New Brunswick Scientific, US
Milli-Q A10 Water purification system	Merck Millipore, Schwalbach
Neubauer Chamber	Carl Roth, Karlsruhe
Particle counter Z1	Beckman Coulter, Krefeld
pH-meter 766 Calimatic	Knick, Berlin
Photometer ultrospec 3000	GE Healthcare, Freiburg
Polymax 1020 shaker	Heidolph, Kelheim
Polymax 1040 shaker	Heidolph, Kelheim
PTFE pestle	B. Braun, Melsungen
RCT classic magnetic stirrer	IKA, Staufen
Reflotron® Plus System Clinical Chemistry Analyser	Roche, Mannheim
Rocking platform	Biometra, Göttingen
Satorius analytical balance	Satorius, Göttingen
Satorius balance LP 6000 200S	Satorius, Göttingen
Sonoplus HD 2200	Bandelin GmbH, Berlin
Sterile bench for cell culture	Heraeus, Osterode
SterilGard® III Advance	The Baker Company, US
Stuart roller mixer SRT9	Bibby Scientific, UK
Tecan Infinite M1000 plate reader	Tecan, CH
Thermoblock 1	Biometra, Göttingen
Thermomixer 5436	Eppendorf, Hamburg

Device	Manufacturer
Thermomixer compact	Eppendorf, Hamburg
Ultrospec 1100 pro	GE Healthcare, Freiburg
Water bath 1228-2F	VWR, Darmstadt

3.15 Consumables

Product	Manufacturer
1.5 mL tubes	Sarstedt, Nümbrecht
2 mL tubes	Sarstedt, Nümbrecht
6, 12, 24 and 96 well plates	Greiner Bio One, Frickenhausen
BD Microtrainer LH	BD Biosciences, USA
Cell counter cuvettes	VWR, Darmstadt
Cell culture dishes, TC dish 100 (100 x 20 mm)	Sarstedt, Nümbrecht
Cell scraper	TPP, CH
Centrifugation tubes (15 and 50 mL)	Greiner Bio One, Frickenhausen
Developer type E 1-3	C & L GmbH, Planegg
Fixer type F 1+2	C & L GmbH, Planegg
Hybond-P, PVDF membrane	Merck Millipore, Schwalbach
Hypercassette™	GE Healthcare, Freiburg
Hyperfilm ECL	GE Healthcare, Freiburg
IV Catheter	BD Biosciences, USA
LightCycler capillaries (polycarbonate)	Genaxxon, Biberach
Microscope cover slips	Carl-Roth, Karlsruhe

Product	Manufacturer
Microscope slides Standard	Carl-Roth, Karlsruhe
Microscope slides SuperFrost Plus	Carl-Roth, Karlsruhe
Nunc™ Cell culture dishes 60 mm	Thermo Scientific, Karlsruhe
Nylon Cell strainer 70 µm	BD Biosciences, USA
Omnifix®-F Syringes (1, 5, 10, 20 mL)	B. Braun, Melsungen
Phase lock gel heavy, 2 mL	5Prime, Hilden
Pipette tips	Sarstedt, Nümbrecht
Pipette tips with filters	4titude, Berlin
Reflotron® ALT (GPT) test strips	Roche, Mannheim
Reflotron® AST (GOT) test strips	Roche, Mannheim
RotiLabo® Syringe filters (0,22 / 0,45 µm)	Carl-Roth, Karlsruhe
Round Bottom FACS tubes	BD Biosciences, USA
Sterican® Disposable Canulas (20, 23, 26, 27G)	B. Braun, Melsungen
Surgical Disposable Scalpel	B. Braun, Melsungen
Tissue culture bottles T25, T75, T175	Greiner Bio One, Frickenhausen
Whatman paper	GE Healthcare, Freiburg

3.16 Software

Software	Manufacturer
BD Accuri 6 Software	BD Biosciences, Heidelberg
Citavi 4	Swiss Academic Software GmbH, CH
FlowJo 10	Tree Star Inc., US

Software	Manufacturer
GraphPad Prism 5.0	GraphPad, US
Image Studio Lite	LI-COR, Bad Homburg
ImageJ	Wayne Rasband, NIH, US
Infinity Capture 6.2	Lumenera, Canada
INTAS GDS	INTAS, Göttingen
Light Cycler Software 3.5	Roche, Mannheim
LSM Image Browser	Zeiss, Jena
MS Office	Microsoft, US
Photoshop CS6	Adobe, US
ZEN Lite 2012	Zeiss, Jena
Light Cycler Software 480 SW 1.5	Roche, Mannheim

4 Methods

4.1 Cell biology

4.1.1 Cultivation of *E. coli*

E. coli strain TOP10 cells were cultivated for 16 h in LB medium at 37 °C with constant shaking in Erlenmeyer flasks. Transformed bacteria were selected by addition of 100 µg/mL ampicillin or 30 µg/mL kanamycin to the medium. Frozen stocks were stored in 30 % (v/v) glycerol at -80 °C.

4.1.2 Mammalian cells

4.1.2.1 Cultivation

In this study, the human hepatoma-derived cell lines HepG2 and Huh7.5 as well as HBV-positive stable cell lines HepAD38 (Ladner et al., 1997) and HepG2.2.15 (Sells et al., 1987) were used. All cell lines were cultivated in a CO_2 incubator (5 % CO_2) at 37 °C and 95 % relative humidity. Cells were grown in DMEM (4.5 g/L glucose) containing 10 % FCS, 0.1 U/mL penicillin, 100 µg/mL streptomycin and 2 mM L-glutamine (DMEM complete). In addition, 25 µg/mL hydrocortisone was added to the cell culture medium of HepAD38 cells. Since insulin-dependent signaling pathways were investigated in this study, all cell culture media were prepared without addition of insulin. For passaging of adherent cells, cells were washed with PBS and detached from cell culture flasks by incubation with a trypsin/EDTA-solution for 5 min at 37 °C. Activity of trypsin was stopped by adding 8 mL DMEM complete. Cells were resuspended and seeded in fresh medium at different dilutions (1:3 – 1:10).

4.1.2.2 Transfection

For transfection of mammalian cells, the linear polyethylenimine (PEI) (1 mg/mL) was used (Ehrhardt et al., 2006) according to the manual of ExGene500 transfection agent (Fermentas). Briefly, 0.5–1 *µ*g plasmid DNA were resuspended in 200 *µ*L PBS, supplemented with 6 *µ*L (for HuH7.5 cells) or 24 *µ*L (for HepG2, HepAD38, HepG2.2.15) PEI/*µ*g plasmid DNA and mixed by vortexing for 15 sec. After 20 min incubation at room temperature, the reaction mixture was added dropwise to 2 mL medium in a six well plate. After 16 h, the medium was changed.

4.1.2.3 Stimulation

For stimulation with insulin, insulin was added to the cell culture medium to a final concentration of 100 nM and cells were incubated at 37 °C for different time periods as indicated in the results section. To activate the transcription factor Nrf2, cells were incubated for 8 h at 37 °C with a final concentration of 50 *µ*M *tert*-Butylhydrochinone (tBHQ) in the cell culture medium.

4.1.2.4 Cell harvest and lysis

To generate total cell lysates for Western Blot and ELISA analysis, cells were washed with PBS and lysed by adding 200–300 *µ*L of cell lysis buffer (see 3.11) supplemented with protease- and phosphatase-inhibitors (see 3.8). After 10 min incubation on ice, cells were scraped off the wells, transferred to reaction tubes and sonicated (10 sec, 15–20 % intensity). Lysates were centrifuged (5 min, 21.000 x *g*, 4 °C). The supernatant was subjected to protein quantification (see chapter 4.3.1).

4.2 Molecular biology

4.2.1 Transformation of chemically competent *E. coli*

For transformation of chemically competent ($CaCl_2$) TOP10 *E. coli*, 100 ng of plasmid DNA were added to 100 µL of competent cells. After incubation for 30 min on ice, cells were incubated at 42 °C for 2 min and then for 2 min on ice. 250 µL of LB medium were added to the suspension and bacteria were incubated with constant shaking at 600 rpm for 1 h at 37 °C. Subsequently, the suspension was added to an Erlenmeyer flask containing 300 mL LB medium with the appropriate antibiotic for resistance selection and incubated for 16 h at 37 °C with constant shaking.

4.2.2 Agarose gel electrophoresis

For separation of DNA and RNA molecules depending on size, agarose gel electrophoresis was used. Agarose was dissolved in 1x TAE buffer by heating, yielding a solution of 1 % (w/v). After cooling of the solution, 0.1 µg/mL ethidiumbromide was added and the warm liquid agarose was poured into a horizontal gel chamber complemented with a comb. Once the gel became solid, it was given into a gel chamber containing 1x TAE. The DNA samples were supplemented with 6x loading buffer, loaded into the pockets of the gel and were separated at 100 V. DNA bands were visualized by UV light (254/365 nm) using the INTAS-imaging system.

4.2.3 Isolation of plasmid DNA

Plasmid DNA was isolated using the *QIAGEN Plasmid Maxi* Kit according to the manufacturer's instructions. The principle relies on the lysis of the bacteria under alkaline conditions in the presence of SDS (Birnboim et al., 1979). Plasmid DNA was extracted from 300 mL bacterial culture. DNA was precipitated by the addition of isopropanol. The precipitate was washed and air-dried and subsequently dissolved in ddH_2O. Plasmid DNA was stored at -20 °C.

4.2.4 Determination of nucleic acid concentration

The concentration of nucleic acids was determined spectrophotometrically at a wavelength of 260 nm using Ultraspec 3000. At this wavelength, an absorption of 1.0 corresponds to a concentration of 50 mg/mL double-stranded DNA or 40 mg/mL RNA. At the same time, the absorbance of proteins at a wavelength of 280 nm was determined to assay the purity of DNA/RNA preparations. Pure samples should obtain an OD_{260}/OD_{280} ratio of 1.8−2.0. Lower values indicate contamination with protein or phenol.

4.2.5 Phenol/Chloroform extraction of RNA

Total RNA was extracted using peqGOLD TriFast according to the manufacturer's instructions. In brief, the cells were lysed with the TriFast reagent that includes phenol, in which RNA dissolves. After addition of chloroform and centrifugation, a phase separation occurred. The upper aqueous phase contained RNA that was precipitated by adding of isopropanol. The quality of the isolated RNA was controlled by agarose gel electrophoresis.

4.2.6 cDNA synthesis

Before cDNA synthesis, the isolated RNA was digested with DNase to degrade potential DNA contaminations. For this, 4−5 µg RNA was mixed with 1 µL DNaseI in a final volume of 10 µL and incubated for 1 h at 37 °C. DNase was inactivated by adding 1 µL 25 mM EDTA and incubation for 10 min at 65 °C. Afterwards, the RNA was reverse transcribed to cDNA using M-MuLV reverse transcriptase and random hexamer primer. For this, RNA was incubated with 1 µL random hexamer primer for 15 min at 65 °C. Afterwards, 2 µL dNTPs (10 mM), 4 µL 5x reverse transcriptase buffer, 1 µL DEPC-treated H_2O and 1 µL M-MulV reverse transcriptase was added and incubated for 10 min at RT and 1 h at 42 °C. Reverse transcriptase was inactivated by incubation for 5 min at 72 °C. The cDNA was used for qRT-PCR analysis at a 1:10 dilution.

4.2.7 Quantitative real time PCR (qRT-PCR)

The LightCycler 1.5 system and LightCycler 480 system served for the detection and quantification of specific transcripts using Maxima SYBR Green qPCR-Kit. The principle of the quantification is based on the intercalation of the DNA binding fluorescent dye SYBR Green to double-stranded DNA during the PCR reaction. The intensity of fluorescence increases proportionally to the amount of the amplified DNA. The fluorescence was measured after each cycle. The amount of specific transcripts was either determined using different standard dilutions of cDNA with known concentrations or was calculated as n-fold expression using the $2^{-\Delta\Delta Ct}$ method. The reaction mixture consisted of 5 µL 2x Maxima SYBR Green qPCR Master Mix, 0.25 µL of each primer (10 µM) and was filled up to 10 µL with

ultrapure ddH_2O. For normalization of the measured values, the house-keeping genes GAPDH or RPL27 were used. The qRT-PCR program is described in **Tab. 4.1**.

Tab. 4.1: qRT-PCR program

Program	Temperature (°C)	Hold time (sec)	Slope (°C/sec)	Cycles
Initial denaturation	95	600	20	1
Denaturation	95	15	20	
Annealing	56	30	20	45
Elongation	72	30	5	
	95	30	20	
Melting curve	60	30	20	1
	95	0	0.1	
Cooling	40	30	20	

4.3 Protein biochemistry

4.3.1 Protein quantification with Bradford reagent

In order to compare different samples, the protein amount in total cell lysates was quantified using the Bradford reagent (Bradford, 1976). The reagent includes the dye Coomassie Brilliant Blue G-250 whose shift in absorbance under acidic conditions is measured upon binding of proteins at 595 nm. For this, 5 µL of the cell lysates were mixed with 100 µL Bradford reagent and absorbance was measured with the Tecan reader (Infinite M1000).

4.3.2 Polyacrylamide gel electrophoresis

Sodium dodecyl sulfate polyacrylamide gel electrophoresis (SDS-PAGE) is a method to separate proteins depending on their molecular weight (Laemmli, 1970). The gel is composed of a stacking gel, in which the proteins get concentrated, followed by a separation gel, in which the SDS-denaturated proteins are separated. For the stacking gel a polymer density of 4 % was used, while the density of the separation gel was in the range of 8–10 %, depending on the expected molecular weight of the target protein. The composition of the gels is summarized in **Tab. 4.2**. Equal amounts of protein (75−100 µg) were denatured in 1x SDS-PAGE sample buffer by heating for 10 min at 95 °C and separated in a vertical chamber at 100–120 V.

Tab. 4.2: Composition of SDS polyacrylamide gels. The indicated volumes are sufficient for 10 mini gels with dimensions of 10 x 8.2 cm.

Stacking gel	**4 %**	**Separation gel**	**8 %**	**10 %**
Stacking gel buffer	15 mL	Separation gel buffer	20 mL	20 mL
Rotiphorese 40 (29:1)	6 mL	Rotiphorese 40 (29:1)	16 mL	20 mL
ddH_2O	45 mL	ddH_2O	44 mL	40
TEMED	60 μL	TEMED	80 μL	80 μL
APS	600 μL	APS	800 μL	800 μL

4.3.3 Western blot

After separation by SDS-PAGE, proteins were transferred onto a methanol pretreated PVDF membrane, using a semi-dry blotting chamber and a discontinuous buffer system (1.3 mA/cm² for 1 h) (Towbin et al., 1979) (**Fig. 4.1**). After transfer, the membrane was blocked using 10 % (w/v) skim milk powder in 1x TBST buffer or 1x Roti®-Block blocking solution for 1 h at room temperature followed by incubation with the primary antibody diluted in blocking solution for 2–3 h at room temperature. After three washing steps for 5 min each with 1x TBST buffer, the membrane was incubated with a horseradish peroxidase (HRP)- or IRDye-coupled (Li-Cor) secondary antibody for 1 h at room temperature. Unbound secondary antibody was removed by three washing steps for 10 min each with 1x TBST buffer, and protein bands were detected and exposed to a scientific imaging

film using a peroxidase substrate reagent (ECL) or the Li-Cor Odyssee detection system.

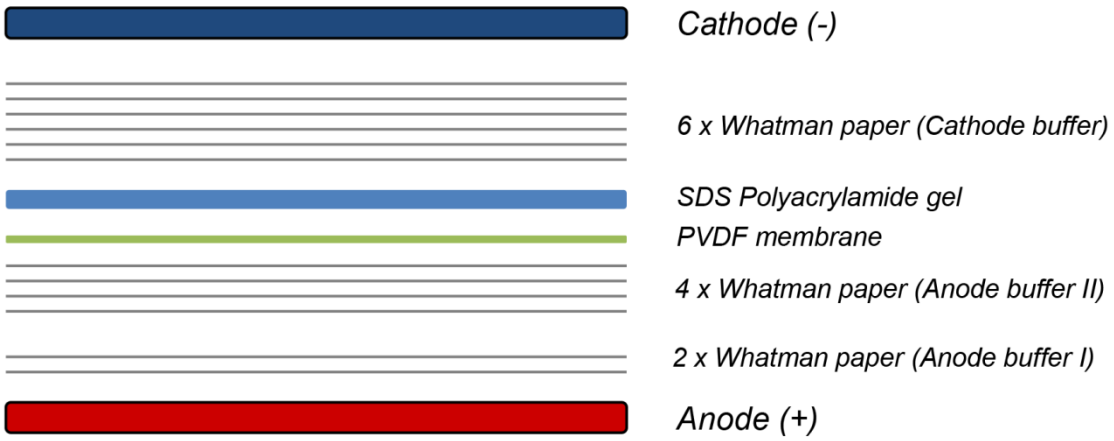

Fig. 4.1: Scheme of a semi-dry blotting stack. 4 Whatman papers soaked in anode buffer I were placed in a blotting chamber, followed by 2 Whatman papers soaked in anode buffer II. The methanol-pretreated PVDF membrane was placed on the Whatman paper stack and the gel was placed on it. 6 Whatman papers soaked in cathode buffer were placed on top.

4.3.4 Western blot with phospho-specific antibodies

Western Blot analysis with phospho-specific antibodies was performed as described in the previous section (see 4.3.3) with the following exceptions. The PVDF membrane after protein transfer was blocked with 5 % BSA or 1x Roti®-Block blocking solution in 1x PBS, supplemented with 0.3 % Triton X-100 (PBST). Antibodies were diluted in 5 % BSA or 1x Roti®-Block solution in 1x PBS, supplemented with 0.3 % Triton X-100 overnight at 4 °C. Washing steps were performed three times for 10–15 min each with PBS, supplemented with 0.3 % Triton X-100 after each antibody incubation period. As secondary antibodies exclusively HRP-coupled antibodies were used.

4.3.5 FITC-insulin binding assay

Cells were seeded in a 96-well microplate. 24 h after seeding, DAPI was added to the medium (5 μg/µL) and cells were incubated for 30 min in the dark at room temperature. Cells were washed two times with ice-cold PBS and then incubated with 4 µM of FITC-labeled insulin for 30 min in the dark at 4 °C. Cells were washed three times with ice-cold PBS and DAPI- (λ_{ex} = 358 nm, λ_{em} = 461 nm) and FITC- (λ_{ex} = 488 nm, λ_{em} = 518 nm) fluorescence was measured using a Tecan microplate reader. FITC fluorescence signal was normalized to the DAPI fluorescence signal.

4.3.6 Galactoysltransferase assay

To determine galactosyltransferase activity as an indicator for the presence of Golgi membrane fragments after subcellular fractionation, a pH-sensitive assay based on the absorbance shift of phenol red was employed (Deng et al., 2004). For this assay, 0.01 mM phenol red, 0.1 mM $MnCl_2$, 10 mM N-acetylglucosamine and 50 μL of each fraction to be analyzed were mixed with phosphate buffer. The total reaction volume was 100 μL in each well of a 96-well plate. The reaction was started by adding UDP-galactose to a final concentration of 2 mM, and the absorbance at 557 nm was recorded for each sample at 10s intervals for a total of 5 min. All measurements were carried out at 30 °C. While galactose is transferred by galactosyltransferase activity to N-acetylglucoseamine yielding N-acetyllactosamine, UDP and a proton are generated (**Fig. 4.2**). The pH will decrease as the reaction proceeds and phenol red changes from red to yellow, with a corresponding absorbance decrease which is measured at a wavelength of

557 nm. There is a quantitative linear relationship between proton concentration and absorbance. The slope of the regression line from the reaction of each fraction was calculated. The slope from the fraction with the highest decrease in absorbance was set as 1 and the slope from each fraction was divided by this slope to calculate the relative galactosyltransferase activity of each fraction.

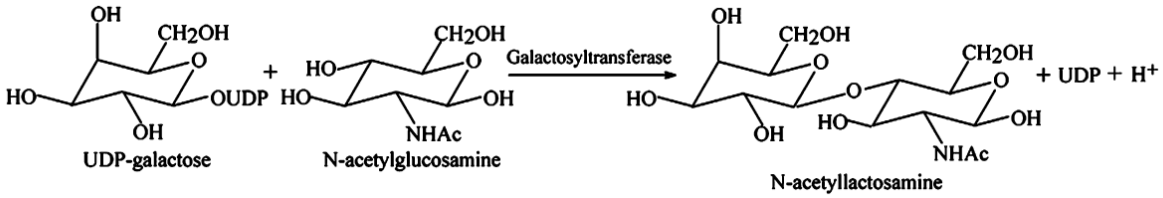

Fig. 4.2: Reaction catalyzed by galactosyltransferase (galT). Galactose from UDP-galactose is transferred to N-acetylglucoseamine catalyzed by galactosyltransferase, yielding N-acetyllactosamine. As by-products UDP and a proton (H^+) are generated (taken from Deng et al., 2004).

4.3.7 Subcellular fractionation

Cells were cultured to confluency on 10 cm dishes. The medium was removed and cells were washed once with PBS. To each plate, 1 mL of homogenization buffer (0.25 M sucrose, 1 mM EDTA, 10 mM HEPES-NaOH, pH 7.4), supplemented with a protease inhibitor mixture, was added and cells were scraped off. Cells were disrupted by 15–20 passages through a 26 gauge needle. Nuclei and unbroken cells were pelleted by centrifugation at 3000 x *g* for 10 min at 4 °C. The postnuclear supernatant was layered on top of a pre-formed 1–20 % iodixanol linear gradient and centrifuged in a Beckman SW41Ti rotor at 200.000 x *g* for 3 h at 4 °C. Linear iodixanol gradients were prepared from a discontinuous gradient (1,

3, 5, 10, 15 and 20 % iodixanol in 0.25 M sucrose, 60 mM HEPES-NaOH, p 7.4) by laying the tube 90° on the side for 1 h at room temperature. After centrifugation, fractions of 900 µL each were collected from top to bottom. Fractions were analyzed by SDS-PAGE and Western blot.

4.3.8 Isolation of plasma membrane fragments

Plasma membrane fragments were enriched according to *Procino et al.* (Procino et al., 2010). For this, cells were cultured to confluency on 10 cm dishes. The medium was removed and cells were washed once with PBS. To each plate, 1 mL of homogenization buffer (0.25 M sucrose, 1 mM EDTA, 10 mM HEPES-NaOH, pH 7.4), supplemented with a protease inhibitor mixture, was added and cells were scraped off. Cells were disrupted by 15–20 passages through a 26 gauge needle. The homogenate was spun at 4,000 x *g* for 15 min, and the pellet was discarded. The supernatant was spun at 17,000 x *g* for 30 min to obtain a pellet enriched with plasma membrane. The pellet was resuspended in PBS and subjected to Western blot analysis.

4.3.9 TUNEL staining

To detect apoptotic cells in paraffin-embedded and formalin-fixed liver sections, TUNEL staining was performed using the DeadEnd™ Fluorometric TUNEL System (Promega) according to manufacturer's instructions. The method is based on fluorescent labeling of free 3'-OH ends by the enzyme TdT of fragmented DNA originating during apoptosis. Fluorescence signals can be measured by confocal laser scanning microscopy (see 4.6.1).

4.3.10 Flow cytometry

For flow cytometry analysis, cells were detached from cell culture dishes by accutase treatment for 15 min at 37 °C. For the staining of the insulin receptor, cells were washed and resuspended in FACS buffer (see 3.12) and incubated with anti-IRβ (rabbit) for 30 min at room temperature. Cells were washed three times and then incubated with Alexa Fluor 488-conjugated anti-rabbit antibody for 30 min at room temperature in the dark. As control, cells were also incubated only with the secondary antibody without prior addition of anti-IRβ. Cells were fixed with 4 % formaldehyde in PBS for 10 min at room temperature, washed three times and were analyzed on a BD Accuri C6 flow cytometer. For FITC-insulin binding of mCherry and mCherry-α-taxilin-transfected cells 48 h post transfection, cells were detached by accutase treatment, resuspended in PBS and stained for 30 min at 4 °C in the dark with the fixable viability dye eFluor450 according to the manufacturer's instructions. After staining, cells were washed and incubated with 100 nM FITC-insulin for 30 min at 4 °C in the dark. Cells were fixed with 4 % formaldehyde in PBS for 10 min on ice and were analyzed on a LSRII SORP flow cytometer.

4.4 Immunological methods

4.4.1 Indirect immunofluorescence microscopy

Intracellular localization and distribution of proteins was analyzed by indirect immunofluorescence microscopy using fluorophore-conjugated antibodies for detection. Cells were seeded on cover slips in 12-well plates. Cells were fixed with 4 % formaldehyde in PBS for 20 min at room temperature and washed twice with PBS. Cells were permeabilized for 10 min with 0.5 % Triton X-100 in PBS and washed three times with PBS. Unspecific antibody binding was blocked by incubation for 1 h at room temperature with 1 % (w/v) BSA in PBS (blocking solution). The cells were incubated with the primary antibody for 1 h at room temperature in a humidified chamber. After three washing steps with PBS, cells were incubated with a fluorophore-conjugated secondary antibody for 1 h at room temperature in a humidified chamber. Primary and secondary antibodies were diluted in blocking solution. Nuclei were stained with DAPI. Cover slips were mounted on microscope slides and sealed with Mowiol.

4.4.2 Immunohistochemistry

Formalin-fixed and paraffin-embedded liver sections mounted on microscope slides were deparaffinized for 15 min in xylene and rehydrated for 10 min in 99 % ethanol, 10 min in 75 % ethanol and 5 min in ddH_2O. Afterwards, the slides were boiled in 10 mM citrate buffer (pH 6) for 2−3 min and incubated for 40 min until the buffer has cooled down. For BrdU immunohistochemistry, incubation with citrate buffer was omitted. Instead, DNA was denatured by incubation of the

sections with 1 M HCl for 10 min on ice, 10 min with 2 M HCl at room temperature and 20 min with 2 M HCl at 37 °C. HCl was neutralized for 10 min with 0.1 M borate buffer (pH 8.5) and slides were washed three times with for 5 min PBS or TBST. Liver sections were then incubated for with 10 % BSA in TBS buffer containing 0.1 % Tween 20 (blocking buffer) for 1 h at room temperature in a humidified chamber. Subsequently, primary antibody diluted in blocking buffer was added to the sections and slides were incubated again for 1 h at room temperature in a humidified chamber. Antibody solution was removed and slides were washed three times for 5 min in TBST. Secondary antibody diluted in blocking buffer was added to the sections and slides were incubated again for 45 min − 1 h at room temperature in a humidified chamber. Finally, antibody solution was discarded and slides were again washed for three times for 10 min each. Slides were sealed with coverslips using Mowiol as mounting medium. Slides were analyzed by fluorescent microscopy.

4.4.3 ELISA

The enzyme-linked immunosorbent assay (ELISA) is a solid-phase enzyme immunoassay that serves to detect specific proteins or antigens in liquid samples such as cellular lysates. The method used in this thesis is called the “sandwich” ELISA (**Fig. 4.3**). The antigen in the sample of interest is specifically captured *via* an antigen-specific antibody (capture antibody), immobilized on a 96-well polystyrene microtiter plate. A second antigen-specific antibody added to this complex then binds to a different epitope in the antigen of interest (detection antibody), trapping it in a “sandwich”-like fashion. Subsequently, a third antibody

that is added binds to the Fc portion of the detection antibody. This antibody is coupled to a horseradish peroxidase enzyme (HRP) which catalyzes the conversion of a chromogenic substrate into a detectable form. The absorbance of the converted substrate is then measured at a wavelength of 450 nm and is proportional to the amount of antigen present in the sample. In this thesis, cellular lysates from mouse liver were obtained as described (4.7.3) and subsequently used for ELISA analysis. All ELISAs were performed as recommended by the manufacturer and measured using a microplate reader (Tecan).

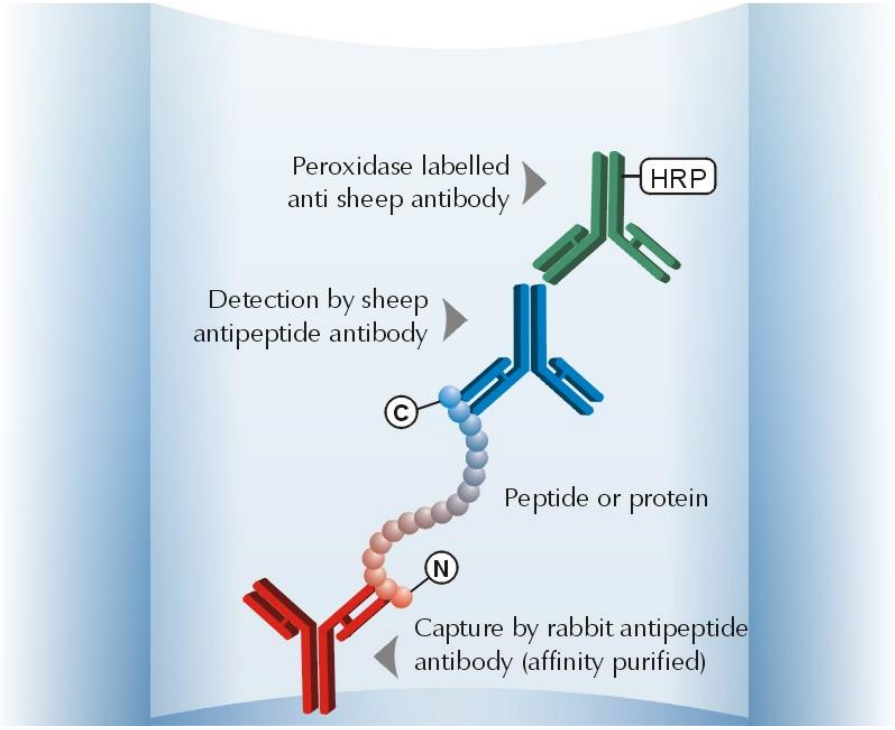

Fig. 4.3: Schematic representation of a "sandwich" ELISA. The capture antibody is immobilized on a polystyrene microtiter plate. The capture antibody binds to the target protein or peptide of interest present in a liquid sample. The detection antibody binds to the same antigen, but to a different epitope. The peroxidase-linked (HRP) antibody binds to the Fc portion of the detection antibody. HRP is able to catalyze the conversion of a chromogenic substrate into a detectable form that is measured at 450 nm (not shown) (taken from http://www.mimotopes.com).

4.5 Histological methods

4.5.1 Hematoxylin and eosin (HE) staining

Since its introduction more than a century ago, Hematoxylin and eosin (HE) staining is one of the oldest and most frequently used tissue staining method in histology (Böhmer, 1865; Schwarz, 1867; Fischer, 1875; Wissowzky, 1876). It involves the dye hematoxylin whose oxidized form hematin, in combination with a mordant (mostly metal ions), binds to cellular DNA and produces a permanent blue color of the nucleus in neutral to basic conditions. It is used in combination with the dye eosin which binds acidophilic structures such as intra- and extracellular proteins and colors them in different shades of red, pink and orange. In this study, HE staining of paraffin-embedded liver sections was kindly performed by Marion Wingerter from the animal pathology department at the Paul-Ehrlich-Institut.

4.5.2 Picro-sirius red staining

Sirius red F3B (CI 35780, Direct red 80) is a polyazo dye that is used in staining procedures for histological visualization of collagen type I and III fibers in tissue sections (Puchtler et al., 1973; Junqueira et al., 1979). The dye was dissolved in a saturated (1.3 %) aqueous solution of picric acid. For staining, a 1 % (w/v) Picro-sirius red solution was used. Formalin-fixed and paraffin-embedded liver sections were deparaffinized for 15 min in xylene and rehydrated for 10 min in 99 % ethanol, 10 min in 75 % ethanol and 5 min in ddH_2O. The slides were then incubated for 1 h at room temperature in the Picro-sirius red solution. After

staining, the slides were washed in two changes of 0.5 % (v/v) acetic acid and dehydrated in three changes of 100 % ethanol. Finally, slides were cleared in xylene and coverslips were mounted by Entellan mounting medium. Staining was visualized by brightfield microscopy and the amount of collagen was quantified using ImageJ. **Fig. 4.4** shows the chemical structure of the dye Direct red 80.

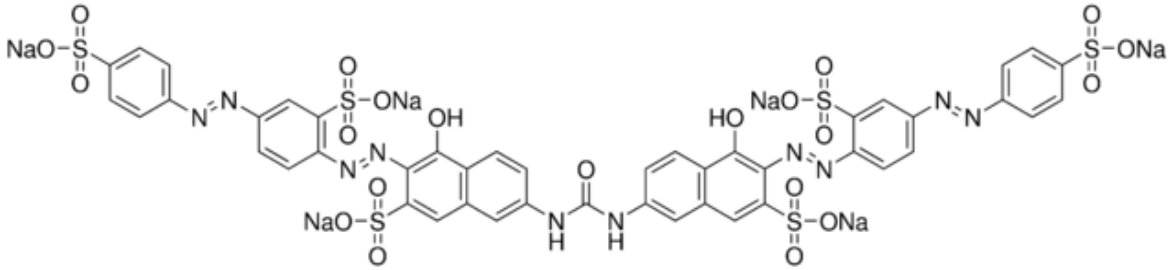

Fig. 4.4: Chemical structure of the polyazo dye Sirius red F3B (CI 35780, Direct red 80). The dye is used for the staining of collagen fibers in tissue sections.

4.6 Microscopy

4.6.1 Confocal laser scanning microscopy (CLSM)

Fluorescent-labeled cells (see 4.4.1 and 4.4.2) were analyzed by confocal laser scanning microscopy. This method allows the detecting of labeled proteins in a defined layer within the cell. The analysis was performed using the LSM 510 microscope and ZEN 2012 software. The 20x, 40x and 100x objectives were used.

4.6.2 Bright-field microscopy

For bright-field microscopy to visualize HE- or Picro-sirius red-stained liver tissue, sections a Leica DRBME microscope equipped with an Infinity 2 camera system from Lumenera was used. The used objectives were 10x and 20x.

4.7 Animal experimentation

4.7.1 CCl_4 and BrdU injections

Carbon tetrachloride (CCl_4) is an established hepatotoxin which is used to experimentally induce liver damage in mice and investigate liver regeneration (Iredale, 2007). Specific hepatotoxicity of CCl_4 is initiated by formation of the trichloromethyl free radical (CCl_3•) by the action of cytochrome P450 oxygenase system in the liver. The free CCl_3• radical subsequently reacts with a variety of biomolecules such as amino acids, proteins, nucleic acids and lipids. It triggers oxidative stress and peroxidation of membrane lipids and finally impairs crucial cellular processes leading to hepatocyte death (Weber et al., 2003). For short-term treatment, mice were treated intraperitoneally (i.p.) with a single dose (0.4 mg/g body weight) of a 2 % solution of CCl_4 in olive oil. At the respective days after the treatment (1, 2, 3, 5 and 7 days) mice were sacrificed and the liver was harvested. For long-term treatment, mice were treated i.p. with 7 doses of CCl_4 (0.25 mg/g body weight) over a time period of 52 days (one injection per week). Mice were sacrificed and the liver was harvested 3 days after the last injection. Livers from mice treated with olive oil only served as control. 120 min before sacrifice, mice

were i.p. injected with 200 mg 5-bromo-2'-deoxyuridine (BrdU) dissolved in ultrapure water (10 mg/mL).

4.7.2 Blood taking and liver excision

Mice were narcotized by CO_2 inhalation and euthanized by cervical dislocation. The belly fur was disinfected with 70 % EtOH. The fur and abdominal was then opened with sterile scissors. Whole blood was obtained by cardiac puncture with a sterile 23G cannula and transferred either into an EDTA-containing (50 μL, 0.5 M) reaction tube or a Microtainer tube (BD) with lithium-heparin additive for capillary blood collection. Serum was obtained by centrifugation of whole blood (2000 x *g*, 10 min, RT). Serum was either directly analyzed or shock-frozen using dry ice and stored at −80 °C. The liver was completely excised and separated into two parts by sterile scalpel. One part containing the gall bladder was fixed in 4 % formaldehyde in PBS. Fixed livers were stored at room temperature. The second part was shock-frozen on a thin layer of aluminum foil placed above pellets of dry ice and cut into smaller pieces (5 x 5 x 5 mm) for storage in reaction tubes at -80 °C.

4.7.3 Preparation of liver lysates

For Western blot or ELISA analysis, lysates were prepared from shock-frozen liver pieces. For this, 1−2 liver pieces were transferred to a *Potter-Elvehjem* glass homogenizer containing 400−500 μL of cell lysis buffer and were disrupted and homogenized by 15−20 strokes with a PTFE pestle on ice. Liver lysates were transferred to a reaction tube and sonicated (10 sec, 15–20 % intensity). Cell

debris was removed by centrifugation (21,000 x *g*, 5 min, 4 °C). The supernatant was subjected to protein quantification (see 4.3.1).

4.7.4 Determination of alanine transaminase (ALT) activity

Quantitative determination of alanine transaminase (ALT) activity in the serum of C57BL/6 wild type and HBV transgenic mice was determined using the Reflotron system and the respective Reflotron test strips. Samples were diluted 1:10−1:100 in PBS for analysis.

4.7.5 Isolation of primary mouse hepatocytes (PMHs).

Mice were narcotized by CO_2 inhalation and euthanized by cervical dislocation. The belly fur was disinfected with 70 % EtOH. The fur and abdominal was then opened with sterile scissors and organs were rinsed with PBS once. The organs below the liver (stomach, intestine, etc.) were carefully pushed aside with sterile gloves. The *inferior vena cava* was cannulated with an IV catheter. The cannula was removed, so only the catheter remained. The portal vein was cut. Using a sterile syringe, 20 mL of EGTA solution were injected into the liver through the *inferior vena cava*. The red color of the liver should slightly vanish. Using a new sterile syringe, altogether 40–50 mL of collagenase/$CaCl_2$ solution was injected into the liver through the *inferior vena cava* within 5–10 min. The liver should turn bright-yellowish and starts to soften. The gall bladder was removed and the liver excised. The liver was transferred to a small petri dish filled with PMH medium. Using sterile scissors, the liver was cut in small pieces. Subsequently, the backside of syringe plunger was used to mash the liver pieces. Suspension was

sieved by a 70 µm cell strainer into sterile 50 mL tube. Primary hepatocytes were washed by centrifugation for three times (2 min, 50 x *g*, 4 °C) with PMH medium and finally seeded no collagen-coated plates. After 4h, the medium was changed.

4.8 Statistical analyses

Results are described as mean ± SEM. * $P < 0.05$, ** $P < 0.01$. The significance of results was analyzed by ratio t test and two-tailed unpaired t-test using GraphPad Prism version 5.04 for Windows, GraphPad Software, San Diego California USA, www.graphpad.com.

5 Results

5.1 CCl_4 induces liver injury in wild type and HBV transgenic mice

HBV transgenic mice express the whole HBV genome specifically in the liver (Guidotti et al., 1995). However, due to immunotolerance, these mice do not exhibit pathological changes in liver morphology or develop signs of hepatitis (Inuzuka et al., 2014). To investigate the process of liver regeneration after liver injury in HBV transgenic mice, the liver therefore needs to be damaged artificially. There are several experimental approaches to induce liver injury and trigger liver regeneration in mice (see 1.3). In this thesis, liver injury was exclusively induced by the hepatotoxin CCl_4. At the different time points after initial injection, wild type (WT) and HBV transgenic mice were sacrificed, the abdominal wall was opened and macroscopic appearance and morphology of the liver were assessed before the liver was excised from the animal. CCl_4-treated mice present obvious changes in liver morphology, starting on day 1 after initial treatment compared to the liver of untreated mice (**Fig. 5.1 A**) and mock-treated mice (**Fig. 5.1 B**). These morphological changes are characterized by scattered patches of necrosis and inflammation, which are most prominent on day 2 and 3 after treatment. Also the color of the liver brightens from dark red-brown to light brown, especially on day 1 and 2. Beginning on day 5 after treatment, these changes start to recede until liver appearance has mostly been restored on day 7. Conclusively, at first glance, between WT and HBV transgenic there are no apparent macroscopic differences in liver morphology on the macroscopic level after CCl_4 treatment. However, liver injury is reliably and specifically induced by CCl_4.

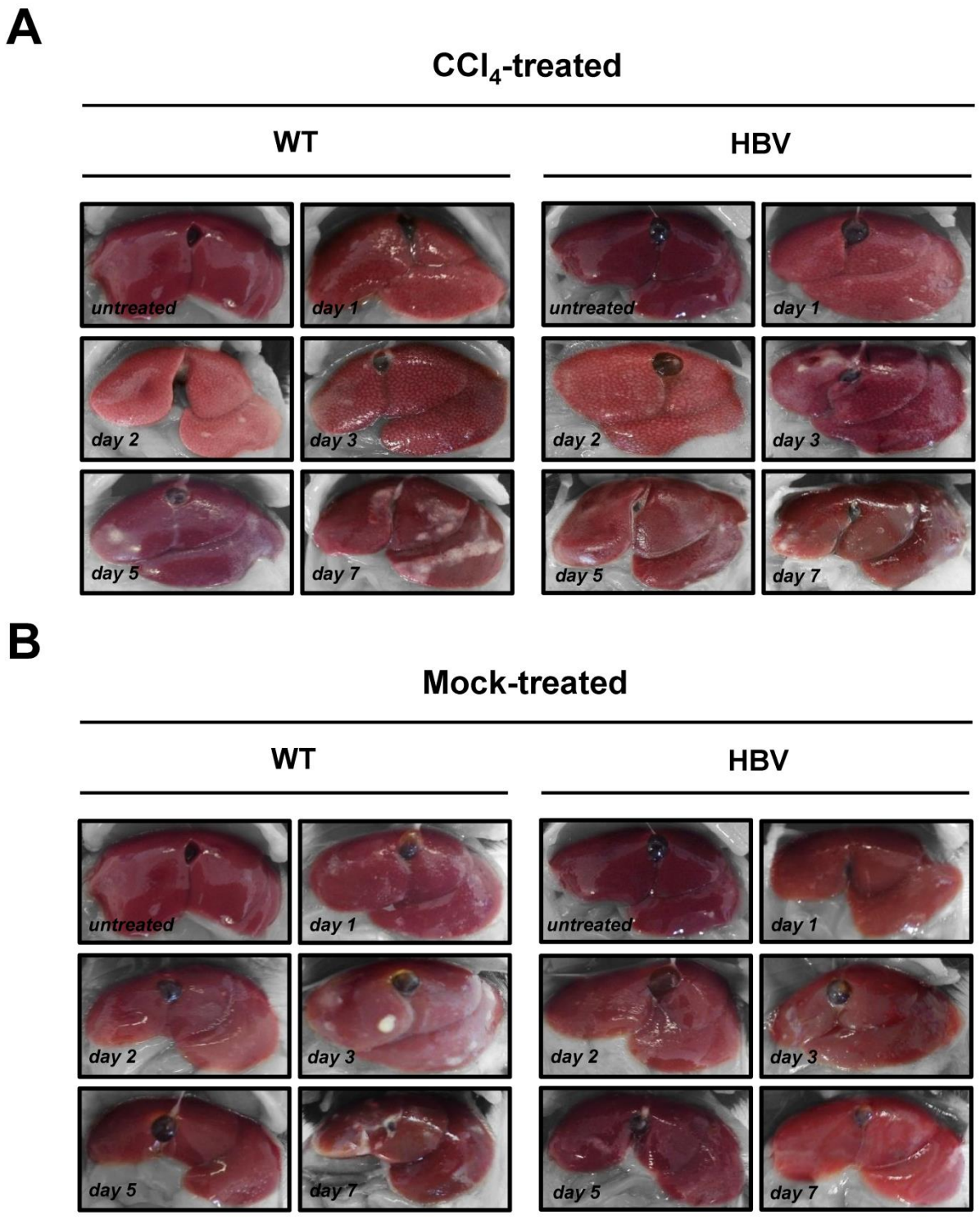

Fig. 5.1: CCl_4 induces liver injury in mice. Morphological structure of representative CCl_4- (**A**) and mock-treated (**B**) mice livers of male WT and HBV transgenic mice which were treated with a single dose of CCl_4 (0.4 mg/g body weight), only olive oil (mock) or were left untreated. At the indicated time points after initial treatment, mice were sacrificed and the liver was photographed.

Presence of alanine transaminase (ALT) in the blood is an established indicator of liver injury since ALT is highly expressed in hepatocytes (Pratt and Kaplan, 2000). Hence, ALT activity was determined in the serum of WT and HBV transgenic mice after CCl_4 treatment. Here, the serum of WT and HBV transgenic mice reveals highly increased ALT activity, especially on day 1 and 2 after initial treatment, compared to untreated mice (**Fig. 5.2**). ALT activity starts to decrease on day 3, until basal levels are finally reached on day 5 and 7. Interestingly, the serum of HBV transgenic mice shows slightly lower ALT activity on day 1, 2 and 3 compared to WT mice.

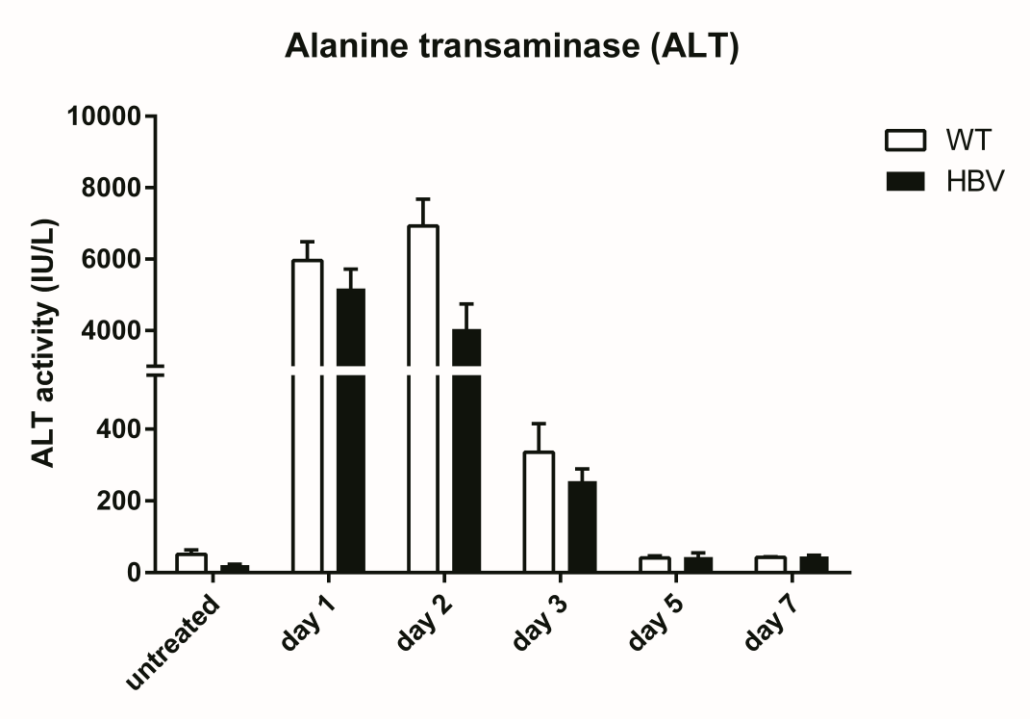

Fig. 5.2: Increased ALT activity after CCl_4-induced liver damage. ALT activity in the serum of CCl_4-treated WT and HBV transgenic mice. Male WT and HBV transgenic mice were treated with a single dose of CCl_4 (0.4 mg/g body weight) or left untreated. Mice were sacrificed at the indicated time points and blood was obtained by cardiac puncture. The graph represents the mean ± SEM from 4−6 animals for each day and each group after treatment and the mean ± SEM from 2 untreated animals each.

Collectively, these results indicate that short-term CCl_4 treatment induces severe liver injury in WT and HBV transgenic mice and represents a feasible tool to investigate liver regeneration in mice.

5.2 HBV transgenic mice reveal persistent liver damage after CCl_4-induced liver injury

Since on the macroscopic level no apparent differences after short-term CCl_4 treatment on liver morphology between WT and HBV transgenic are observed, liver damage was assessed histologically by hematoxylin and eosin (HE) staining of formalin-fixed and paraffin-embedded liver sections of the above described mice. After CCl_4 treatment, liver sections of WT and HBV transgenic mice show numerous necrotic areas, most prominently around the blood vessels where CCl_4 enters the tissue *via* the bloodstream and damages the surrounding hepatocytes (**Fig. 5.3**). These hepatic lesions are highly pronounced on day 1 and 2 after treatment in both, WT and HBV transgenic mice, but appear to be stronger in HBV transgenic mice. However, in WT mice hepatic lesions start to recede on day 3 after treatment, until the liver has ultimately regenerated on day 5 and 7. Remarkably, HBV transgenic mice in contrast reveal long-lived hepatic lesions up to day 5 after initial treatment with lesions larger and more pronounced in size on day 3 as compared to the WT. Taken together, these results indicate a prolonged and increased liver damage in HBV transgenic mice after CCl_4-induced liver injury compared to WT mice.

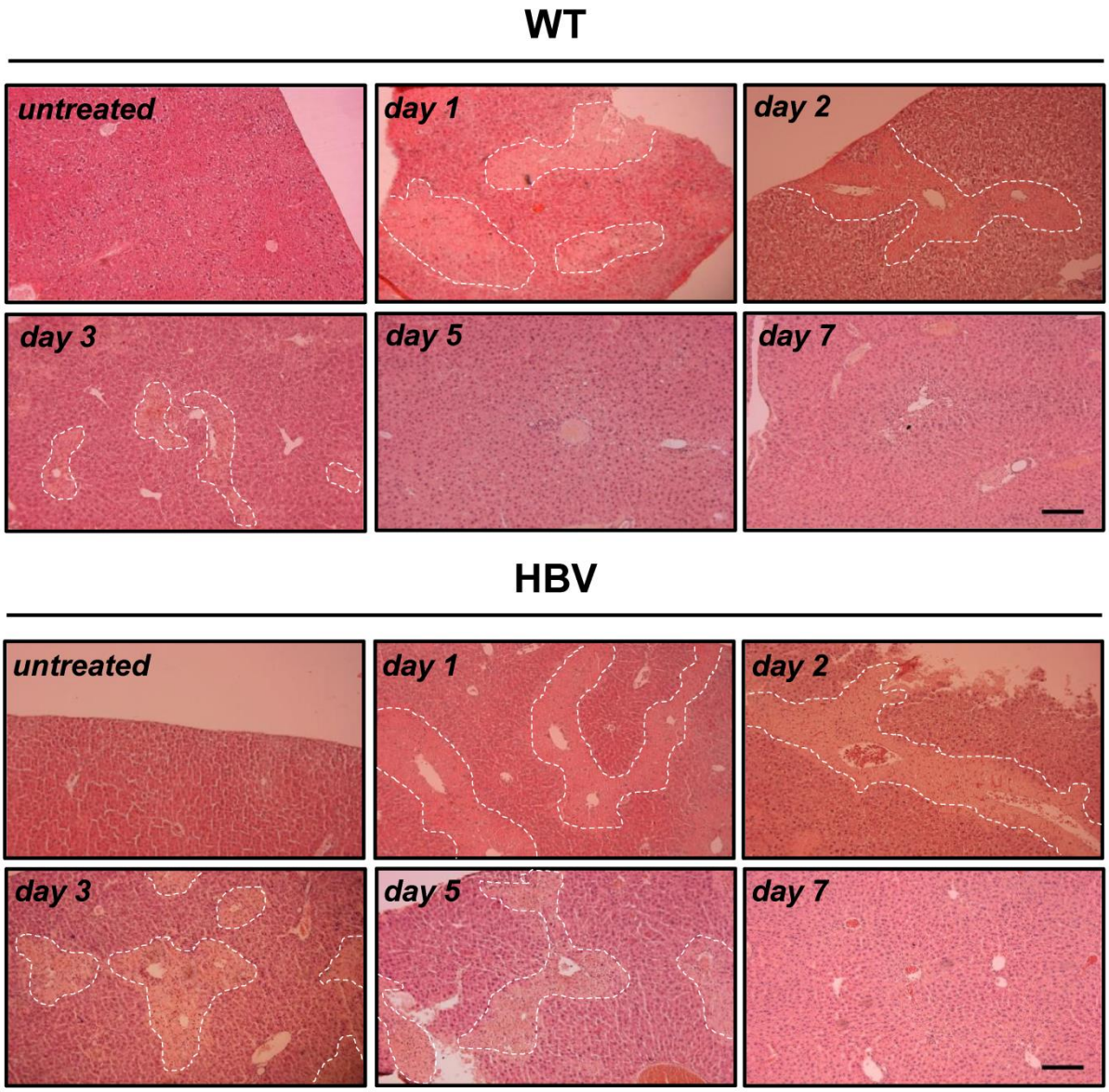

Fig. 5.3: Prolonged liver damage in HBV transgenic mice. HE staining of representative paraffin-embedded liver sections of male WT and HBV transgenic mice either untreated or at different time points after intraperitoneal injection of a single dose (0.4 mg/g body weight) of CCl_4. Hepatic lesions are outlined in white dashed lines. 5 animals per day were analyzed with comparable results (magnification 100x). Scale bar represents 500 μm.

5.3 Increased apoptosis in the liver of HBV transgenic mice after CCl_4-induced liver injury

As illustrated in **Fig. 5.3**, short-term CCl_4 treatment causes severe hepatocyte death. To determine the extent of apoptosis in the liver of WT and HBV transgenic mice after CCl_4 treatment, paraffin-embedded liver sections were stained for apoptotic cells employing the TUNEL method (*T*erminal deoxynucleotidyl transferase d*U*TP *n*ick *e*nd *l*abeling). With this method, fragmented DNA in the nucleus of apoptotic cells is fluorescently labeled and can be visualized by fluorescent microscopy. On day 1 after initial CCl_4 treatment, numerous TUNEL-positive nuclei can be detected in the liver of WT and HBV transgenic mice indicating hepatocyte death induced by the toxic effect of CCl_4. However, in the liver of HBV transgenic mice an elevated amount of TUNEL-positive cells is observable compared to the liver of WT mice (**Fig. 5.4**). This observation implies that in HBV transgenic mice immediately after liver injury apoptosis is increased and leads to more pronounced cell death.

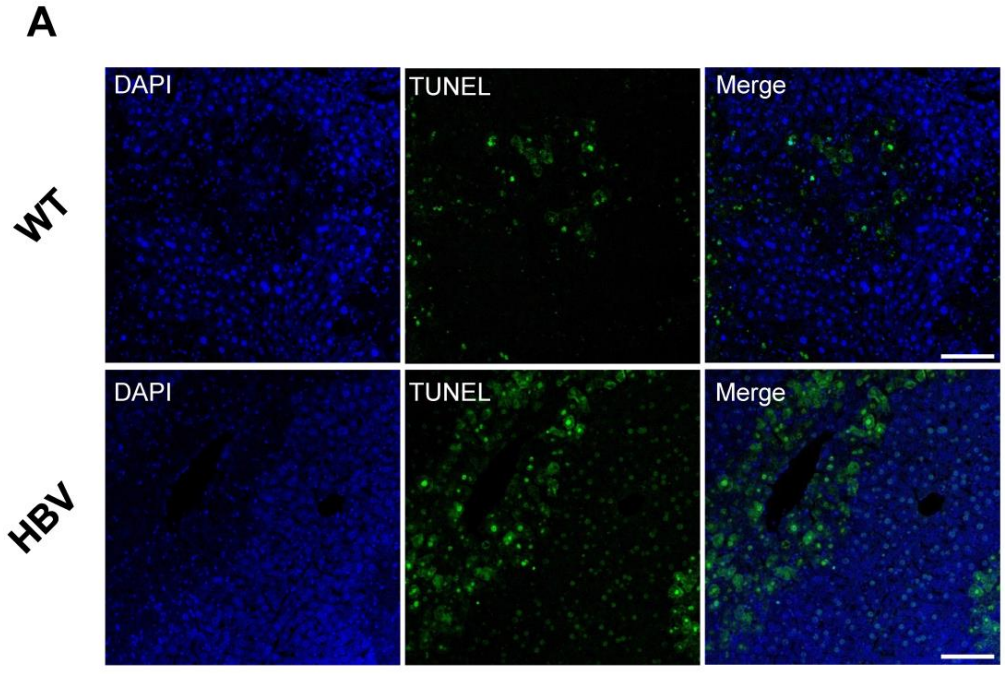

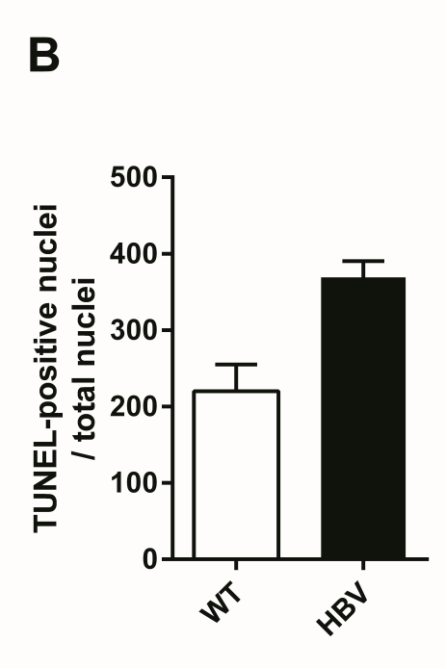

Fig. 5.4: Increased apoptosis in the liver of HBV transgenic mice. A, TUNEL staining of paraffin-embedded liver sections of WT and HBV transgenic mice 1 day after CCl_4 treatment (green fluorescence). Nuclei were visualized by DAPI (blue fluorescence) (magnification 200x). A representative image of one animal each is shown. Scale bar represents 100 μm. **B**, The graph represents the ratio of TUNEL-positive nuclei and total nuclei quantified from three different visual fields (mean ± SEM) from one animal each (n=1).

5.4 Hepatocyte proliferation is reduced in HBV transgenic mice after CCl_4-induced liver injury

A principal prerequisite for liver regeneration is the induction of hepatocyte cell proliferation after liver injury to compensate for the loss of functional hepatocytes. Hepatocytes in the adult liver are normally quiescent and are predominantly in the G_0 state of the cell cycle but retain their ability to reenter the cell cycle and proliferate during liver regeneration (Taub, 2004). As observed in **Fig. 5.3** and **5.4**, HBV transgenic mice exhibit increased and prolonged liver damage after CCl_4-induced liver injury compared to WT mice. It was therefore investigated whether hepatocyte proliferation and liver regeneration in HBV transgenic mice are inhibited and whether this inhibition could be causative for persistent liver damage in the context of HBV expression. One experimental approach to analyze and monitor cell proliferation is the detection of DNA-incorporated bromodeoxyuridine (BrdU) in the nucleus of the cells. For this purpose, BrdU was injected into the mice 2 h before sacrifice to permit BrdU incorporation into the DNA of hepatocytes. After the liver was obtained, liver sections of WT and HBV transgenic mice were then analyzed for BrdU-positive cells by immunohistochemistry using a BrdU-specific antibody and a Cy3-coupled secondary antibody. In the liver of untreated mice as well as in the liver of mice on day 1 after CCl_4 treatment, no BrdU-positive hepatocytes can be detected, whereas on day 2 after initial treatment proliferation initiates and BrdU-positive hepatocytes are readily detectable (**Fig. 5.5 A**). Remarkably, on day 2 after CCl_4 treatment, HBV transgenic mice exhibit decreased numbers of BrdU-positive hepatocytes compared to WT mice, indicating that hepatocyte proliferation is decreased in HBV

transgenic mice after liver damage (**Fig. 5.5 A**). This is in accordance with the observation that liver damage persists in HBV transgenic mice after liver injury (**Fig. 5.3**). After hepatocyte proliferation has reached its peak 2 days after treatment, only low numbers of BrdU-positive hepatocytes are detected on day 3 and differences between WT and HBV transgenic mice are not so pronounced as for day 2. For this reason, only the amount of BrdU-positive hepatocytes for day 2 was quantified and compared for WT and HBV transgenic mice. The quantification confirms the observations made by immunohistochemical staining of the liver sections, showing a significant decrease in BrdU-positive hepatocytes in HBV transgenic mice 2 days after liver injury (**Fig. 5.5 B**). Collectively, these results confirm that in HBV transgenic mice liver regeneration and hepatocyte proliferation are impaired as reflected by persistent liver damage after CCl_4-induced liver injury.

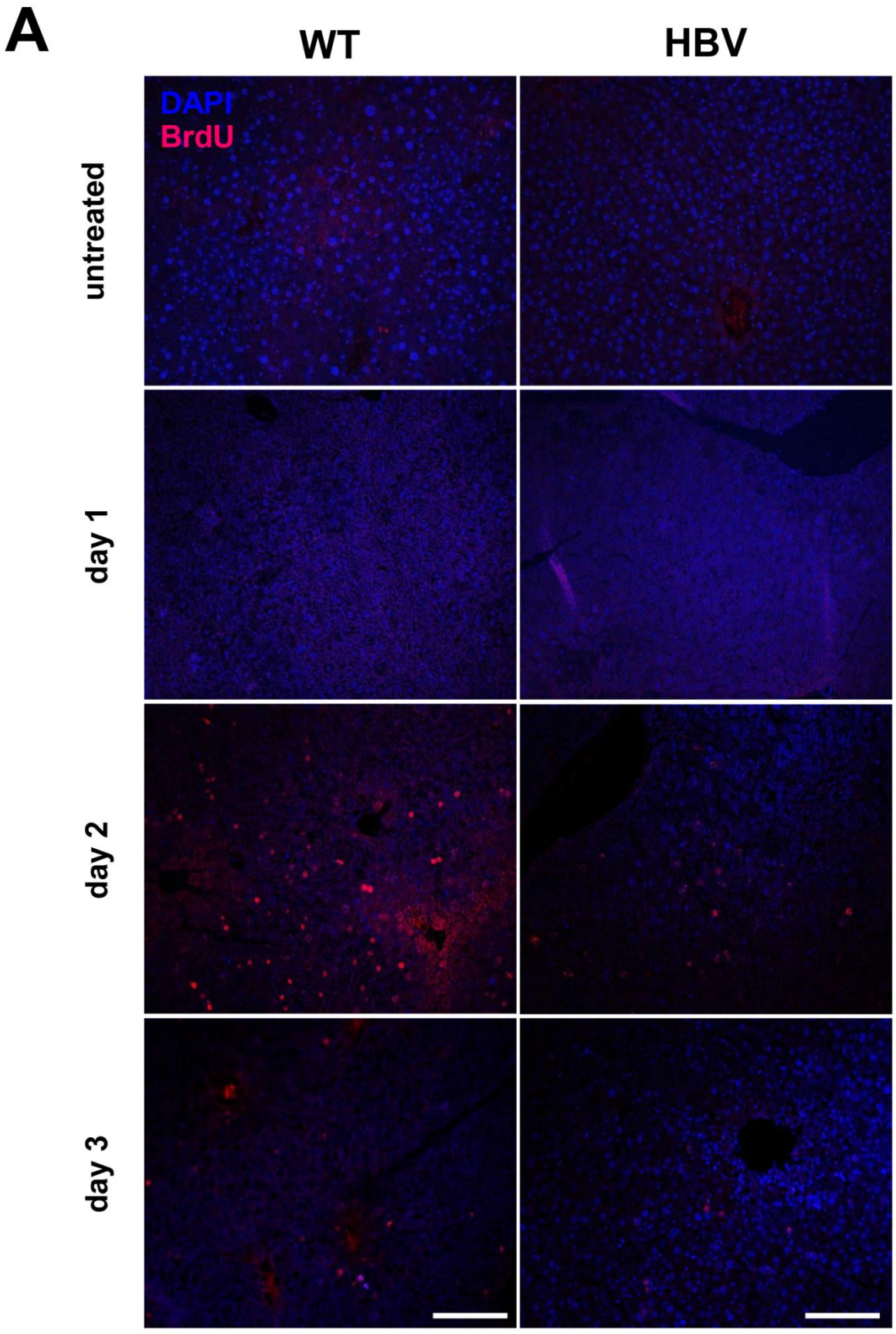
A
WT
HBV
DAPI
BrdU
untreated
day 1
day 2
day 3

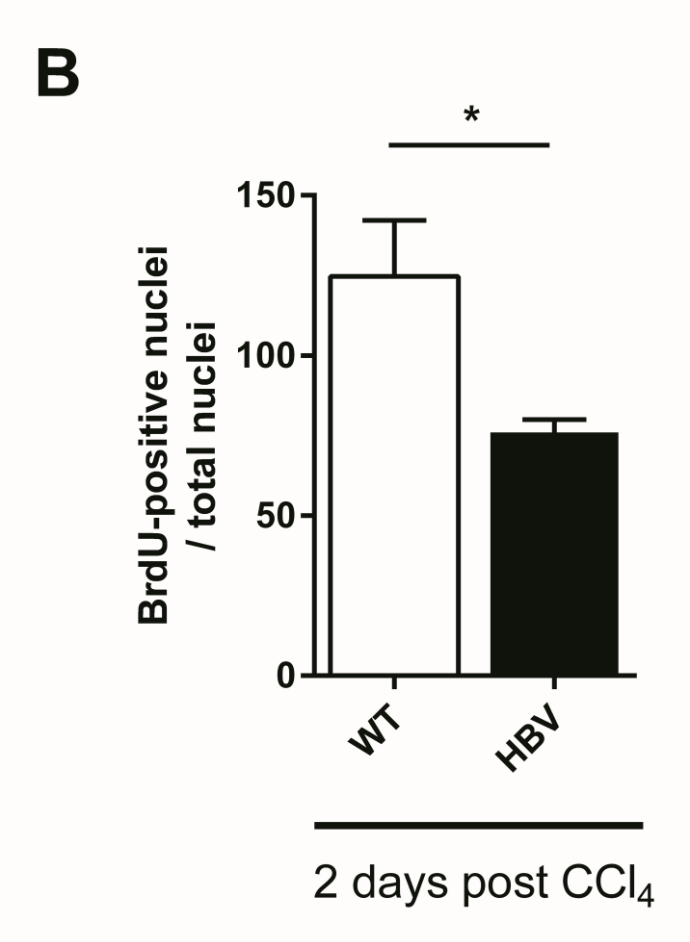

Fig. 5.5: Reduced hepatocyte proliferation in HBV transgenic mice. A, BrdU staining of paraffin-embedded liver sections derived from WT and HBV transgenic mice 2 days after CCl_4 treatment. Liver sections were deparaffinized and stained for BrdU using a mouse-derived primary antibody and a donkey-derived Cy-3 conjugated anti-mouse secondary antibody (red fluorescence). Nuclei were visualized by DAPI (blue fluorescence) (magnification 200x). A representative image of one animal per group and day is shown. Scale bar represent 50 μm. **B**, The graph represents the ratio of BrdU-positive nuclei and total nuclei per visual field in male WT and HBV transgenic mice 2 days after CCl_4 treatment (mean ± SEM, n = 3). Three visual fields have been analyzed per animal. * $p < 0.05$.

5.5 Insulin receptor activation is reduced in HBV transgenic mice after CCl_4-induced liver injury

The hitherto presented results reveal persistent liver damage after CCl_4-induced liver injury in HBV transgenic mice as a consequence of impairment of liver regeneration and hepatocyte proliferation. To uncover a possible mechanism for this observation, insulin receptor-dependent signaling moved into the focus of the present investigations since it is a key pathway involved in the control of liver regeneration and hepatocyte proliferation (Yamada et al., 1977; Beyer et al., 2008a; Beyer et al., 2008b; Böhm et al., 2010). Since liver regeneration and hepatocyte proliferation are impaired in HBV transgenic mice after liver injury, it was tempting to investigate whether inhibition of insulin receptor signaling could be causative for this observation. For this reason, the extent of insulin receptor (IR) activation reflected by tyrosine phosphorylation of the β-subunit (pY-IRβ) was determined 1 day after CCl_4 treatment in liver lysates derived from HBV transgenic and WT mice by phospho-IRβ-specific ELISA and was referred to the total amount of IRβ determined by IRβ-specific ELISA (**Fig. 5.6**). Strikingly, liver lysates from HBV transgenic mice reveal diminished phosphorylation of insulin receptor β (IRβ) 1 day after CCl_4 treatment as compared to liver lysates from WT mice. This result indicates that, after liver damage, in HBV transgenic mice insulin receptor activation is impaired and could contribute to diminished hepatocyte proliferation and deceleration of liver regeneration.

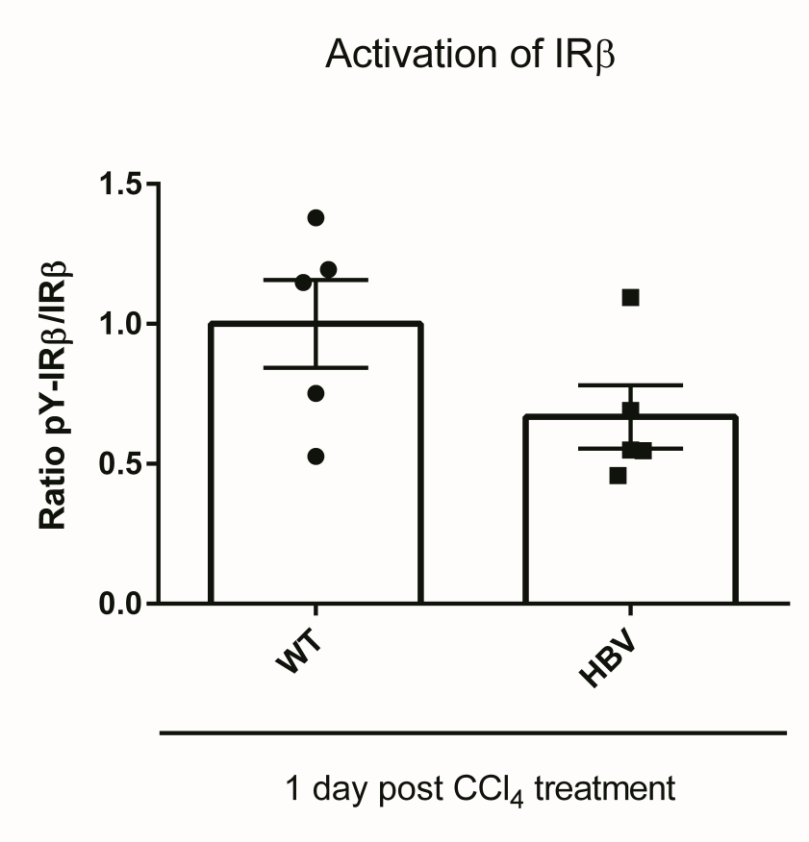

Fig. 5.6: Reduced insulin receptor activation in HBV transgenic mice after liver damage. Quantification of tyrosine-phosphorylated IRβ (pY-IRβ) by phospho-IRβ-specific ELISA in liver lysates from male WT (n = 5) and HBV transgenic mice (n = 5) 1 day after CCl_4 treatment. The graph represents the ratio of pY-IRβ and the total amount of IRβ as determined by IRβ-specific ELISA (mean ± SEM). The mean of the ratio of WT mice was set as 1. p = 0.1103.

5.6 HBV expression results in elevated amounts of insulin receptor mRNA

Since HBV transgenic mice after liver injury exhibit reduced insulin receptor activation, it was initially assumed that HBV-expressing hepatocytes of HBV transgenic mice might possess diminished amounts of the insulin receptor that could contribute to the reduced proliferative capacity in these cells. Strikingly, as already outlined in the thesis objectives, transiently and stably HBV-expressing cells as well as HBV-positive hepatocytes from HBV transgenic and chronic HBV patients possess elevated amounts of the insulin receptor (see 2.1). In light of impaired hepatocyte proliferation and reduced hepatic insulin receptor activation in HBV transgenic mice, this appears contradictory at first glance. However, the amount of the insulin receptor upon HBV expression so far has not been investigated on the transcriptional level. Hence, to clarify whether HBV expression also induces transcription of the insulin receptor gene, total RNA was isolated from stably HBV-expressing cells and corresponding HBV-negative control cells. After reverse transcription to cDNA, the amount of insulin receptor-specific transcripts was analyzed *via* quantitative real-time PCR (qRT-PCR) using sequence-specific primers (see 3.4). Expression of the HBV genome in the stable cell lines was confirmed by using specific primers against the 3.5 kb HBV transcript (see 3.4). In accordance with the elevated amount of insulin receptor on the protein level, qRT-PCR analysis reveals significantly increased amounts of insulin receptor mRNA in stably HBV-expressing cells compared to HBV-negative controls (**Fig. 5.7**). Taken together, these data indicate that upon HBV expression, transcription of the insulin receptor gene is induced and this results in increased amounts of the insulin receptor protein.

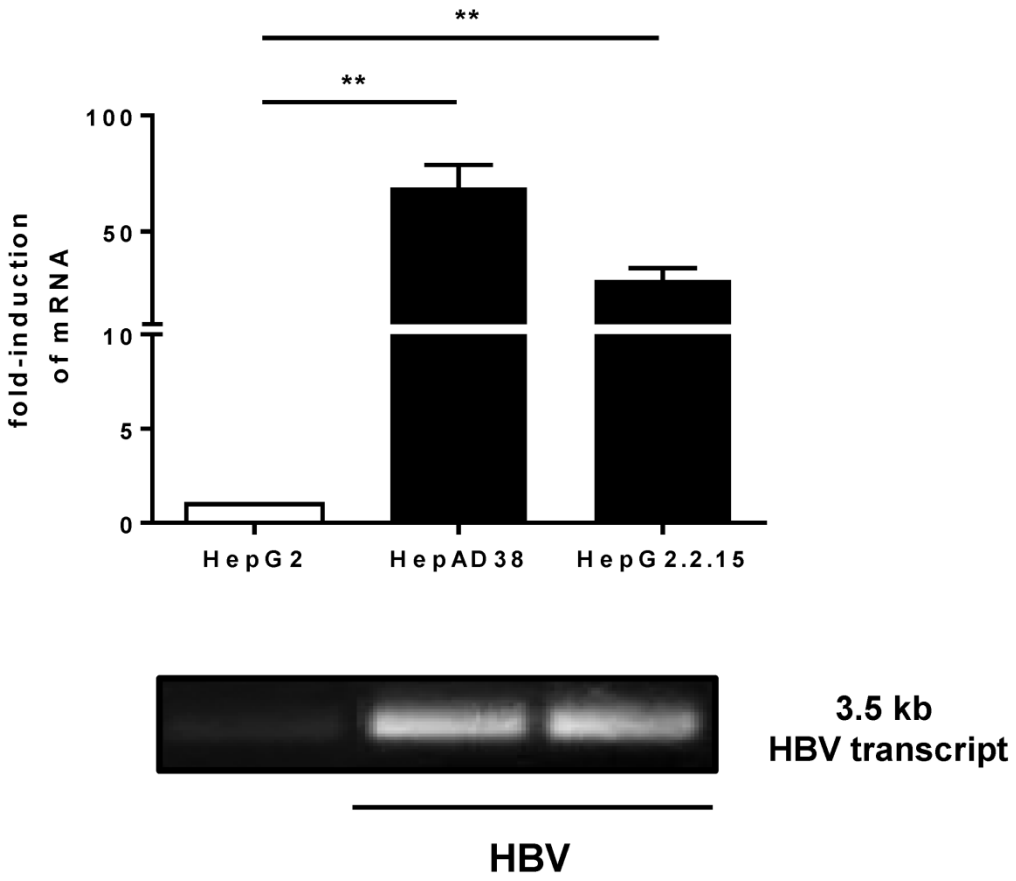

Fig. 5.7: Elevated amounts of insulin receptor-specific transcripts in stably HBV-expressing cells. qRT-PCR analysis of insulin receptor-specific transcripts in HBV-negative (HepG2) and stably HBV-expressing cells (HepAD38, HepG2.2.15). Values were referred to *GAPDH* as internal control. The values for HBV-negative HepG2 cells were set as 1. Results are shown as the fold induction of HBV-expressing cells relative to HBV-negative cells (mean ± SEM, n = 3). The band for the 3.5 kb HBV-specific transcript shown below the chart was detected using HBV-specific primers and was visualized by agarose gel electrophoresis and subsequent ethidium bromide staining. ** $p > 0.01$.

5.7 Activation of Nrf2 induces expression of the insulin receptor

HBV is known to induce activation of transcription factor Nrf2 and increased expression of Nrf2/ARE-regulated genes (Schädler et al., 2010). A classical Nrf2-regulated gene is NAD(P)H quinone oxidoreductase 1 (*NQO1)*. So far, increased expression of Nrf2-regulated genes has not been confirmed in the liver of HBV transgenic mice. Paraffin-embedded liver sections from HBV transgenic mice and WT mice were analyzed by immunohistochemical staining for NQO1. Confirming the data on HBV-dependent activation of Nrf2, HBV-expressing hepatocytes of HBV transgenic mice indeed reveal increased amounts of NQO1 compared to WT mice (**Fig. 5.8**).

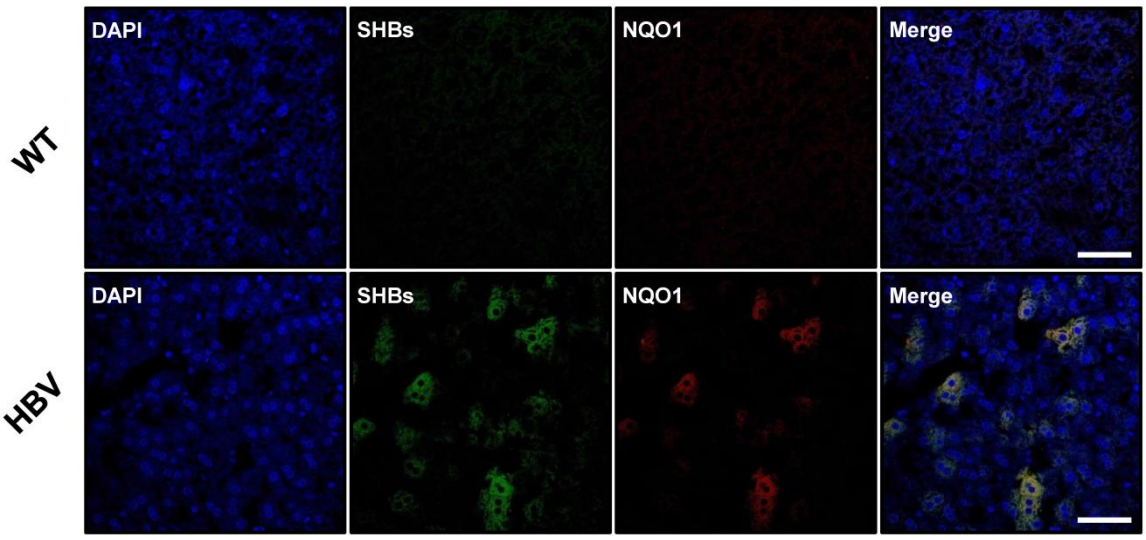

Fig. 5.8: Increased amounts of NQO1 in HBV-expressing hepatocytes from HBV transgenic mice. Paraffin-embedded liver sections from WT and HBV transgenic mice were stained for NQO1 using a rabbit-derived antibody and a donkey-derived Cy3-coupled anti-rabbit secondary antibody (red fluorescence). HBV-expressing cells were visualized using a goat-derived SHBs-specific antiserum and a donkey-derived Alexa488-coupled anti-goat secondary antibody (green fluorescence). Nuclei were visualized by DAPI (blue fluorescence) (magnification 400x). A representative image of one animal each is shown. Scale bar represents 50 μm.

Nrf2-dependent activation of gene transcription requires the presence of an antioxidant response element (ARE), located in the promoter region of Nrf2-regulated genes which binds Nrf2 (Wasserman et al., 1997). The typical ARE comprises the consensus sequence *TGACnnnGC*. The human insulin receptor promoter was analyzed for putative ARE sites to analyze whether the presence of potential ARE sites in the promoter could be causative for increased insulin receptor expression in HBV-expressing cells. Indeed, two ARE sites can be identified in the insulin receptor promoter (**Fig. 5.9**).

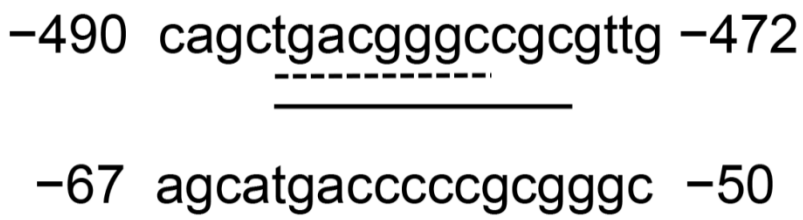

Fig. 5.9: Two putative antioxidant response elements (ARE) in the human insulin receptor promoter. Two segments of the sequence of the human insulin receptor promoter are shown. The numbers refer to the upstream position of the element within the promoter. The putative ARE sequences in the promoter region of the insulin receptor gene are underlined. The dashed line indicates an alternative ARE sequence.

After these sequences had been identified in the human insulin receptor promoter, it was necessary to check whether they were functional. For this purpose, activation of Nrf2 was induced by treatment of human hepatoma cells (HuH7.5) with *tert*-Butylhydrochinone (tBHQ). tBHQ is a widely used activator of Nrf2. Total RNA was isolated and reverse transcribed to cDNA. The amount of insulin receptor-specific transcripts (*IR*) was quantified by qRT-PCR. As a control for activation of Nrf2 and induction of Nrf2-dependent gene expression, the amount of specific transcripts of the catalytic subunit of the glutamate-cysteine ligase (*GCLC*) – an established Nrf2 target gene – was quantified in parallel. Upon activation of Nrf2 by tBHQ, *IR* mRNA expression as well as expression of *GCLC* mRNA is increased compared to untreated cells (**Fig. 5.10 A**). In addition, transfection with a constitutively active mutant of Nrf2 also induces insulin receptor expression (**Fig. 5.10 B**). *Vice versa*, when cells are transfected with a transdominant negative mutant of Nrf2 (tdnNrf2) to abrogate Nrf2 activity, mRNA expression of the *IR* and *GCLC* is prevented upon tBHQ stimulation compared to the control-transfected cells (**Fig. 5.10 A**). Taken together, these analyses corroborate the functionality of the ARE sites in the insulin receptor promoter and that activation of Nrf2 by HBV contributes to the induction of gene transcription of the insulin receptor.

A

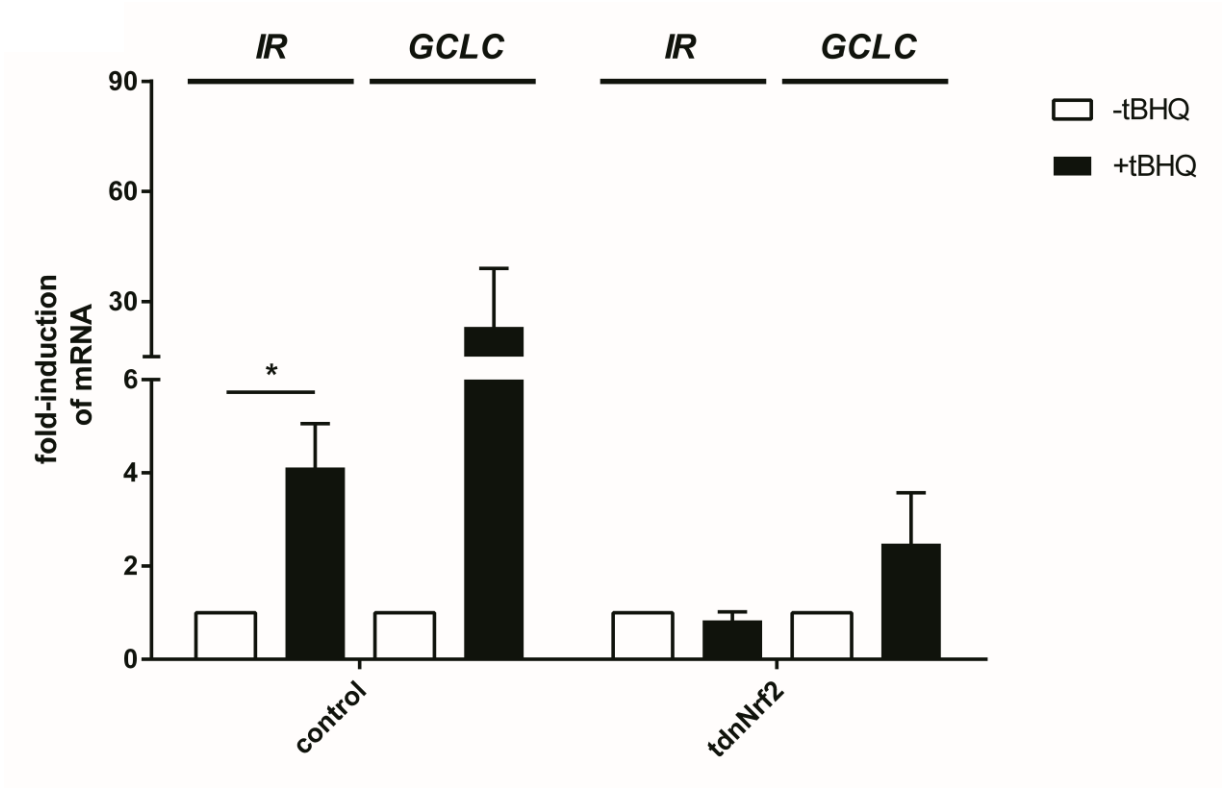
IR
GCLC
IR
GCLC
-tBHQ
+tBHQ
fold-induction of mRNA
90
60
30
6
4
2
0
*
control
tdnNrf2

B

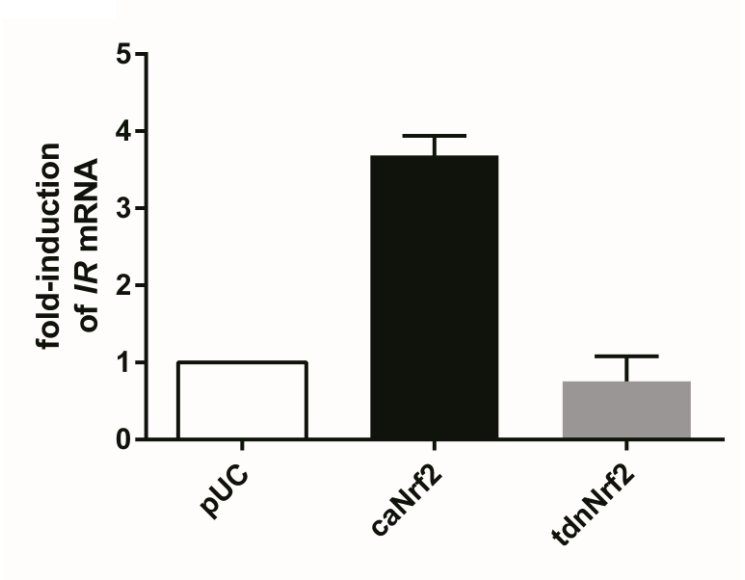
fold-induction of IR mRNA
5
4
3
2
1
0
pUC
caNrf2
tdnNrf2

◄ **Fig. 5.10: Activation of Nrf2 induces increased amounts of insulin receptor mRNA. A,** qRT-PCR analysis of *IR*- and *GCLC*-specific transcripts in HuH7.5 cells transfected with gfp (as control) or a transdominant negative Nrf2 mutant (tdnNrf2) stimulated with tBHQ or left untreated (mean ± SEM, n = 3). Unstimulated cells served as control and were set as 1. Values were referred to *GAPDH* as internal control. * $p < 0.05$. **B**, qRT-PCR analysis of *IR*-specific transcripts in HuH7.5 cells transfected with a pUC plasmid (as control), a constitutively active Nrf2 mutant (caNrf2) or a transdominant negative Nrf2 mutant (tdnNrf2) (mean ± SEM, n = 2). Control transfected cells served as control and were set as 1. Values were referred to *GAPDH* as internal control.

To further confirm that Nrf2-dependent induction of the insulin receptor gene also leads to increased protein amounts of the insulin receptor, Western blot analysis of HuH7.5 cells stimulated with tBHQ was performed. After stimulation with tBHQ, increased amounts of the insulin receptor are detected compared to unstimulated cells. In addition, increased protein amounts of the established Nrf2-induced target proteins γ-glutamylcysteine synthetase catalytic subunit (γ-GCSc) and NQO1 confirm the activation of Nrf2 upon tBHQ stimulation (**Fig. 5.11 A**). *Vice versa*, when Nrf2 activity is inhibited by transfection of the cells with the transdominant negative mutant of Nrf2 (tdnNrf2), protein amounts of the insulin receptor as well as γ-GCSc and NQO1 remain unaffected after stimulation with tBHQ (**Fig. 5.11 A**). These results confirm the observations made on the transcriptional level. In accordance with this, transfection of HBV-expressing HepG2.2.15 cells with tdnNrf2 diminishes insulin receptor expression compared to control-transfected cells (**Fig. 5.11 B**). Taken together, these results demonstrate that elevated expression of the insulin receptor in HBV-expressing cells depends on the activation of Nrf2.

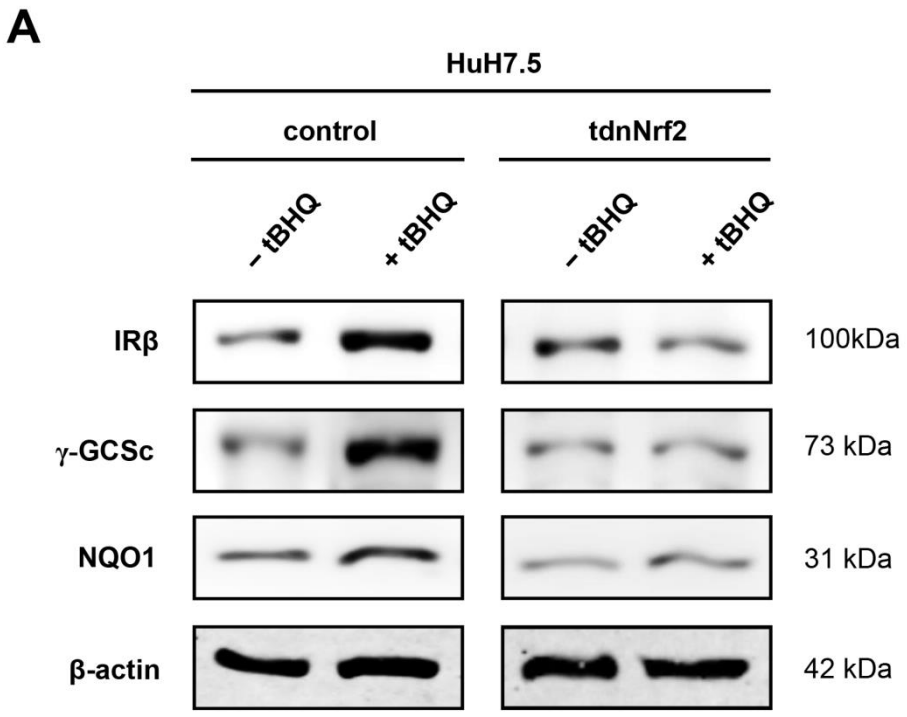
A
HuH7.5
control
tdnNrf2
– tBHQ
+ tBHQ
– tBHQ
+ tBHQ
IRβ
γ-GCSc
NQO1
β-actin
100kDa
73 kDa
31 kDa
42 kDa

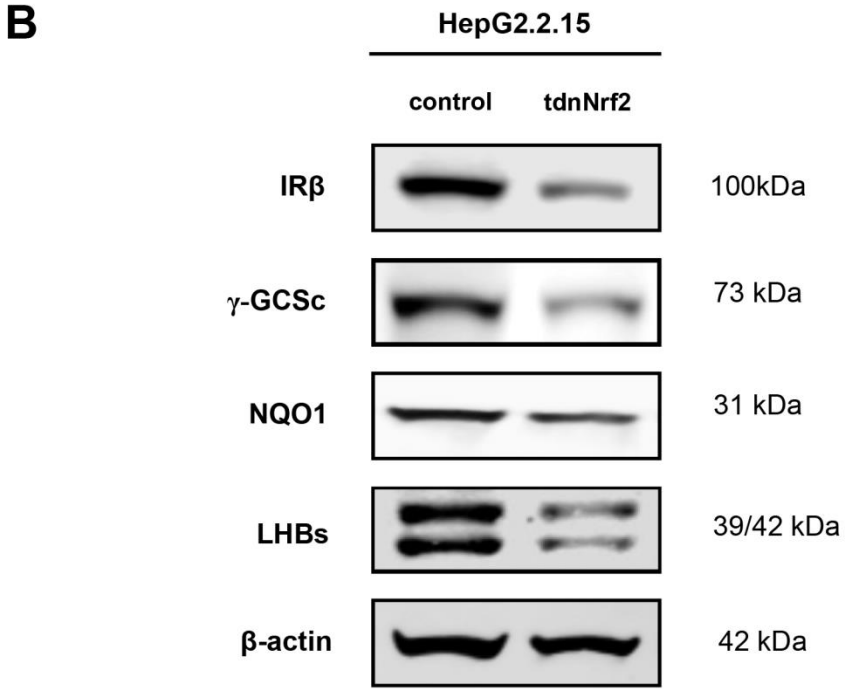
B
HepG2.2.15
control
tdnNrf2
IRβ
γ-GCSc
NQO1
LHBs
β-actin
100kDa
73 kDa
31 kDa
39/42 kDa
42 kDa

◄ **Fig. 5.11: Activation of Nrf2 leads to increased protein amounts of the insulin receptor. A,** Western blot analysis of cellular lysates derived from HuH7.5 cells transfected with gfp (control) or a transdominant negative mutant of Nrf2 (tdnNrf2) stimulated with tBHQ or left untreated. IRβ, γ-GCSc and NQO1 were detected using specific antisera. Detection of β-actin served as a loading control. **B**, Western blot analysis of cellular lysates derived from HBV-expressing HepG2.2.15 cells transfected with gfp (control) or a transdominant negative mutant of Nrf2 (tdnNrf2). IRβ, γ-GCSc, NQO1 and LHBs were detected using specific antisera. Detection of β-actin served as a loading control.

5.8 HBV-expressing hepatocytes bind less insulin *in vitro* and *in vivo*

After liver damage, HBV transgenic mice display impaired liver regeneration and hepatocyte cell proliferation in correlation with reduced activation of the insulin receptor. Since activation of the insulin receptor is initiated by insulin binding, these results imply that in the liver of HBV transgenic mice insulin binding may be diminished leading to attenuation of insulin receptor activation despite the increased amounts of the insulin receptor in HBV-expressing hepatocytes. To confirm this hypothesis, primary mouse hepatocytes were isolated from WT and HBV transgenic mice by liver perfusion and were incubated with fluorescein-isothiocyanate (FITC)-labeled insulin to determine insulin binding to the insulin receptor on the cell surface. In addition, also stably HBV-expressing cells as well as HBV-negative cells were incubated with FITC-insulin and fluorescence intensity of bound FITC-insulin was measured. Strikingly, in these experiments, primary hepatocytes from HBV transgenic mice as well as stably HBV-expressing cells bind significantly less insulin than hepatocytes from WT mice and HBV-negative

control cells as measured by lower fluorescence intensity originating from FITC-labeled insulin. These data thereby confirm that reduced insulin binding is causative for diminished insulin receptor activation after liver damage *in vivo* (**Fig. 5.12**).

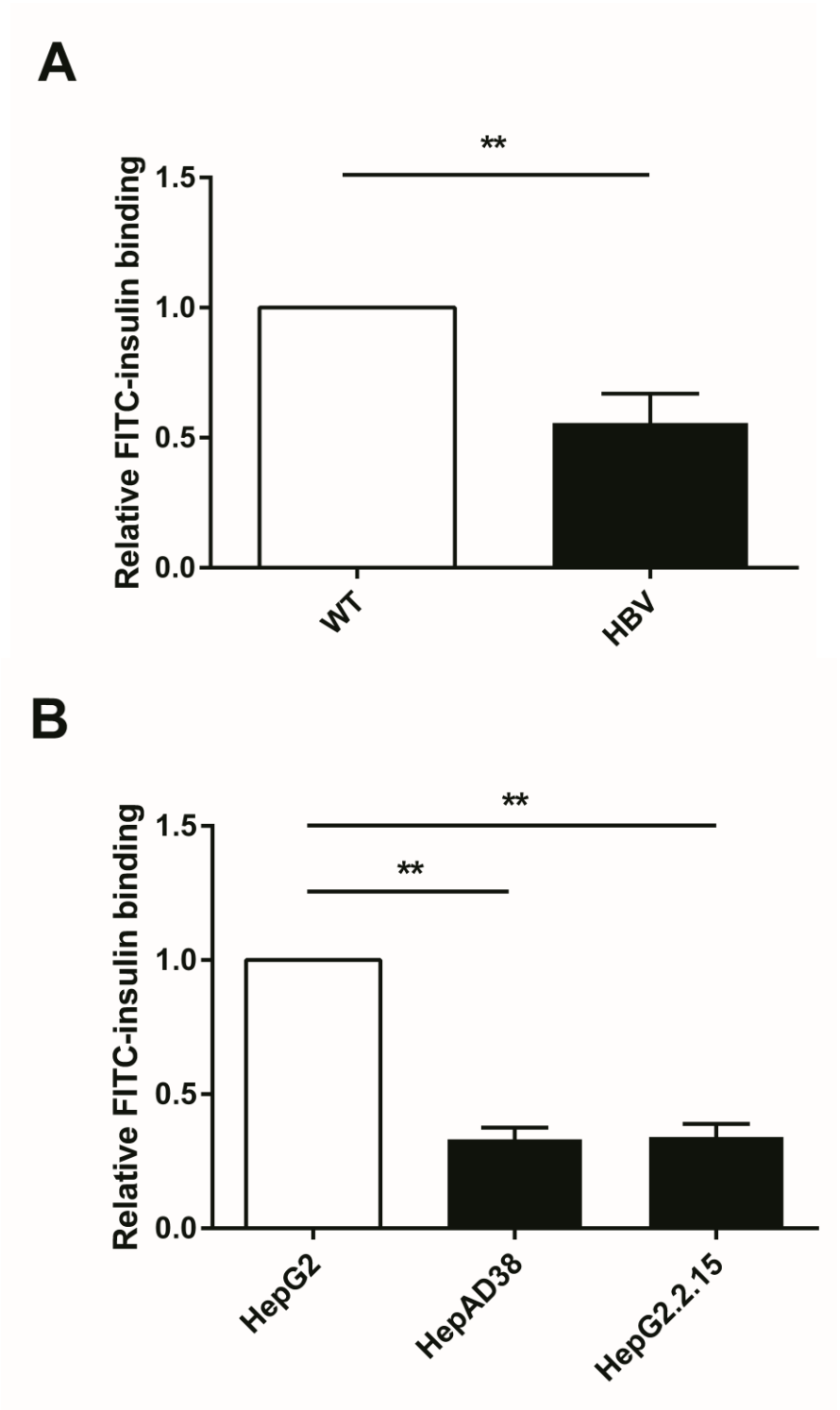

◄ **Fig. 5.12: Less insulin binding in HBV-expressing hepatocytes. A**, Primary hepatocytes from WT and HBV transgenic mice were isolated by liver perfusion and incubated with FITC-labeled insulin. Relative FITC-fluorescence was measured in a microplate fluorescent plate reader (mean ± SEM, n = 3). Values for hepatocytes from WT cells were set as 1. ** $p < 0.01$. **B**, HepG2, HepAD38 and HepG2.2.15 cells were incubated with FITC-labeled insulin and relative FITC-fluorescence was measured in a microplate fluorescent plate reader (mean ± SEM, n = 3). Values for HepG2 cells were set as 1. ** $p < 0.01$.

5.9 HBV-expressing cells reveal reduced amounts of insulin receptor on the cell surface

The reduced binding capacity for insulin in HBV-expressing hepatocytes suggests that these cells may possess decreased amounts of the insulin receptor on the cell surface. It was therefore tempting to investigate the amount of plasma membrane-associated insulin receptors in HBV-expressing cells. For this purpose, non-permeabilized HBV-expressing cells were analyzed by flow cytometry using an IRβ-specific antibody. Consistent with the reduced insulin binding capacity, this experiment reveals a significantly diminished percentage of insulin receptor-positive cells in the population of HBV-expressing cells compared to HBV-negative controls (**Fig. 5.13**). To further determine the amount of the insulin receptor localized on the cell surface, plasma membrane fragments of HBV-expressing and HBV-negative control cells were enriched by centrifugation from total cell lysates and were analyzed by Western blot for the presence of the insulin receptor (**Fig. 5.14**). Enrichment of the plasma membrane (PM) was confirmed by detection of the alpha subunit of the sodium potassium ATPase (Na,K-ATPase α), a typical plasma membrane marker protein. *Vice versa*, detection of the cytosolic

protein GAPDH served as a marker for the depletion of cytosolic proteins in the plasma membrane-enriched fractions. **Fig. 5.14** shows increased levels of the insulin receptor in HBV-expressing cells (HepG2.2.15) compared to HBV-negative cells (HepG2) in the total cell lysate. This finding confirms the previous observations that HBV-expressing cells possess elevated total amounts of the insulin receptor. Moreover, while only slight amounts of Na,K-ATPase α are detected, GAPDH protein is readily detectable in the total cell lysate of both cell types. However, the Western blot analysis of the PM-enriched pellet confirms the enrichment of plasma membrane fragments by increased amounts of Na,K-ATPase α and depletion of GAPDH protein in contrast to the total cell lysate. Most importantly, in contrast to the increased amounts in the total cell lysate, the PM-enriched fraction of HBV-expressing cells reveals diminished amounts of insulin receptor compared to HBV-negative controls. This confirms the reduced amounts of the insulin receptor on the cell surface of HBV-expressing cells as already observed by flow cytometry (**Fig. 5.13**).

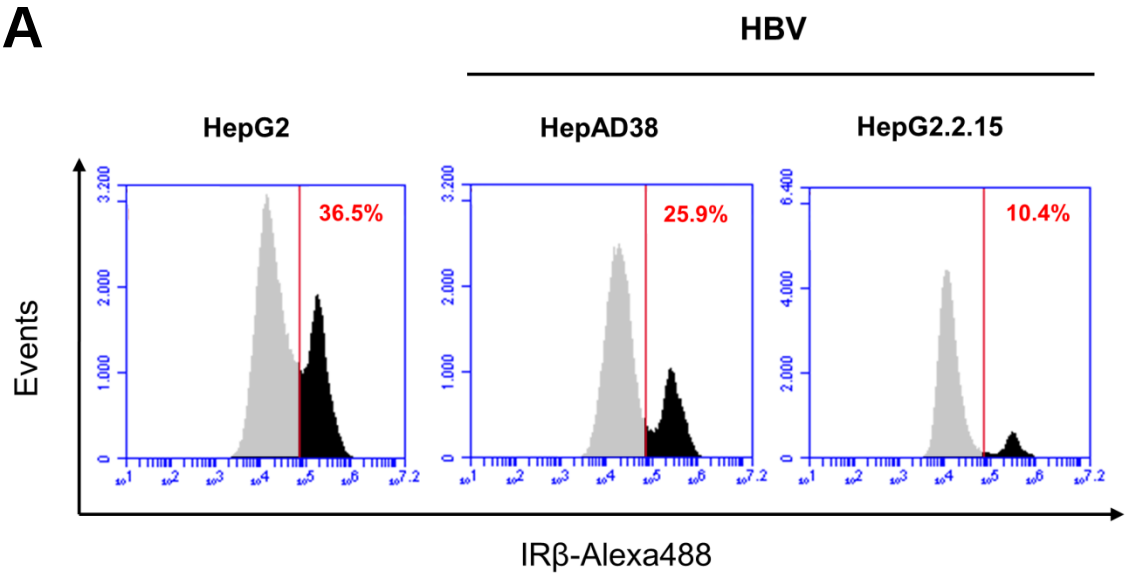

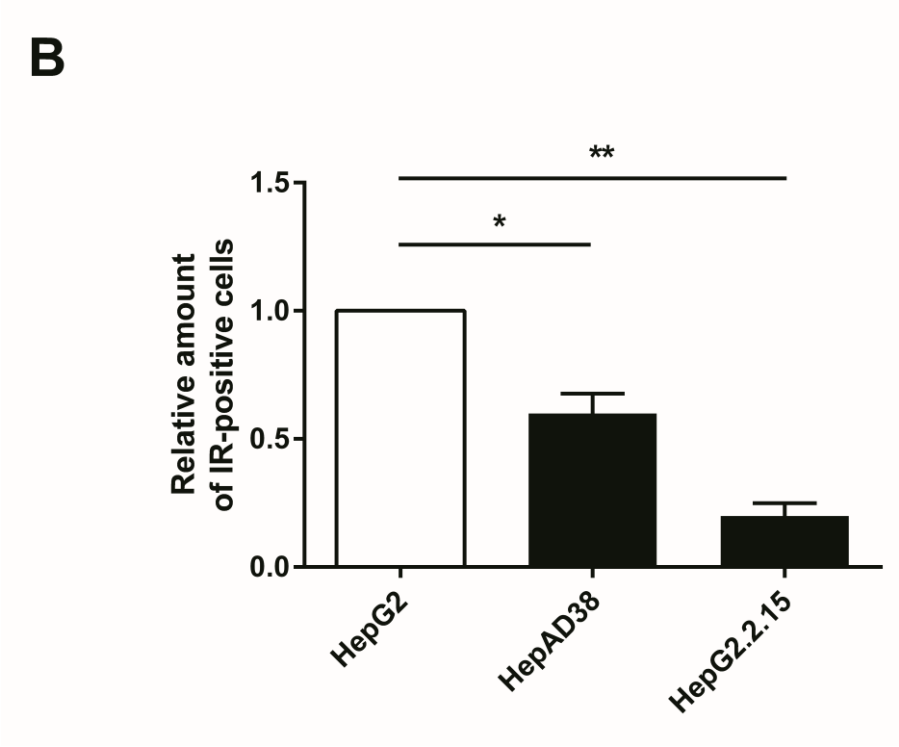

Fig. 5.13: Decreased amounts of insulin receptor on the cell surface of HBV-expressing cells. A, Non-permeabilized HepG2, HepAD38 and HepG2.2.15 cells were incubated with a rabbit-derived IRβ-specific antiserum and a goat-derived Alexa488-coupled anti-rabbit secondary antibody. Viable cells were gated by flow cytometry and percentage of cells expressing insulin receptor on the cell surface were analyzed. One representative histogram of three independent experiments per cell line is shown. As a control, the cells were only incubated with the Alexa488-coupled secondary antibody to determine background fluorescence originating from the cells (grey-shaded peaks). **B**, The graph represents the relative amount of IRβ-positive cells determined by flow cytometry from three independent experiments (mean ± SEM, n = 3). Values for HepG2 cells were set as 1. * $p < 0.05$, ** $p < 0.01$.

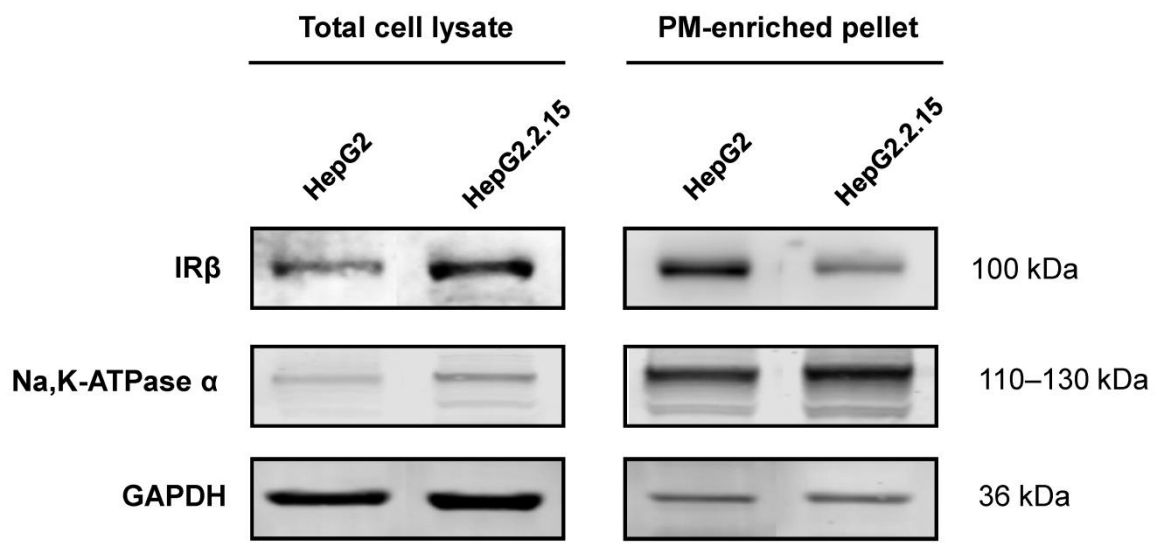

Fig. 5.14: Decreased amounts of insulin receptor on the cell surface of HBV-expressing cells. Western blot analysis of total cellular lysates and plasma membrane (PM)-enriched fractions derived from HepG2 and HepG2.2.15 cells using IRβ-specific antisera. Enrichment of plasma membrane was confirmed by detection of membrane-localized Na,K-ATPase α and depletion of cytosolic GAPDH. Residual amounts of GAPDH after enrichment represent membrane-associated GAPDH.

To investigate whether the reduction of insulin receptors on the cell surface of HBV-expressing cells is specific for the insulin receptor, the total cell lysates and PM-enriched pellets were also analyzed for the protein amount of insulin-like growth factor I receptor (IGF-IRβ) (**Fig. 5.15**). Here, the Western blot analysis reveals comparable amounts of IGF-IRβ in the total cell lysate of HBV-expressing and HBV-negative control cells. Furthermore, the amount of plasma membrane-associated IGF-IRβ also appears not to be affected by HBV expression since the amount of IGF-IRβ in the PM-enriched pellet in HBV-expressing cells is not reduced in comparison to the amount in HBV-negative cells.

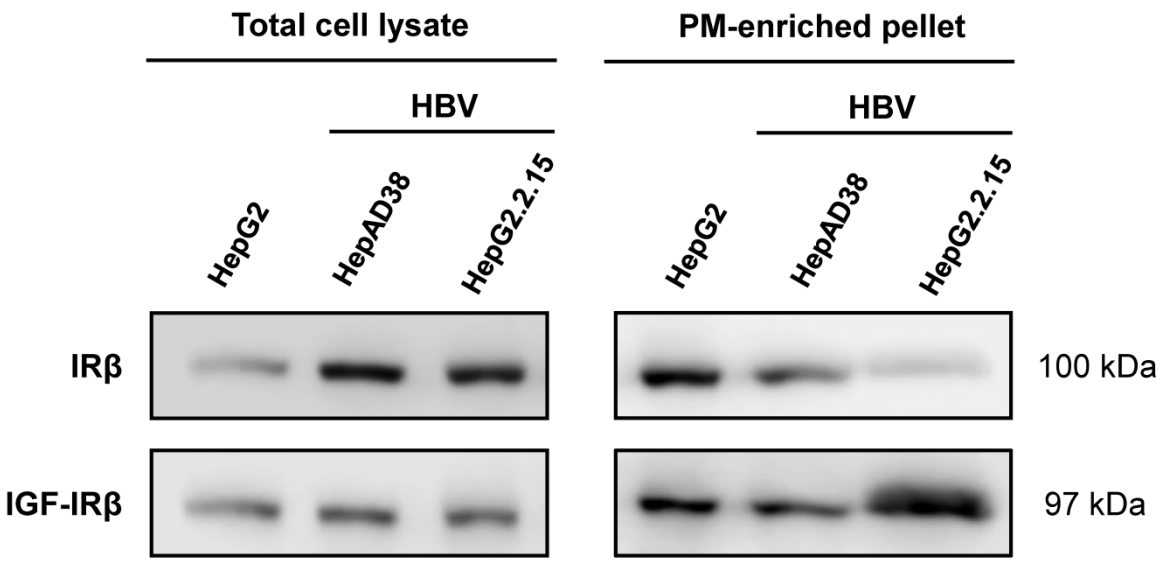

Fig. 5.15: Total amount and plasma membrane localization of insulin-like growth factor receptor (IGF-IRβ) is not affected in HBV-expressing cells. Western blot analysis of total cellular lysates and plasma membrane (PM)-enriched fractions derived from HepG2, HepAD38 and HepG2.2.15 cells using IRβ- and IGF-IRβ-specific antisera.

Collectively, these data demonstrate that HBV-expressing cells exhibit specifically decreased levels of the insulin receptor on the cell surface that are causative for reduced insulin binding.

5.10 The insulin receptor is intracellularly retained in HBV-expressing cells

The reduced amounts of the insulin receptor on the cell surface suggest that correct translocation of the insulin receptor to the plasma membrane in HBV-expressing cells is prevented and that the receptor may accumulate intracellularly. To therefore investigate the intracellular localization of the insulin receptor, cellular lysates derived from HBV-expressing and HBV-negative cells were subjected to subcellular fractionation by iodixanol density centrifugation. Subsequently, fractions were collected and analyzed by Western blot for the presence of the insulin receptor (**Fig. 5.16**). ER-specific fractions were detected with an antibody for the ER marker protein disulfide isomerase (PDI). Golgi-specific fractions were identified by analysis of galactosyltransferase activity (**Fig. 5.16**). Remarkably, subcellular fractionation reveals that high amounts of the insulin receptor in HBV-expressing cells (HepAD38) are predominantly detected in the ER-specific fractions and only to a minor extent in the Golgi-specific fractions. In contrast, in HBV-negative controls the insulin receptor is detectable in all of the fractions analyzed, not only in the ER-specific but also in the Golgi-specific fractions. This observation implies that in HBV-expressing cells the insulin receptor is retained in the fractions which mark the transition of the ER to the Golgi apparatus and is not further transported to the cell membrane. In sum, these results confirm that HBV-expressing cells show defective translocation of the insulin receptor to the plasma membrane resulting in intracellular receptor retention at the ER which is causative for attenuated insulin binding *in vitro* and *in vivo*.

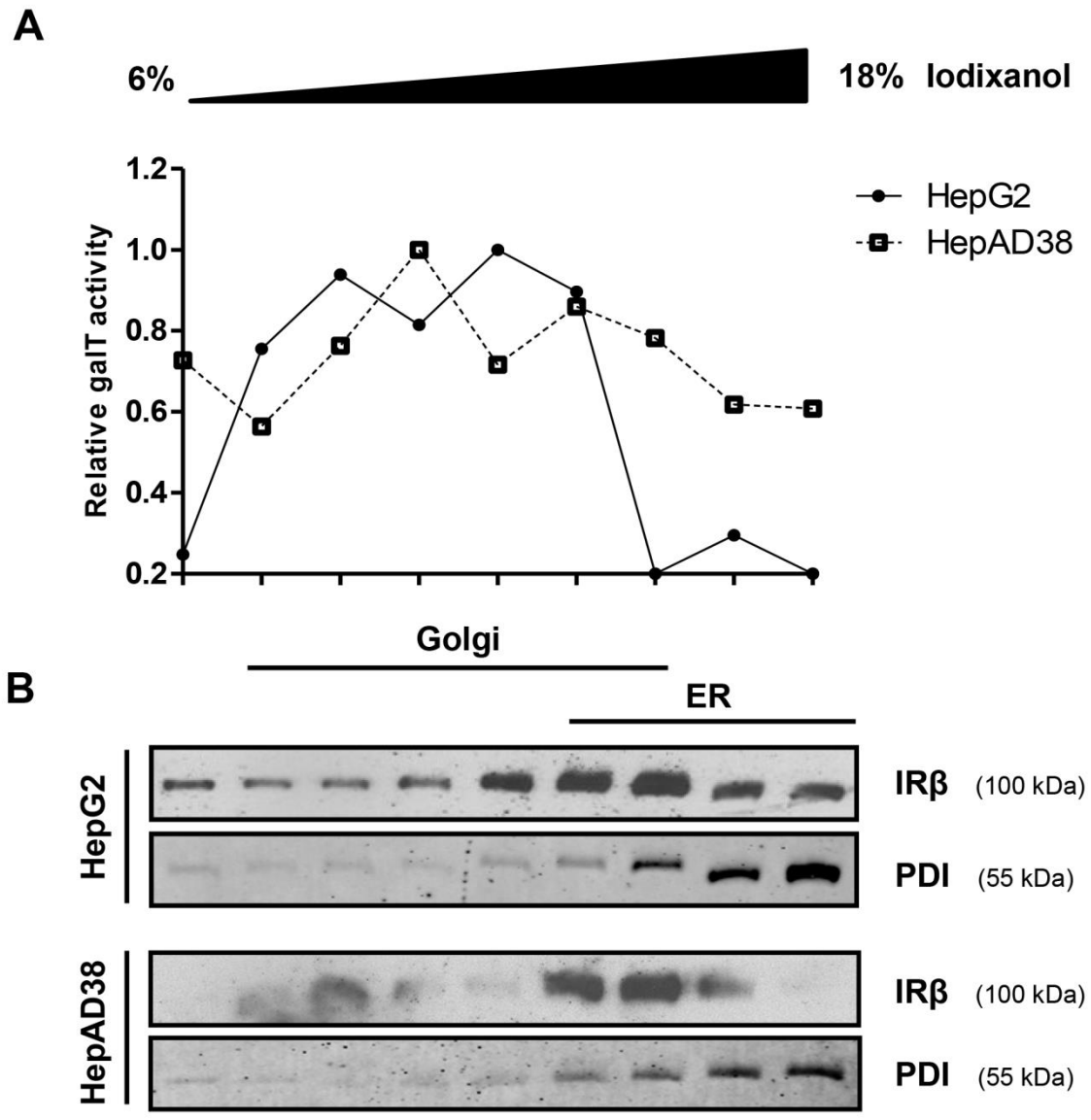

Fig. 5.16: The insulin receptor is intracellularly retained in HBV-expressing cells. Cellular lysates from HepG2 and HepAD38 cells were subjected to subcellular fractionation by iodixanol density gradient centrifugation. Fractions were collected from top to bottom and analyzed by galactosyltransferase (galT) activity assay for the presence of Golgi membranes (**A**) and the presence of IRβ and ER-resident protein PDI by Western blot using IRβ- and PDI-specific antisera (**B**). The range of iodixanol concentration of the analyzed fractions is indicated above the graph in A. The fractions analyzed in the galT assay above the blot correspond to the fractions analyzed by Western blot.

5.11 Elevated amounts of α-taxilin in HBV-expressing cells contribute to insulin receptor retention

HBV-expressing cells show diminished insulin binding capacity due to intracellular insulin receptor retention. However, the underlying reason for insulin receptor retention had yet to be determined. Previously, HBV-expressing cells were observed to express increased levels of α-taxilin (Hoffmann et al., 2013). α-taxilin is a protein involved in intracellular vesicle trafficking and exerts a negative regulatory effect on SNARE-mediated vesicle transport to the cell membrane (Nogami et al., 2003a). Given these properties and the increased levels in HBV-expressing cells, α-taxilin was assumed to be responsible for intracellular insulin receptor retention and thus became the focus of attention in this thesis. α-taxilin was therefore overexpressed in HBV-negative HuH7.5 cells to investigate whether HBV-induced insulin receptor retention could be mimicked. For this, an expression vector encoding an mCherry-tagged α-taxilin fusion protein (mCherry-Txlna) was used. Cells were transfected with this construct and subsequently incubated with FITC-insulin. Using flow cytometry, transfected cells were first gated for mCherry-Txlna expression. Cells that were positive for mCherry-Txlna expression were then analyzed for FITC-fluorescence. In contrast to control cells that were transfected with a plasmid solely encoding mCherry, the population of Txlna-overexpressing cells displays a significantly diminished percentage of FITC-insulin-positive cells (**Fig. 5.17**). These results indicate that overexpression of α-taxilin independent from HBV expression in human hepatoma cells attenuates insulin binding. Conclusively, these results confirm that increased amounts of α-taxilin are

responsible for intracellular insulin receptor retention and cause diminished insulin binding in HBV-expressing hepatocytes.

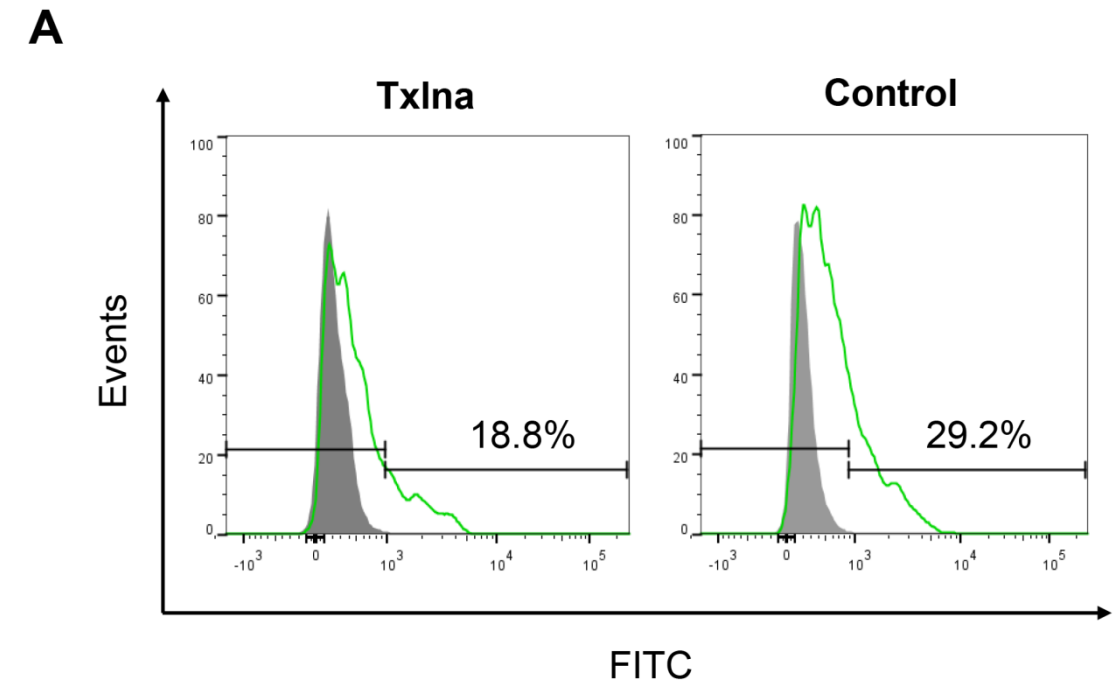

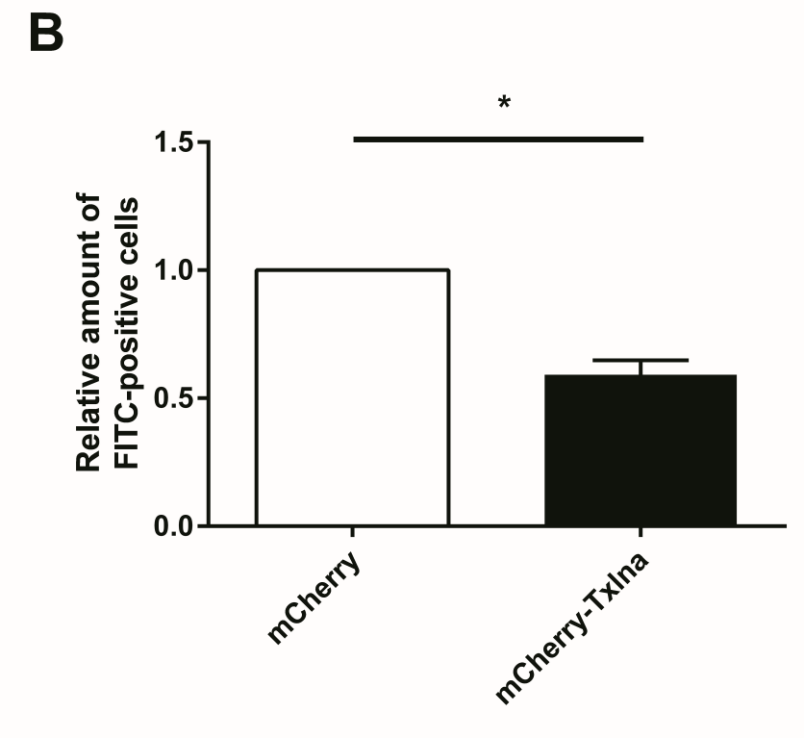

◄ **Fig. 5.17: Increased amounts of α-taxilin contribute to insulin receptor retention in HBV-expressing cells. A,** HuH7.5 cells were either transfected with a plasmid encoding an mCherry-tagged α-taxilin fusion protein (Txlna) or mCherry alone (Control). 48 h after transfection, cells were incubated with 100 nM FITC-insulin. mCherry-Txlna- or mCherry-expressing cells were gated by flow cytometry and analyzed for FITC-fluorescence. Grey-shaded peaks represent background fluorescence originating from cells that were not incubated with FITC-insulin. A representative histogram shows percentage of FITC-insulin-positive cells from mCherry-Txlna- or mCherry-expressing control cells. **B,** Summary of flow cytometry analysis (mean ± SEM, n = 4). Control cells were set as 1. * $p < 0.05$.

5.12 Insulin sensitivity is impaired in HBV-expressing cells

The *in vitro* data presented in this thesis demonstrate that HBV-expressing cells bind less insulin due to reduced amounts of the insulin receptor on the cell surface which is intracellularly retained by elevated amounts of α-taxilin. As a consequence of diminished amounts of cell surface-localized insulin receptors, it can be hypothesized that activation of the insulin receptor as well as further downstream signaling after insulin binding are impaired. To substantiate this hypothesis, the extent of insulin receptor tyrosine phosphorylation in stably HBV-expressing cells was determined by Western blot analysis. As depicted in **Fig. 5.18**, insulin treatment induces tyrosine phosphorylation of IRβ (pY-IRβ) in contrast to untreated cells. However, the amount of tyrosine-phosphorylated IRβ in HBV-expressing HepAD38 cells is reduced compared to HBV-negative HepG2 cells, while total amounts of IRβ are higher than in HepG2 cells (**Fig. 5.18**). This corroborates that reduced insulin binding in HBV-expressing cells results in diminished insulin sensitivity and impaired insulin receptor activation.

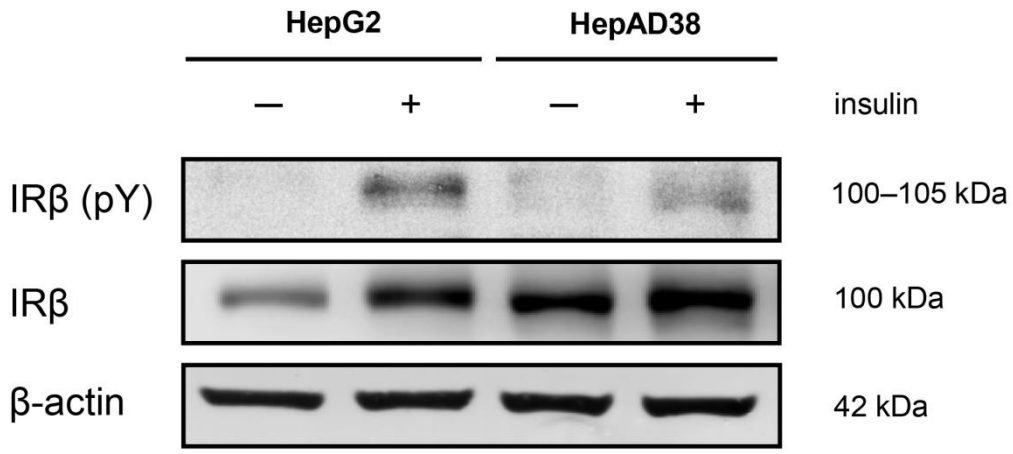

Fig. 5.18: Reduced insulin receptor activation in HBV-expressing cells. Western blot analysis of cellular lysates derived from HBV-negative HepG2 cells and stably HBV-expressing HepAD38 cells that were incubated for 5 min with 100 nM insulin or left untreated. For detection of tyrosine-phosphorylated (pY) and total insulin receptor β (IRβ) specific antisera were used. Detection of β-actin served as a loading control.

Since insulin receptor activation in HBV-expressing cells is impaired, it was tempting to analyze whether insulin-dependent induction of gene transcription is also affected. The glucokinase gene (*GCK*) is a principal target gene whose transcription is regulated by the action of insulin (Iynedjian et al., 1989; Parsa et al., 1996). In this regard, transcription of the *GCK* gene was determined by qRT-PCR in the context of insulin treatment in HBV-negative and HBV-expressing cells. Total RNA from untreated and insulin-treated cells was isolated and reverse transcribed to cDNA. Subsequently, the amount of *GCK*-specific mRNA transcripts was analyzed using sequence-specific primers (see 3.4). Strikingly, insulin-dependent induction of *GCK* transcription is significantly reduced in HBV-expressing cells upon insulin treatment in contrast to HBV-negative cells (**Fig. 5.19**).

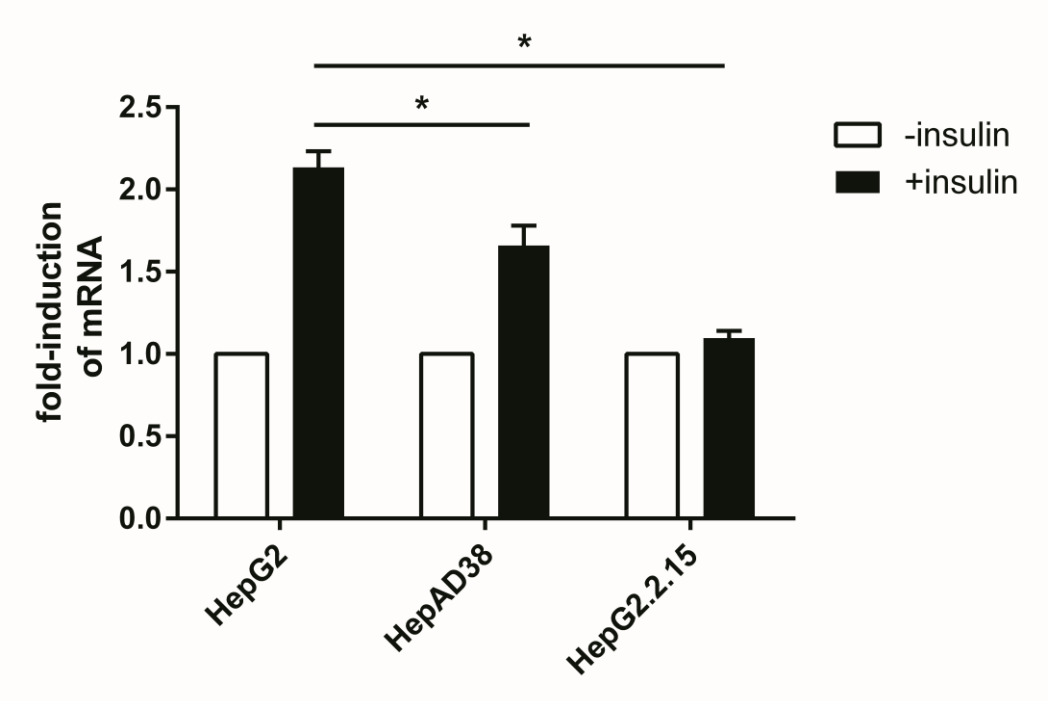

Fig. 5.19: Reduced amounts of human glucokinase (*GCK*) mRNA in HBV-expressing cells. qRT-PCR analysis of *GCK*-specific transcripts in HBV-negative HepG2 cells and stably HBV-expressing HepAD38 and HepG2.2.15 cells after treatment with 100 nM insulin for 2-3 h. Values were referred to RPL27 as internal control. Values for untreated cells were set as 1. Results are shown as the fold induction of insulin-treated cells relative to untreated cells (mean ± SEM, n = 3). * $p > 0.05$.

In summary, these results reveal that HBV-expressing cells – as a consequence of intracellular insulin receptor retention and attenuated insulin binding – exhibit deficient insulin sensitivity, leading to inhibition of insulin-dependent signaling and impaired induction of insulin-dependent gene expression.

5.13 Decreased expression of GLUT4 in HBV-expressing cells

Previous results have revealed that HBV-expressing cells fail to respond to insulin stimulation and show defective glucose uptake from the cell culture supernatant in contrast to HBV-negative cells (see 2.1). In addition, HBV transgenic mice display increased serum glucose levels in comparison to WT mice (see 2.1). These observations are in agreement with the hitherto presented data in this thesis. Upon insulin-stimulation, GLUT4 is translocated from intracellular vesicles and inserted into the plasma membrane to enable glucose uptake into the cell (Suzuki et al., 1980). By this means, GLUT4 contributes to the regulation and homeostasis of glucose metabolism and blood glucose levels (Saltiel et al., 2001). GLUT4 is predominantly expressed in adipose tissue and skeletal muscle but was also observed to be expressed in liver-specific cell lines, e.g. HepG2 cells (Bose et al., 2012). Hence, expression of GLUT4 was determined in HBV-expressing and HBV-negative hepatocytes by qRT-PCR using sequence-specific primers (see 3.4) after total RNA was isolated from the cells and reverse transcribed to cDNA. Interestingly, HBV-expressing hepatocytes show significantly decreased expression of GLUT4 in comparison to HBV-negative hepatocytes (**Fig. 5.20**). This result suggests that HBV-expressing hepatocytes cause downregulation of GLUT4 expression and by this impede glucose uptake into the cell.

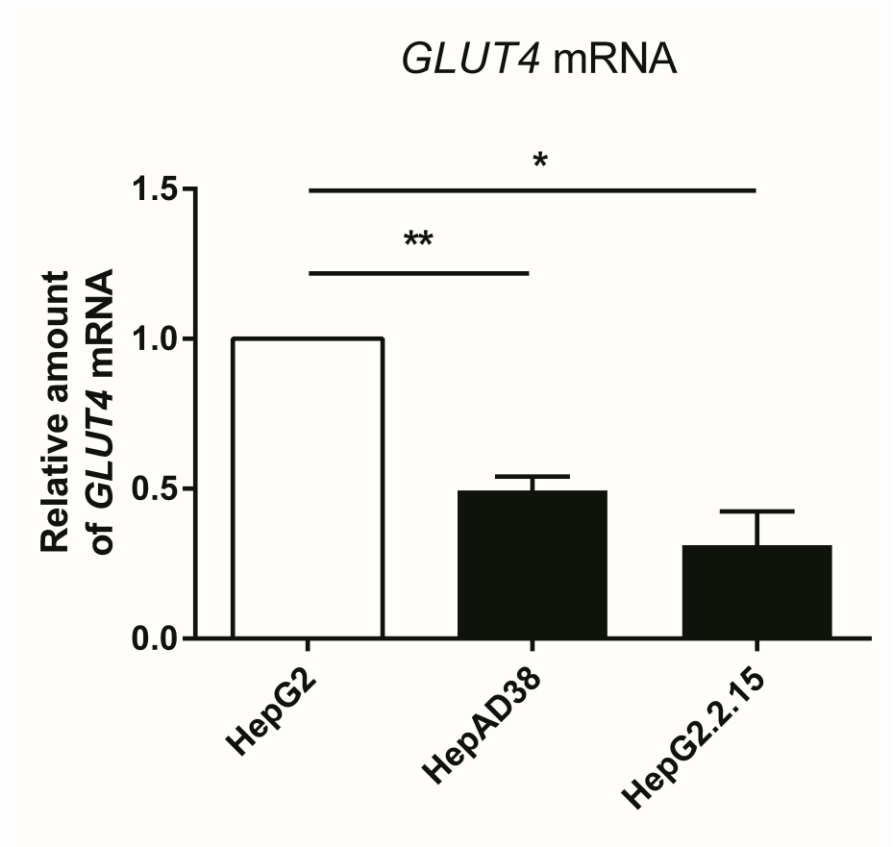

Fig. 5.20: Decreased expression of GLUT4 in HBV-expressing cells. qRT-PCR analysis of GLUT4-specific transcripts in HBV-negative (HepG2) and stably HBV-expressing cells (HepAD38, HepG2.2.15). Values were referred to *RPL27* as internal control. The values for HBV-negative HepG2 cells were set as 1. Results are shown as the fold induction of HBV-expressing cells relative to HBV-negative cells (mean ± SEM, n = 5). * $p > 0.05$, ** $p > 0.01$.

5.14 HBV transgenic mice reveal more pronounced liver damage and fibrosis after long-term CCl_4 treatment

Taken into consideration the hitherto obtained results, it can be concluded that in HBV-expressing cells as a consequence of elevated levels of α-taxilin, the insulin receptor undergoes intracellular retention and fails to translocate to the plasma membrane thereby causing reduced insulin sensitivity and impaired insulin receptor signaling. After liver injury in HBV transgenic mice, the impairment of this key pathway in the control of liver regeneration thus provokes decreased hepatocyte proliferation and increased apoptosis, finally resulting in prolonged liver damage and a decline in hepatic regenerative capacity. Since these observations are based on short-term liver injury experiments, it was not clear until this point whether the inhibition of insulin receptor signaling is also able to promote the development of chronic liver disease such as fibrosis in the context of long-term liver injury. To address this issue, male WT and HBV transgenic mice were treated for 7 weeks in total with a single injection of CCl_4 each week. Long-term CCl_4 treatment is an established model to induce and study liver fibrosis in mice (Constandinou et al., 2005). The liver of untreated WT and HBV transgenic mice shows its typical dark red-brown color and a soft and smooth appearance (**Fig. 5.21**). In contrast, after long-term treatment, the liver of WT and HBV transgenic mice has changed its color to a light brown and the surface appears rough with scattered patches of necrosis and inflammation (**Fig. 5.21**), as already observed for the liver after short-term treatment (compare **Fig. 5.1**). Moreover, activity of liver transaminases ALT and aspartate transaminase (AST) was measured after long-term treatment in the serum of WT and HBV transgenic mice as an

indicator for hepatocyte damage. Compared to the untreated controls, the serum of the treated mice exhibits a marked increase in transaminase activity. In addition, HBV transgenic mice here reveal significantly increased transaminase activity compared to WT mice, indicating more pronounced liver injury (**Fig. 5.21 B**). In summary, macroscopic changes in liver morphology as well as strongly increased serum transaminase activity confirm the induction of long-term liver injury by CCl_4 in HBV transgenic as well as WT mice.

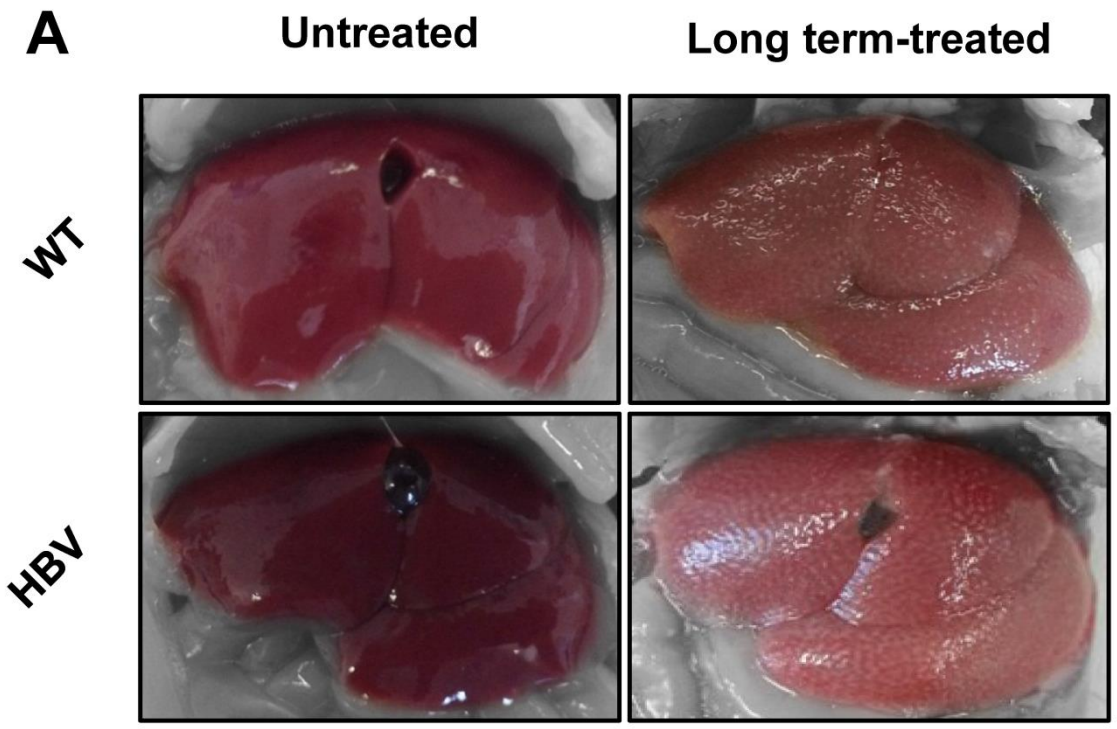

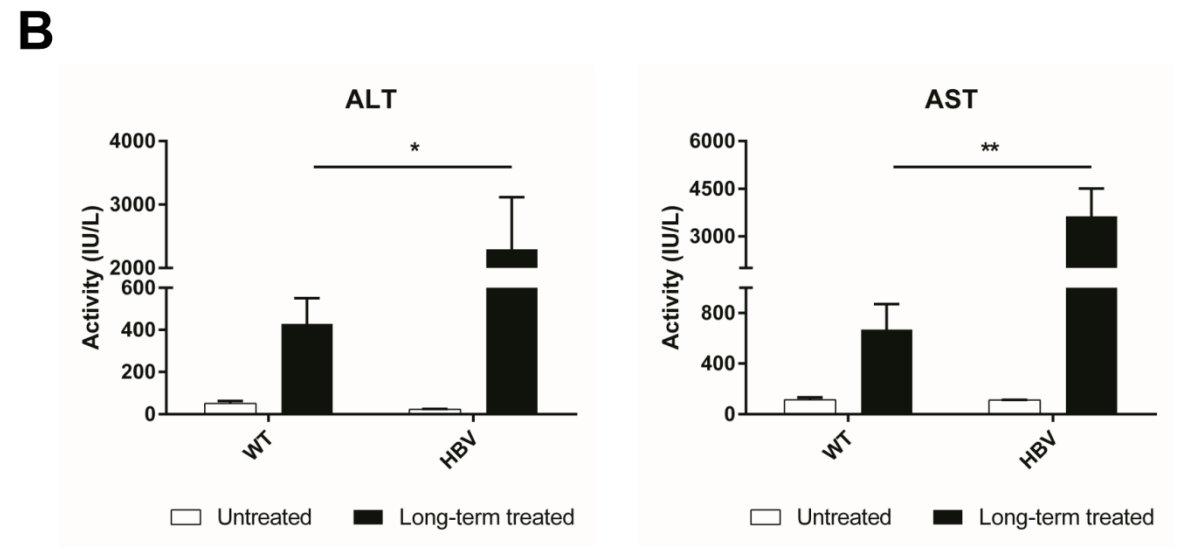

Fig. 5.21: Altered liver morphology and increased transaminase activity in mice after long-term CCl_4 treatment. Male WT and HBV transgenic mice were treated with CCl_4 (0.25 mg/g body weight) for 7 weeks in total with a single injection each week or left untreated. Mice were sacrificed 72 h after the final injection. **A**, Representative photographic images from untreated and long term-treated WT and HBV transgenic mice. **B**, ALT (left graph) and AST (right graph) activity was determined in the serum of untreated and long term-treated WT and HBV transgenic mice. The graphs represent the mean ± SEM from 6 long term-treated animals in each group (n = 6). The serum of untreated mice (WT: n = 2; HBV: n = 3) served as control. * $p > 0.05$, ** $p > 0.01$.

To further investigate the magnitude of liver injury on the histological level, liver sections of WT and HBV transgenic mice were analyzed by HE staining. After treatment, in the liver of both, WT as well as HBV transgenic mice, a clear infiltration of small mononuclear inflammatory cells can be recognized, indicating the presence of an inflammatory response (**Fig. 5.22 A**). In contrast, in healthy untreated liver tissue of WT and HBV transgenic mice no such infiltration is observable (**Fig. 5.22 B**). Moreover, in the liver of long term-treated mice there is notable hepatocyte damage due to necrosis and/or apoptosis which is visible by either nuclear shrinkage or swelling, nuclear deformation or fragmentation,

cytoplasmic shrinkage and cytoplasmic clearing (i.e. the cytoplasm appears white). In general, an overall loss in tissue integrity is observable (**Fig. 5.23**). Some cells also show ballooning degeneration which is accompanied by cytoplasmic clearing and swelling and increase in hepatocyte size. In comparison, liver damage appears to be more severe in HBV transgenic mice than in WT mice. This is in accordance with the increased transaminase activity in the serum of HBV transgenic mice compared to WT mice (**Fig. 5.21**). Conclusively, long-term CCl_4 treatment induces significant liver injury and hepatic inflammation in mice.

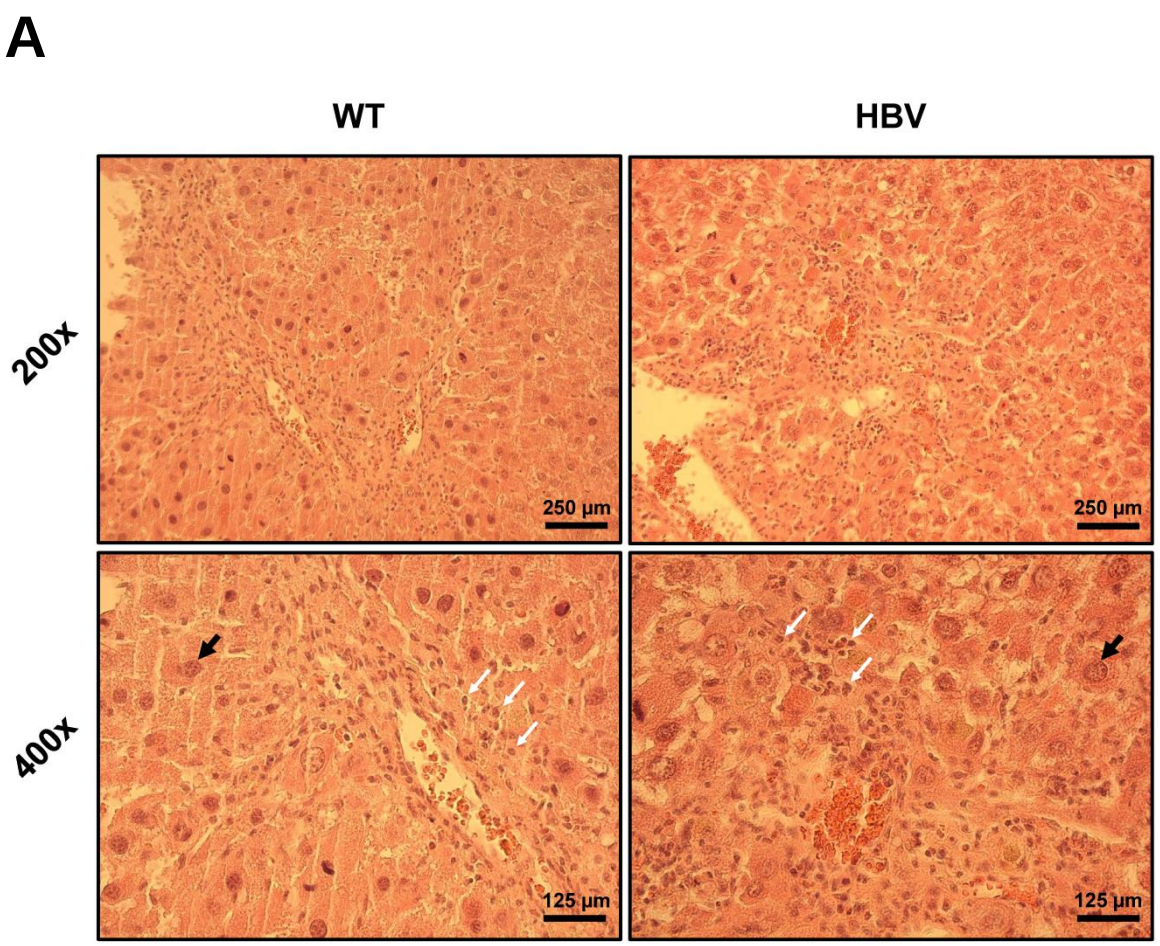

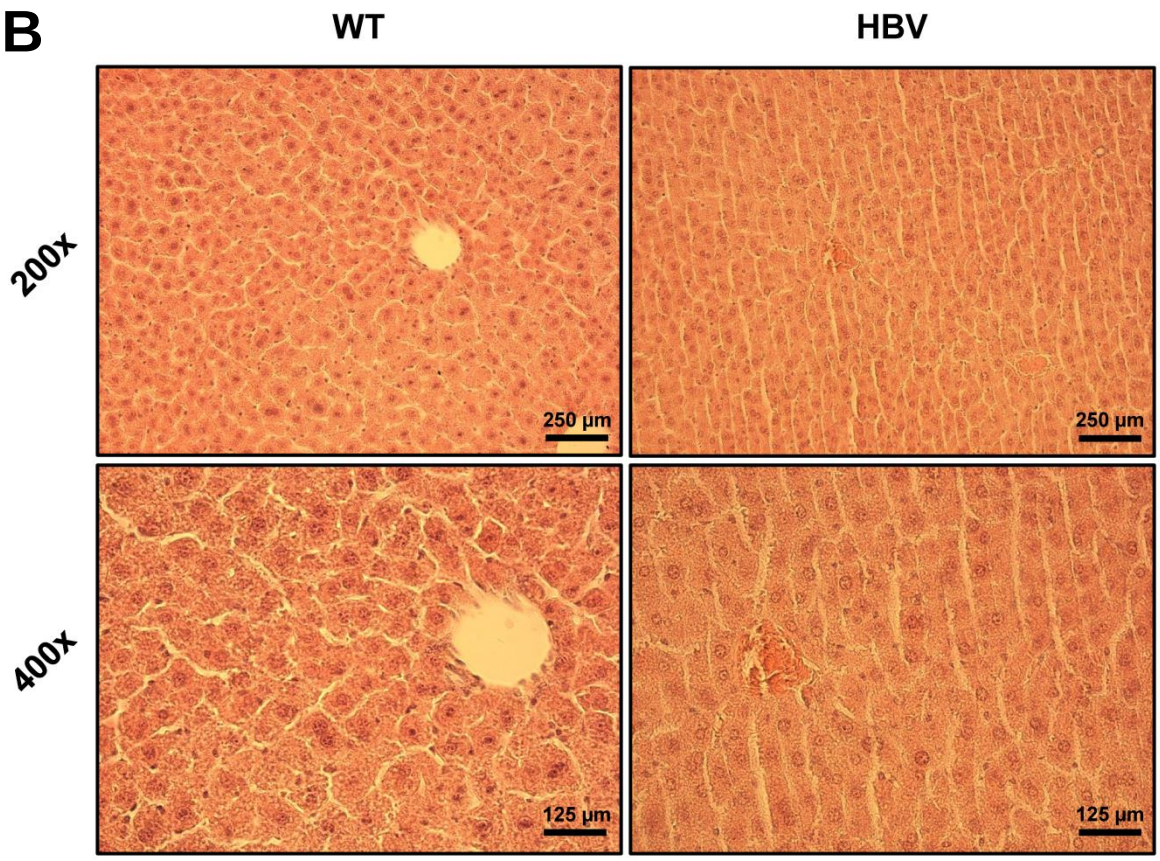

Fig. 5.22: Long-term CCl_4 treatment induces infiltration of mononuclear inflammatory cells into the liver. HE staining of representative paraffin-embedded liver sections of male WT and HBV transgenic mice either treated with CCl_4 (0.25 mg/g body weight) for 7 weeks in total with a single injection each week (n = 6–8) (**A**) or left untreated (n = 3–4) (**B**). Mice were sacrificed 72 h after the final injection. The liver was excised and fixed in 4 % formalin. Magnification (200x and 400x) of the images is indicated on the left hand side. Bold black arrows indicate at the nucleus of parenchymal hepatocytes. Thin white arrows indicate at small mononuclear inflammatory cells. 6–8 animals were analyzed per group with comparable results. Scale bars represents the indicated size.

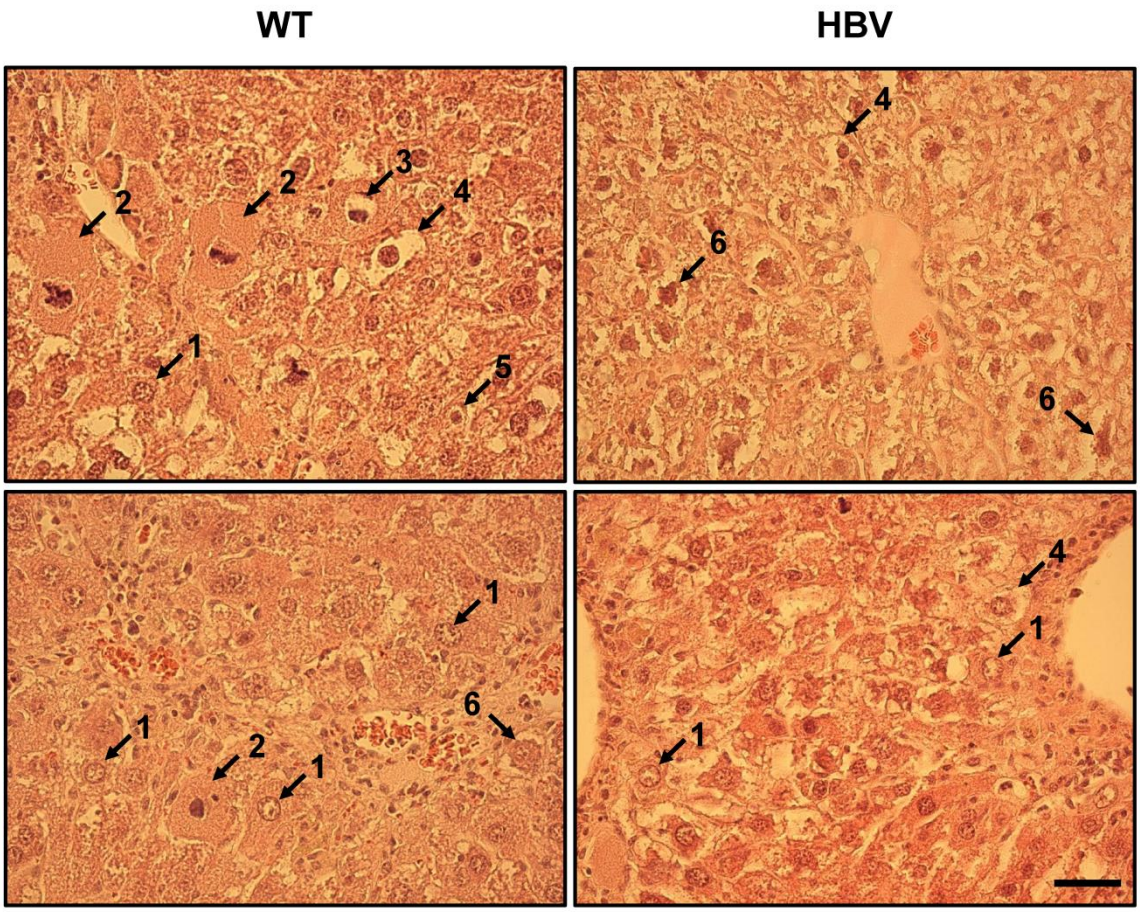

Fig. 5.23: Increased liver damage in HBV transgenic mice after long-term CCl_4 treatment. HE staining of representative paraffin-embedded liver sections of male WT and HBV transgenic mice either treated with CCl_4 (0.25 mg/g body weight) for 7 weeks in total with a single injection each week (n = 6–8) (400x magnification). Black arrows indicate apoptotic or necrotic cells that show (1) nuclear fragmentation, (2) ballooning degeneration with deformed nucleus, (3) nuclear deformation and nuclear swelling, (4) cytoplasmic clearing, (5) nuclear and cytoplasmic shrinkage and (6) nuclear deformation. 6–8 animals were analyzed per group with comparable results. Scale bar represents 125 μm.

A major hallmark of liver fibrogenesis is an increased intrahepatic deposition of collagen within the liver parenchyma (Xu et al., 2012; Pellicoro et al., 2014). To investigate the presence of collagen in the liver after long-term CCl_4 treatment, liver sections of WT and HBV transgenic mice were subjected to Picro-sirius red staining (see 4.5.2). Using this technique, primarily collagen type I and III fibers can be stained in the liver and appear colored in red (Puchtler et al., 1973; Junqueira et al., 1979). While in the liver sections of untreated WT and HBV transgenic mice collagen is almost exclusively found as a thin layer lining the blood vessels, in the liver of long term-treated mice the collagen layer around the portal veins appears thicker, reflecting so-called portal fibrosis. In addition, collagen fibers spread from the vessels into the liver parenchyma partially bridging the vessels together to form fibrous tissue bands, the so-called septa. Interestingly, in the liver of HBV transgenic mice, there is a significantly increased deposition of collagen fibers as compared to the liver of WT mice after long-term treatment (**Fig. 5.24**). Moreover, blood vessels in the liver of HBV transgenic mice are predominantly bridged by septa, reflecting so-called bridging or septal fibrosis, whereas in the liver of WT mice after treatment portal fibrosis with only few septa can be observed. Collectively, from these data it can be inferred that long-term CCl_4 treatment induces liver fibrosis in both, WT and HBV transgenic mice, but fibrosis is more pronounced in HBV transgenic mice as reflected by increased collagen deposition and more severe histological changes in the liver tissue.

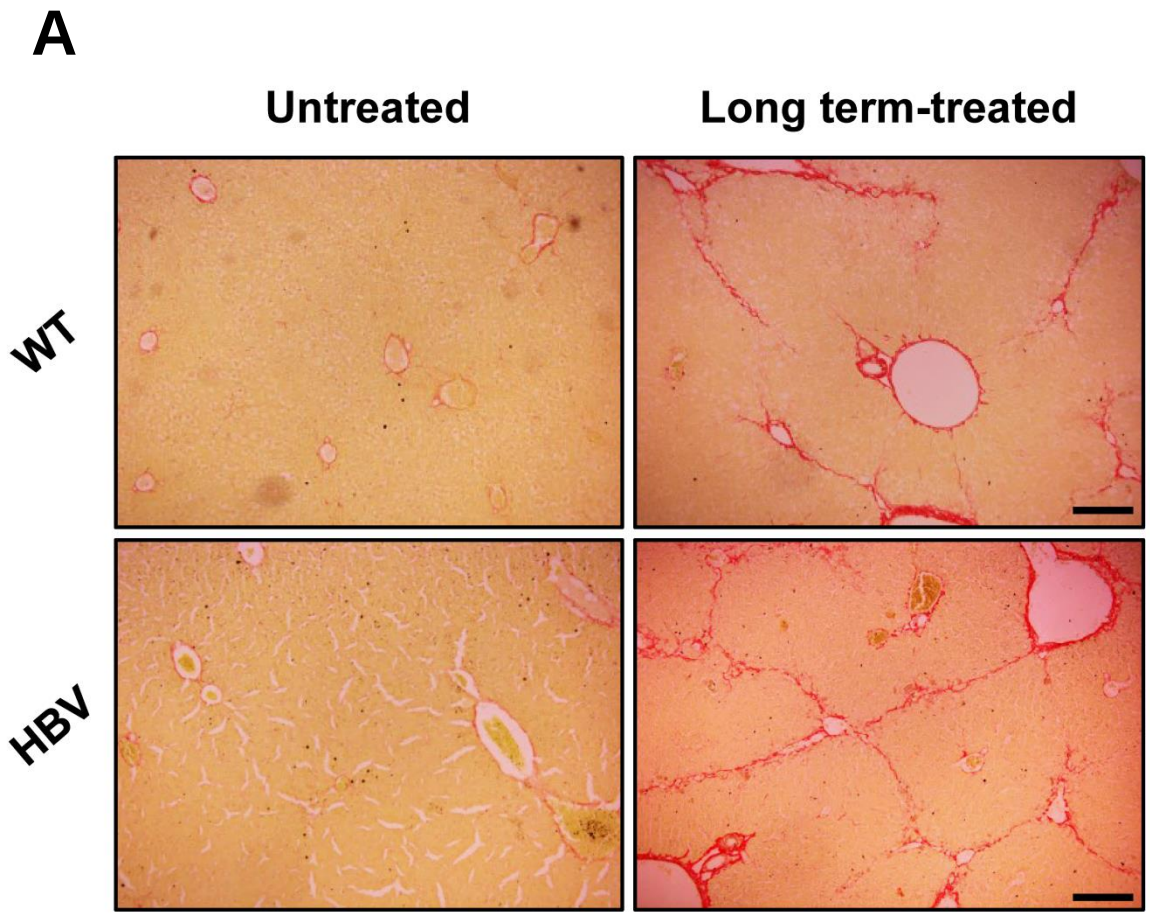
A
Untreated
Long term-treated
WT
HBV

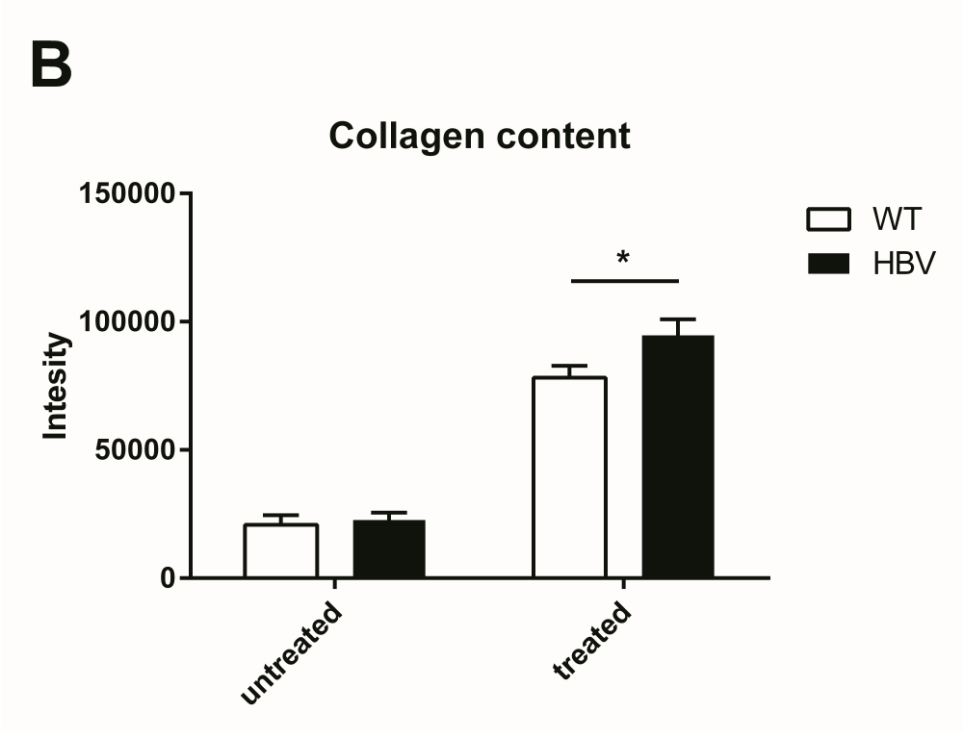
B
Collagen content
150000
100000
50000
0
Intesity
WT
HBV
*
untreated
treated

◄ **Fig. 5.24: Increased collagen deposition in the liver of HBV transgenic mice after long-term CCl_4 treatment.** Male WT and HBV transgenic mice were treated with CCl_4 (0.25 mg/g body weight) for 7 weeks in total with a single injection each week. Mice were sacrificed 72 h after the final injection and the liver was excised and fixed in 4 % formalin. **A**, Paraffin-embedded liver sections were deparaffinized and stained by Picro-sirius red. Representative images are shown in comparison to untreated animals (magnification 100x). The red color indicates collagenous fibers. Scale bar represents 500 μm. **B**, The amount of collagen was quantified by the intensity of the red color using ImageJ. The graph represents the mean ± SEM from untreated (WT: n = 3; HBV: n = 4) and long-term treated WT (n = 10) and HBV transgenic (n = 10) mice. Five visual fields have been analyzed per animal. * $p > 0.05$.

Upon hepatic necroinflammation and damage, hepatic stellate cells (HSC) also called *Ito cells* are activated and can differentiate into myofibroblasts that produce and secrete ECM components such as collagen (Xu et al., 2012; Pellicoro et al., 2014). Activated HSC-derived myofibroblasts show also upregulated expression of alpha-smooth muscle actin (α-SMA) which is another marker for liver fibrosis (Xu et al., 2012; Pellicoro et al., 2014). Therefore, to further investigate the extent of liver fibrosis in HBV transgenic mice after long-term CCl_4 treatment compared to WT mice, liver sections of untreated and long term-treated WT and HBV transgenic mice where stained by immunohistochemistry for the amount of α-SMA. As already observed for collagen, in the liver sections of untreated mice α-SMA is merely detectable in the vasculature of the blood vessels (**Fig. 5.25 A**). In contrast, in the liver sections of treated mice, α-SMA-positive cells as well as α-SMA deposition are readily detectable within the liver parenchyma, spreading from the blood vessels into the tissue (**Fig. 5.25 A**). Remarkably, the amount of α-SMA is considerably increased in HBV transgenic mice in contrast to WT mice after

long-term treatment (**Fig. 5.25 A** and **B**). Taken together, it can be deduced from these results that induction of fibrosis in HBV transgenic mice is increased during long-term liver injury and distinctly marked by elevated deposition of α-SMA.

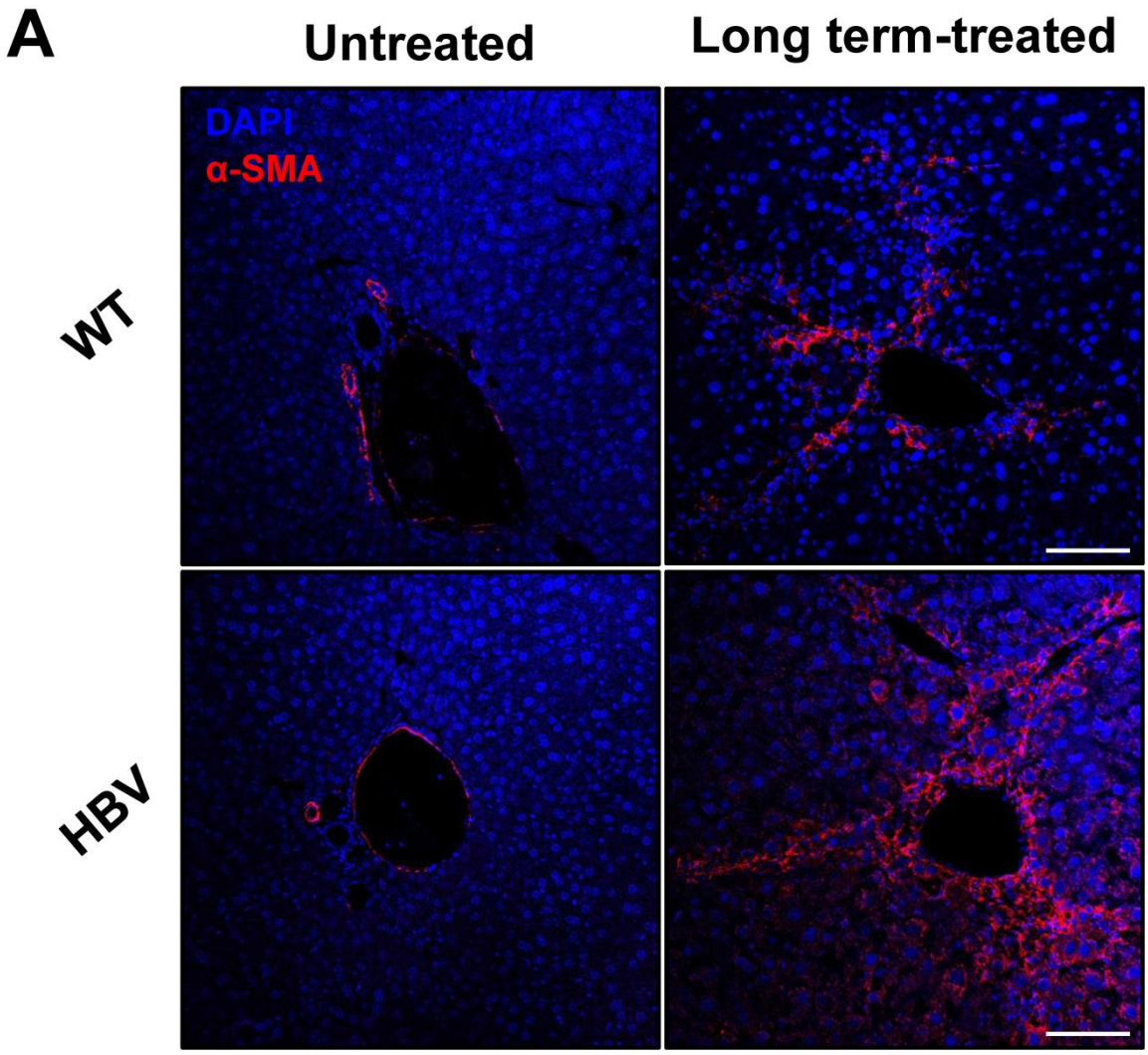

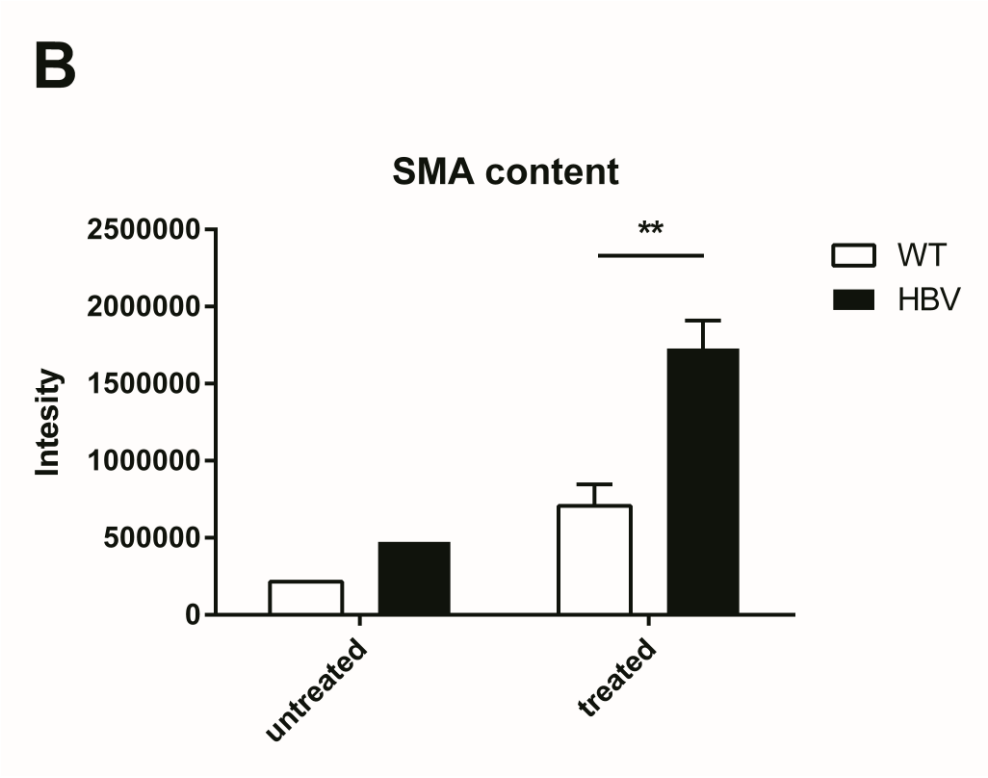

Fig. 5.25: Increased amounts of alpha-smooth muscle actin (α-SMA) in the liver of HBV transgenic mice after long-term CCl_4 treatment. Male WT and HBV transgenic mice were treated with CCl_4 (0.25 mg/g body weight) for 7 weeks in total with a single injection each week. Mice were sacrificed 72 h after the final injection and the liver was excised and fixed in 4 % formalin. **A**, Paraffin-embedded liver sections from WT and HBV transgenic mice were stained for α-SMA using a mouse-derived primary antibody and a donkey-derived Cy3-coupled anti-mouse secondary antibody (red fluorescence). Nuclei were visualized by DAPI (blue fluorescence) (magnification 200x). Scale bar represents 100 μm. Representative images are shown in comparison to untreated animals. **B**, The amount of α-SMA was quantified by the intensity of the red color using ImageJ. The graph represents the mean ± SEM from untreated (WT: n = 1; HBV: n = 1) and long-term treated WT (n = 5) and HBV transgenic (n = 5) mice. Five visual fields have been analyzed per animal. ** $p > 0.01$.

6 Discussion

6.1 Impairment of liver regeneration by HBV

Liver pathology in chronic HBV infection is associated with disturbances in hepatocyte proliferation and liver regeneration (Tachtatzis et al., 2015). Chronic hepatocyte turnover due to immune-mediated liver damage leads to telomere shortening and can cause ‘replicative senescence’ of hepatocytes, rendering them incapable of exerting their regenerative potential (Wiemann et al., 2002; Tachtatzis et al., 2015). In addition, HBV expression has been linked to an inhibitory effect on cell cycle progression and hepatocyte proliferation (Friedrich et al., 2005). After liver damage, dysregulation of cell cycle entry and an impairment of liver regeneration, primarily by the action of the HBV X protein (HBx), has been reported (Tralhao et al., 2002; Wu et al., 2006; Hodgson et al., 2008). Several mechanisms for impairment of liver regeneration by HBV have been proposed, including an involvement of activated hepatic NKT cells (Dong et al., 2007), an epigenetic regulation of HGF activation (Park et al., 2013) as well as HBx-induced overexpression of IL-6 (Quétier et al., 2013). However, it should be noted that most of these studies were conducted using transgenic mice solely expressing the HBx protein and not the whole HBV genome. In addition, HBx transgenic mice highly overproduce the HBx protein and do not reflect the physiological situation of HBV infection. Therefore, HBV transgenic mice serve as a more appropriate model for human HBV infection (Inuzuka et al., 2014; Iannacone et al., 2015). So far, the influence of HBV expression on liver regeneration has not been investigated in depth in HBV transgenic mice, or otherwise no specific effect has

been observed in these mice after partial hepatectomy (PHx) (Tian et al., 2012). Furthermore, liver damage in all of these studies has been exclusively induced by PHx. Hence, in this thesis, the influence of HBV on liver regeneration was investigated, on the one hand in transgenic mice expressing the whole HBV genome and on the other hand using CCl_4 instead of PHx to induce liver damage. CCl_4 has proven to be a reliable inducer of hepatotoxicity (Weber et al., 2003). CCl_4 treatment induces severe liver damage in WT as well as HBV transgenic mice as the liver dramatically changes its morphological appearance (**Fig. 5.1**) and shows significant tissue damage (**Fig. 5.3**). This is further corroborated by increased presence of high concentrations of liver-specific transaminase ALT in the serum of WT and HBV transgenic mice (**Fig. 5.2**). Highest concentrations of ALT are detected on day 1 and day 2 after initial CCl_4 treatment. Interestingly, compared to the wild type, ALT concentrations in the serum of HBV transgenic mice are slightly lower. One explanation could be that increased activity of Nrf2 in HBV-expressing hepatocytes of HBV transgenic mice (**Fig. 5.8**) better protects these cells from CCl_4-induced liver damage. The basis of CCl_4-induced liver damage is the generation of the trichloromethyl radical (see 4.7.1) which could be more effectively detoxified by Nrf2-induced cytoprotective enzymes in HBV transgenic mice, thereby lowering the local cellular concentration of CCl_4 radicals and thus the extent of liver damage and ALT concentrations compared to wild type mice. This assumption may be supported by significantly higher ALT concentrations in the serum of HBV transgenic mice compared to WT mice on day 1 after PHx, where liver damage is mechanically induced and is independent from chemical injury by radicals (unpublished results by T. Heinrich). Nevertheless,

even though increased Nrf2 activity in the liver of HBV transgenic may mitigate the toxic effect of CCl_4, liver damage is strongly induced in both, WT and HBV transgenic mice (**Figs. 5.1, 5.2** and **5.3**). But, while WT mice exhibit rapid reduction of hepatic lesions with complete restoration of liver tissue on day 5 and day 7 after treatment, hepatic lesions in HBV transgenic appear stronger on day 3 and even persist until day 5 (**Fig. 5.3**). This observation suggests prolonged liver damage and an impairment of liver regeneration in HBV transgenic mice after CCl_4-induced liver damage. Impairment of liver regeneration is confirmed by significantly reduced hepatocyte proliferation in HBV transgenic mice as quantified by BrdU incorporation, most significantly on day 2 after initial CCl_4 treatment (**Fig. 5.5**). A similar result is obtained when hepatocyte proliferation is quantified by BrdU incorporation after PHx. Here, HBV transgenic mice also display an overall decrease and a delayed onset of hepatocyte proliferation after mechanical liver damage (unpublished results by T. Heinrich). Unfortunately, due to time reasons, liver sections from HBV transgenic and WT mice 5 and 7 days after CCl_4 treatment could not be analyzed for BrdU incorporation in this thesis. But, since the amount of proliferating hepatocytes in HBV transgenic mice is significantly reduced on day 2 compared to WT mice, it can be assumed that in the liver of HBV transgenic mice proliferation may be delayed and may start to initiate on day 5 to compensate for the reduced regenerative response. However, in murine hepatocytes proliferation normally peaks around 40 h after PHx (Taub, 2004). This appears to be true also for CCl_4-induced liver damage, since on day 2 after initial treatment the highest numbers of BrdU-positive hepatocytes are detectable in WT and HBV transgenic mice, in contrast to the other days that were analyzed post CCl_4

treatment (**Fig. 5.5**). While hepatocyte proliferation is reduced in HBV transgenic mice after liver damage, hepatocyte cell death is increased compared to WT hepatocytes (**Fig. 5.4**). This can be explained by previous observations that in the liver of HBV transgenic mice the activity of the anti-apoptotic transcription factor NF-κB is reduced compared to WT mice, thereby promoting apoptosis in HBV-expressing cells (unpublished data T. Heinrich). Interestingly, recent reports described that increased Nrf2 activation is associated with decreased NF-κB activity, rendering the cells more sensitive for apoptotic stimuli (Masoudi et al., 2014). This is further supported by another study demonstrating that increased activation of Nrf2 results in an impairment of liver regeneration due to the activation of genes involved in apoptosis, primarily the cyclin-dependent kinase inhibitor p15 and pro-apoptotic protein Bim (Köhler et al., 2014). Taken together, HBV transgenic mice show prolonged liver damage and impaired liver regeneration as a consequence of reduced hepatocyte proliferation and increased apoptosis after CCl_4-induced liver damage. Nonetheless, it has to be noted that CCl_4 treatment to induce liver damage represents an artificial system by using a chemical toxin. Therefore, it would be of great interest to employ other more physiological systems to study the influence of HBV on the process of liver regeneration, such as the autoimmune hepatitis model (Hintermann et al., 2012) or human liver chimeric mice naturally infected with HBV (Tsuge et al., 2005; Bissig et al., 2010).

6.2 Influence of HBV on insulin receptor signaling

Insulin receptor signaling cascades have been reported to be of major importance for liver regeneration (Yamada et al., 1977; Böhm et al., 2010). Patients with severe glucose intolerance or impaired insulin secretion even show high mortality following hepatectomy, indicating that insulin receptor signaling is indispensable for liver regeneration (Ozawa et al., 1976). Insulin receptor signaling is affected by the activity of the redox-sensitive and cytoprotective transcription factor Nrf2 (Beyer et al., 2008a; Beyer et al., 2008b). Translation products of Nrf2-regulated genes are in charge of defusing intracellular oxygen radicals (ROS) and electrophiles and thereby prevent oxidative stress. Oxidative stress is known to inhibit insulin receptor signaling and induce insulin resistance (Urakawa et al., 2003; Besse-Patin et al., 2014). This is further supported by the observation that Nrf2 deficiency in Nrf2 knock-out mice causes elevated intracellular ROS levels that induce inhibition of insulin receptor signaling, leading to impaired hepatocyte proliferation and liver regeneration (Beyer et al., 2008b). Interestingly, HBV has been reported to directly induce the activation of Nrf2 and expression of Nrf2-regulated genes (Schädler et al., 2010). This was also confirmed in this thesis in HBV transgenic mice (**Fig. 5.8**). In addition, previous work has revealed that not only in transiently and stably HBV-expressing cells, but also in the liver of HBV transgenic mice as well as chronic HBV patients elevated amounts of the insulin receptor protein are detected (unpublished results T. Heinrich). A transcriptional activation of the insulin receptor gene in stably HBV-expressing cells could be confirmed in this thesis (**Fig. 5.7**). It was further evidenced that increased activity of Nrf2 is causative for increased transcription and expression of the insulin

receptor gene in HBV-expressing cells (**Figs. 5.10** and **5.11**). This is triggered by the presence of an antioxidant response element (ARE) in the insulin receptor promoter, which is required for the binding of Nrf2 to the cognate promoter and the activation of gene transcription (**Fig. 5.9**). These data suggest that the insulin receptor gene may be a novel direct target of Nrf2 in the liver. Given an increased activity of Nrf2 in combination with elevated amounts of insulin receptor in HBV-expressing cells, this would imply a benefit for insulin receptor signaling and liver regeneration. However, these two findings are in conflict with the previous described observation that HBV transgenic mice after liver damage exhibit impaired liver regeneration (**Figs. 5.3** and **5.5**). In addition, analysis of tyrosine phosphorylation as an indicator for insulin receptor activation revealed reduced insulin receptor activation in the liver of HBV transgenic mice shortly after CCl_4-induced liver damage (**Fig. 5.6**). This suggests that HBV exerts an inhibitory effect on hepatic insulin receptor signaling that would contribute to the reduced proliferative response after liver damage. This assumption is further corroborated by a study which demonstrated that HBx expression is able to impair hepatic insulin signaling by promoting degradation of IRS1 and induction of suppressor of cytokine signaling 3 (SOCS3) (Kim et al., 2010). It was therefore tempting to investigate the molecular basis of insulin receptor signaling inhibition by HBV. In case of HCV, it is well established that HCV infection causes insulin resistance which impairs liver regeneration and fosters liver fibrosis (Hui et al., 2003; Alberstein et al., 2012). Mechanistically, this can be conclusively explained by increased oxidative stress in HCV-positive hepatocytes since HCV has been demonstrated to inhibit Nrf2/ARE-regulated gene expression (Carvajal-Yepes et

al., 2011). In case of HBV, activation of Nrf2 by HBV argues against an inhibitory effect on insulin receptor signaling and hepatocyte proliferation by increased oxidative stress. Hence, another mechanism must be causative for this potential inhibitory effect. From the reduced activation of the insulin receptor upon liver damage in HBV transgenic mice, it can be inferred that HBV-expressing hepatocytes bind less insulin. This was experimentally confirmed by insulin binding studies *in vivo* and *in vitro*. Stably HBV-expressing cells as well as primary mouse hepatocytes reveal diminished insulin binding compared to HBV-negative cells and hepatocytes from WT mice (**Fig. 5.12**). It was further observed *in vitro* that reduced insulin binding occurs as a consequence of diminished amounts of insulin receptor on the cell surface of HBV-expressing cells compared to HBV-negative control cells (**Figs. 5.13** and **5.14**). Strikingly, in HBV-expressing cells the insulin receptor is intracellularly retained and appears to accumulate at the transition of the ER to the Golgi apparatus where it is not further translocated to the cell surface, therefore leading to diminished insulin binding (**Fig. 5.16**). It was recently described that HBV leads to elevated expression of α-taxilin which is required for the release of HBV (Hoffmann et al., 2013). Here, it acts as an adapter by binding to LHBs on the one hand and *via* its late domain to the ESCRT-component tsg101 on the other, thereby enabling multivesicular body (MVB)-dependent viral release. In addition to this, α-taxilin prevents the formation of t-SNARE (target-SNARE) complexes and thereby exerts a negative regulatory effect on SNARE-mediated vesicle trafficking and transport to the cell membrane (Nogami et al., 2003a; Nogami et al., 2003b). Interestingly, when α-taxilin was overexpressed in HuH7.5 human hepatoma cells in the absence of HBV

expression, these cells bind significantly less insulin compared to control cells (**Fig. 5.17**). From this result it can be concluded that increased amounts of α-taxilin in HBV-expressing cells cause or at least partially contribute to – beside other potential factors – the intracellular retention of the insulin receptor. How exactly intracellular retention by α-taxilin occurs in HBV-expressing cells remains to be determined. Interestingly, intracellular transport and membrane translocation of the IGF-IR is not affected by HBV expression (**Fig. 5.15**). This finding suggests that the insulin receptor is specifically retained in HBV-expressing cells. How this specificity is accomplished is also not clear at that time. A possible explanation may be the presence of different syntaxin proteins in the cell, which in concert with α-taxilin are involved in intracellular trafficking and to which α-taxilin can bind. The transport of the insulin receptor may require different syntaxins (e.g. syntaxin-4) than the transport of IGF-IR, and these syntaxins may be more specifically targeted by increased levels of α-taxilin than those required for IGF-IR trafficking. Specific processing and trimming of glycan residues on the insulin receptor protein in the ER might also be differentially affected by HBV expression which consequently could result in insulin receptor retention. This hypothesis may be confirmed by two-dimensional gel electrophoresis analyses of the insulin receptor. Most interestingly, a former study reports that HBV-expressing cells also bind less EGF due to reduced expression of the EGF receptor (EGFR), while levels of TNF-RI are not affected (Friedrich et al., 2005). This implies that the expression of the HBV genome does not result in a general reduction of receptor proteins (Friedrich et al., 2005). Reduced levels of EGFR also impair induction of cell proliferation in HBV-expressing cells. It is tempting to speculate whether the EGFR, like the IR,

may also be intracellularly retained by a similar mechanism which causes reduced EGF binding. However, as a consequence of intracellular retention of the insulin receptor in HBV-expressing cells, insulin sensitivity is decreased. This is obvious from the analysis of insulin receptor activation upon insulin binding. Here, HBV-expressing cells reveal lower amounts of tyrosine-phosphorylated insulin receptor than HBV-negative cells (**Fig. 5.18**). These data corroborate the *in vivo* data where reduced insulin receptor activation is also detectable in HBV transgenic mice upon liver damage (**Fig. 5.6**). Consequently, insulin-dependent gene expression is diminished in HBV-expressing cells upon insulin stimulation as observed for the glucokinase gene, indicating that the insulin receptor signaling pathway is not properly activated, but rather inhibited by HBV-induced insulin receptor retention (**Fig. 5.19**). This can also explain previous observations that upon insulin binding, HBV-expressing cells show impaired glucose uptake from the cell culture supernatant as compared to HBV-negative cells (unpublished results T. Heinrich). In addition, HBV transgenic mice show increased blood glucose levels than WT mice (unpublished results T. Heinrich). Therefore, it can be deduced that impaired glucose uptake is a consequence of the reduced binding capacity for insulin and inhibition of insulin receptor signaling due to insulin receptor retention in HBV-expressing hepatocytes. This is also corroborated by a diminished basal expression of GLUT4 observed in HBV-expressing cells (**Fig. 5.20**). In sum, these data demonstrate that key metabolic changes normally initiated by insulin binding are impeded in HBV-expressing cells, causing a state of insulin resistance and impaired glucose uptake. Conclusively, preventing proliferative insulin receptor signaling by retention of the insulin receptor could be of major importance for HBV

since it preferentially replicates in quiescent hepatocytes (Ozer et al., 1996; Friedrich et al., 2005). It can therefore be hypothesized that HBV-induced expression of α-taxilin – in addition to support viral release – serves to prevent insulin receptor transport and activation of insulin receptor signaling to decelerate hepatocyte proliferation during compensatory liver regeneration in order to support HBV replication. As a consequence, the insulin receptor is hindered to fulfill its proper function as a key player in orchestrating liver regeneration, resulting in a pathological phenotype. At first glance, it appears contradictory why HBV on the one hand triggers increased expression of the insulin receptor via activation of Nrf2, but simultaneously induces its retention on the other. Overall, HBV-dependent activation of Nrf2 is supposed to be beneficial for HBV-infected cells by protecting the viral and the host genome from oxidative stress induced by the immune response (Schädler et al., 2010). The insulin receptor promoter was shown to harbor ARE sites (**Fig. 5.9**), thus its expression is induced by HBV-induced Nrf2 activation (**Figs. 5.10** and **5.11**). However, since HBV preferentially replicates in non-dividing hepatocytes, promotion of mitogenic signaling pathway is counterproductive. Therefore, since Nrf2-dependent expression of the insulin receptor cannot be circumvented, intracellular retention of the insulin receptor may be an effective countermeasure for HBV-infected cells to prevent activation of the insulin receptor signaling pathway which would otherwise lead to induction of proliferation. Beside this rather teleological interpretation, this mechanism could just be the consequence of a co-evolutionary adaptation process between HBV and its host that finally has resulted in an optimal setting for HBV replication.

6.3 Promotion of liver fibrosis by HBV

Liver fibrosis is a physiological and self-limiting wound-healing response to tissue damage that leads to deposition of extracellular matrix (ECM) components within the liver (Pellicoro et al., 2014). In chronic liver injury, such as HBV infection, fibrosis can become dysregulated, causing an imbalance between ECM deposition and degradation (Xu et al., 2012; Pellicoro et al., 2014). Excessive ECM deposition in the liver alters tissue function and elicits liver scaring that ultimately leads to cirrhosis (Friedman, 2008; Pellicoro et al., 2014). Previously, it has been observed that fibrosis in HBV transgenic mice is accelerated (Jin et al., 2011). Therefore, the long-term consequences of HBV-induced inhibition of insulin receptor signaling on liver regeneration were investigated in HBV transgenic mice using CCl_4. Long-term CCl_4 treatment is experimentally used to induce liver fibrosis in rodents (Constandinou et al., 2005). CCl_4 treatment over 7 weeks evokes severe liver damage as indicated by altered liver morphology and increased transaminase activity in both, WT and HBV transgenic mice (**Fig. 5.21**). However, liver damage is significantly stronger in HBV transgenic mice as observed by elevated transaminase activity in the serum compared to WT mice (**Fig. 5.21 B**). This is further corroborated on the histological level where liver sections of HBV transgenic also show intensified cell death as compared to the livers of WT mice, causing increased transaminase activity in the serum of HBV transgenic mice (**Fig. 5.23**). Increased serum bilirubin levels also indicate liver damage and impaired liver function (Gowda et al., 2009). Interestingly, the levels of bilirubin in the serum of WT and HBV transgenic mice after long-term CCl_4 treatment remain unaffected (*not shown*). This indicates that

besides increased liver damage, sufficient functional liver tissue is still present. Fibrosis is normally preceded by inflammation (Pellicoro et al., 2014). As depicted in **Fig. 5.22**, an inflammatory response characterized by infiltration of small-nucleated leukocytes into the liver is indeed observable in WT and HBV transgenic mice after long-term liver damage. Consequently, detection of fibrotic markers such as collagen and α-SMA in the liver of WT and HBV transgenic mice confirms induction of fibrosis by long-term CCl_4 treatment (**Fig. 5.24** and **Fig. 5.25**). Most importantly, HBV transgenic mice reveal more pronounced liver fibrosis than WT mice as reflected by significantly increased deposition of collagen (**Fig. 5.24**) and α-SMA (**Fig. 5.25**). Collectively, these observations imply that HBV transgenic mice exhibit increased liver damage and more pronounced liver fibrosis after long-term liver damage and inflammation than WT mice. It can be concluded that the inhibition of proliferative insulin receptor signaling in hepatocytes from HBV transgenic mice, in combination with sensitization to apoptosis, impairs liver regeneration, so that tissue recovery is counteracted by the replacement of parenchymal hepatocytes by pro-fibrogenic myofibroblasts which initiate liver fibrosis and cause ECM deposition after long-term liver damage. This is in line with the *in vitro* data as well as the *in vivo* data from short-term CCl_4 treatment.

6.4 HBV and diabetes

Taking into consideration that HBV-expressing cells present impaired glucose uptake and reduced insulin sensitivity and that HBV transgenic mice show increased blood glucose levels, one could speculate that chronic HBV patients are at risk to develop type 2 diabetes. Interestingly, the studies on chronic HBV

infection and insulin resistance are conflicting with no clear correlation between HBV infection status and risk of type 2 diabetes (Zhang et al., 2015; Shen et al., 2015). In can be assumed that for regulation of blood glucose levels in mice the liver plays a more critical role than in humans where skeletal muscle, adipose tissue and kidney are more relevant for the regulation of blood glucose levels than the liver (Mårin et al., 1987; Cersosimo et al., 1999; Meyer et al., 2002; Marsenic 2009). In addition, while in HBV transgenic mice every hepatocyte is supposed to express the HBV genome, in chronic HBV infection not every hepatocyte is infected. Hence, the impact of impaired insulin receptor signaling on the glucose uptake in HBV-infected hepatocytes of chronic HBV patients could not become apparent. Nevertheless, elevated blood glucose levels in HBV transgenic mice confirm that insulin receptor signaling is inhibited by HBV and has pathophysiological relevance with respect to liver regeneration. It can therefore be hypothesized that impairment of insulin receptor signaling in HBV-infected cells creates a situation which is not sufficient to establish a diabetic phenotype in chronic HBV patients, but promotes fibrogenesis and liver disease progression by interruption of hepatocyte proliferation and liver regeneration.

6.5 Conclusion and future perspectives

Taken together, in this thesis it was initially observed that HBV transgenic mice reveal prolonged liver damage and impaired liver regeneration after liver injury as a consequence of diminished insulin binding and insulin receptor activation. Furthermore, long-term liver damage induces increased fibrosis in HBV transgenic mice. Consequently, it was the principal goal of this thesis to clarify the molecular

mechanisms that are responsible for these observations. It was further observed that HBV-expressing cells *in vitro* reveal increased expression of insulin receptor by HBV-dependent Nrf2 activation, but simultaneously reduced amounts of insulin receptors on the cell surface which are causative for impaired insulin binding. Due to elevated amounts of the cellular trafficking factor α-taxilin in HBV-expressing cells, the insulin receptor is intracellularly retained which leads to the reduction of functional insulin receptors on the cells surface and diminished insulin sensitivity. By this, HBV-expressing cells fail to respond to insulin stimulation and are uncoupled from proliferative signals that promote hepatocyte proliferation and liver regeneration *in vivo* (**Fig. 6.1**). Future studies need to address whether a functional knock-down of α-taxilin in HBV-expressing cells is able to reverse HBV-dependent insulin receptor retention. Furthermore, the exact intracellular localization of the insulin receptor in HBV-expressing cells could also be investigated by confocal immunofluorescence studies using ER- and Golgi-specific antibodies or fluorescent fusion-proteins of compartment-specific markers. Since expression and translocation of IGF-IR is not affected by HBV, it is debatable why the inhibition of insulin receptor signaling due to loss of functional insulin receptor on the cell surface is not compensated by IGF-IR signaling in HBV-expressing cells. This also needs to be addressed in future studies. With respect to fibrosis progression after long-term CCl_4 treatment, differentially upregulated expression of several marker genes could be checked by qRT-PCR in the liver of WT and HBV transgenic mice. These could include genes such as TGF-β, fibronectin, tissue inhibitor of metalloproteinase (TIMP)-1 and matrix metalloproteinase (MMP)-2 (Jin et al., 2011). Increased presence of fibrosis-promoting HSCs in HBV transgenic

mice may be detected by immunohistochemical staining of glial fibrillary acidic protein (GFAP), which is a specific marker for those cells (Pellicoro et al., 2014). Beside the detection of reduced tyrosine phosphorylation of the insulin receptor, other downstream targets could be analyzed for reduced activating tyrosine phosphorylation in HBV-expressing cells upon insulin stimulation, such as IRS proteins or PKB/Akt. *Vice versa*, inhibitory serine phosphorylation of IRS proteins is supposed to be increased in HBV-expressing cells and could also be quantified experimentally. In addition, it would be worthwhile to determine differences in the expression of cell-cycle dependent genes upon insulin stimulation in HBV-expressing cells in contrast to HBV-negative cells to further confirm inhibition of insulin-stimulated hepatocyte proliferation. The interplay between apoptosis and proliferation in HBV-expressing hepatocytes should be investigated for their respective contribution to increased liver damage and impairment of liver regeneration. In addition, it would be of great interest to investigate the effect of HBV on liver regeneration and pathogenesis in a more physiological context with respect to inflammation and immune-mediated liver damage, such as the autoimmune hepatitis model in HBV transgenic mice or a mouse model of natural HBV infection in immunocompetent mice. Unfortunately, such a model to naturally infect mice with HBV is not available at this time. Finally, it would be tempting to analyze the application of insulin sensitizers (e.g. thiazolidinediones) for their therapeutic potential to mitigate insulin resistance and to improve insulin sensitivity and liver regeneration in HBV transgenic mice as well as in patients suffering from chronic HBV.

Altogether, this thesis highlights a hitherto unprecedented as well as physiological relevant pathomechanism by which HBV inactivates insulin receptor signaling and impairs liver regeneration to promote liver damage and fibrosis. These findings provide valuable insights into a better understanding of HBV-associated liver pathogenesis.

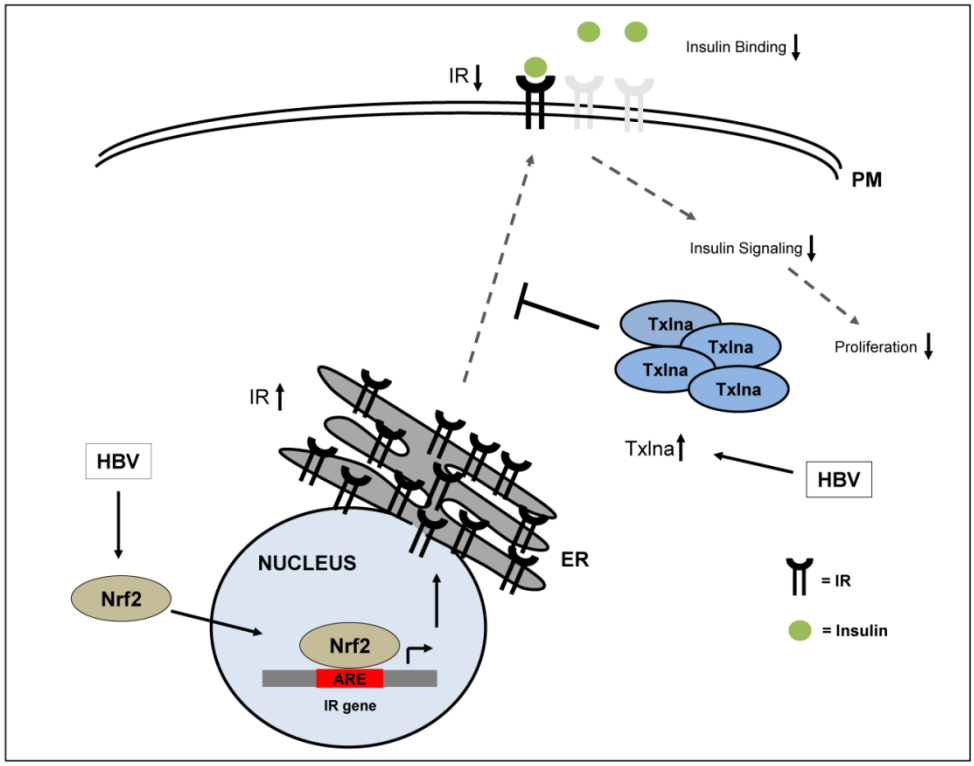

Fig. 6.1: Schematic representation of HBV-induced insulin receptor retention. HBV induces activation of Nrf2 which translocates to the nucleus and activates ARE-mediated expression of the insulin receptor (*IR*). In parallel, HBV also induces increased amounts of α-taxilin (Txlna) which prevent insulin receptor translocation to the plasma membrane (PM), resulting in an accumulation of the insulin receptor at the ER. Reduced amounts of the insulin receptor at the plasma membrane attenuate insulin binding and lead to the inhibition of insulin receptor signaling and retardation of hepatocyte proliferation.

7 Summary

Hepatitis B caused by infection with the hepatitis B virus (HBV) still ranks among the most challenging infectious diseases of our time. Despite the availability of an effective prophylactic vaccine, 240 million people worldwide are estimated to be chronically infected with HBV and are at risk of developing life-threatening liver diseases, including cirrhosis and liver cancer. The underlying pathogenic mechanisms of HBV-associated liver diseases are only incompletely understood. It is widely accepted that liver pathology results from long-term immune-mediated liver injury and inflammation as a consequence of inefficient viral elimination. This injury can be naturally compensated by liver regeneration. However, chronic liver damage and permanent inflammation debilitates the regenerative capacity of the liver and fosters fibrosis as well as accumulation of chromosomal aberrations, which both contribute to cirrhosis and liver cancer. Liver regeneration requires the presence of the redox-sensitive transcription factor Nrf2 and intact insulin receptor signaling. A lack of Nrf2 causes increased intracellular levels of reactive oxygen species (ROS) that inactivate insulin receptor signaling and induce insulin resistance. Interestingly, HBV was observed to activate Nrf2 and the expression of Nrf2-regulated genes. This argues against an inhibitory effect of HBV on insulin receptor signaling by increased ROS levels. However, chronic HBV infection is associated with dysregulation of hepatocyte proliferation and retardation of liver regeneration. Hence, the aim of this thesis was to investigate the influence of HBV on the process of liver regeneration with respect to the insulin receptor signaling pathway. After short-term carbon tetrachloride (CCl_4)-induced liver damage, HBV

transgenic mice present prolonged liver damage and impaired liver regeneration as reflected by reduced hepatocyte proliferation and increased apoptosis. Impaired hepatocyte proliferation in HBV transgenic mice correlates with diminished activation of the insulin receptor. It was further observed *in vitro* that the activation of Nrf2 by HBV induces increased levels of the insulin receptor mRNA and protein in HBV-expressing cells. Strikingly, stably HBV-expressing cells as well as primary mouse hepatocytes from HBV transgenic mice bind less insulin due to reduced amounts of insulin receptor on the cell surface. This is caused by intracellular retention of the insulin receptor in HBV-expressing cells as a consequence of increased amounts of the cellular trafficking factor α-taxilin. The reduced amounts of insulin receptor on the cell surface impair insulin sensitivity in HBV-expressing cells and inactivate downstream signaling cascades that initiate insulin-dependent gene expression and glucose uptake. As a consequence of impaired hepatocyte proliferation and liver regeneration, HBV transgenic mice exhibit increased development of fibrosis after long-term CCl_4-induced liver damage. Taken together, in this thesis, a novel pathomechanism could be uncovered that includes inactivation of insulin receptor signaling by HBV *via* intracellular retention of the insulin receptor leading to impaired liver regeneration after liver damage and promotion of liver fibrosis. These findings significantly contribute to an enhanced understanding of HBV-associated liver pathogenesis.

8 Zusammenfassung

Das Hepatitis-B-Virus (HBV) ist ein behülltes DNA-Virus aus der Familie der *Hepadnaviridae*. Es trägt ein partiell doppelsträngiges DNA-Genom mit einer Länge von 3200 Nukleotiden, welches für sieben virale Proteine kodiert. Nach einer parenteralen Infektion gelangt das Virus zur Leber und infiziert spezifisch Hepatozyten. Eine Infektion mit HBV evoziert eine Entzündung (Hepatitis) der Leber, die akut oder chronisch verlaufen kann. Hepatitis B ist weltweit immer noch eine der bedeutsamsten Infektionskrankheiten. Trotz eines prophylaktischen Impfstoffes, der effektiv vor einer Infektion schützen kann, wird angenommen, dass weltweit ca. 2 Milliarden Menschen aktuell mit HBV infiziert sind oder Anzeichen einer vergangenen Infektion aufweisen. Laut Schätzungen der WHO sind von dieser Zahl ungefähr 240 Millionen Menschen chronisch mit HBV infiziert. Eine chronische Hepatitis-B-Infektion ist die Ursache für schwerwiegende und letale Lebererkrankungen, wie z. B. Leberzirrhose oder Leberkrebs (hepatozelluläres Karzinom). Trotz verfügbarer antiviraler Therapeutika sterben jährlich ca. 780.000 Menschen an den Folgen der chronischen Hepatitis B. Die genauen Mechanismen der HBV-assoziierten Pathogenese sind bisher nicht vollständig verstanden. Da HBV selbst nicht zytopathogen ist, geht man davon aus, dass das Immunsystem des Wirtes für die Schädigung des Lebergewebes verantwortlich ist, indem es versucht, das Virus zu eliminieren. Bei der chronischen HBV-Infektion bleibt jedoch eine vollständige Eliminierung des Virus durch das Immunsystem aus und es manifestiert sich eine dauerhafte Entzündung der Leber, die das Entstehen einer Lebererkrankung begünstigt. Geschädigtes

Lebergewebe kann zwar durch den Prozess der Leberregeneration wiederhergestellt werden, die langjährige, chronische Schädigung und permanente Entzündung der Leber vermindert jedoch deren Regenerationsfähigkeit und fördert eine Fibrosierung der Leber. Hierbei wird funktionelles Lebergewebe sukzessive durch nichtfunktionelles Binde- und Narbengewebe als Form der Wundheilung ersetzt. Das klinische Endstadium dieses Prozesses ist die Leberzirrhose, bei der die Leber nahezu ihre komplette Funktion verloren hat und überwiegend aus vernarbtem Gewebe besteht. Das Auftreten einer Leberzirrhose begünstigt um ein Vielfaches die Entstehung eines hepatozellulären Karzinoms. Für die Leberregeneration sind die Funktion des zytoprotektiven und redoxsensitiven Transkriptionsfaktors Nrf2 sowie ein intakter Insulinrezeptor-Signalweg unabdingbar. Interessanterweise wurde beobachtet, dass HBV in der Lage ist, diesen Transkriptionsfaktor zu aktivieren und dadurch verstärkt die Expression Nrf2-regulierter Gene zu induzieren. Nrf2-regulierte Gene kodieren für Proteine und Enzyme, die dazu befähigt, sind reaktive Sauerstoffspezies (ROS) zu detoxifizieren und so die Zelle vor oxidativem Stress zu schützen. Bei Fehlen von Nrf2 verursachen erhöhte ROS-Konzentrationen in der Zelle oxidativen Stress, welcher über die Aktivierung von entsprechenden Stress-aktivierten Kinasen (z. B. c-Jun N-terminale Kinasen (JNK)) zu einer Inaktivierung des Insulinrezeptor-Signalweges und zu einer Insulinresistenz führt. Die Aktivierung von Nrf2 durch HBV spricht dabei gegen einen inhibitorischen Effekt durch erhöhte ROS-Konzentration auf den Insulinrezeptor-Signalweg in HBV-exprimierenden Zellen. Dennoch ist bekannt, dass HBV mit dem Prozess der Leberregeneration negativ interferiert und dadurch zusätzlich deren

Regenerationsfähigkeit beeinträchtigt. Berücksichtigt man die Relevanz von Nrf2 für die Leberregeneration und den Insulinrezeptor-Signalweg, erscheint dies zunächst widersprüchlich. Hiervon ausgehend war daher das Ziel der vorliegenden Dissertation die Untersuchung des Einflusses von HBV auf den Prozess der Leberregeneration unter besonderer Berücksichtigung des hepatischen Insulinrezeptor-Signalweges. Zunächst wurden HBV-transgene sowie entsprechende Wildtyp-Mäuse mit dem Lebertoxin Tetrachlorkohlenstoff (CCl_4) behandelt, um eine Schädigung der Leber zu evozieren und den Einfluss von HBV auf den Regenerationsprozess *in vivo* zu untersuchen. Hierbei zeigte sich, dass in HBV-transgenen Mäusen im Vergleich zu Wildtyp-Mäusen eine länger anhaltende Schädigung der Leber zu beobachten ist (**Abb. 5.3**). Ursächlich dafür ist eine verminderte Zellproliferation der Hepatozyten nach Leberschädigung und damit verbunden eine verringerte Regenerationsfähigkeit der Leber in HBV-transgenen Mäusen (**Abb. 5.5**). Ergänzend dazu findet sich in der Leber HBV-transgener Mäuse unmittelbar nach Schädigung eine höhere Anzahl apoptotischer Zellen im Vergleich zum Wildtyp (**Abb. 5.4**). Diese Ergebnisse deuten darauf hin, dass nach einer Schädigung die Leberregeneration in HBV-transgenen Mäusen durch eine verminderte Zellproliferation und eine erhöhte Apoptose beeinträchtigt ist. Um einen möglichen Einfluss von HBV auf den Insulinrezeptor-Signalweg während der Leberregeneration zu untersuchen, wurde das Ausmaß der Tyrosin-Phosphorylierung bei Insulinrezeptor-Aktivierung bestimmt. Hierbei zeigte sich, dass Hepatozyten von HBV-transgenen Mäusen unmittelbar nach Leberschädigung eine verringerte Insulinrezeptor-Aktivierung aufweisen im Vergleich zu entsprechend behandelten Wildtyp-Mäusen (**Abb. 5.6**).

Interessanterweise ist aus vorhergehenden Arbeiten bekannt, dass HBV-exprimierende Zellen *in vivo* und *in vitro* erhöhte Proteinmengen des Insulinrezeptors aufweisen. In dieser Arbeit konnte auf transkriptioneller Ebene in stabil HBV-exprimierenden Zellen (HepAD38, HepG2.2.15) eine Induktion des Insulinrezeptor-Gens nachgewiesen werden (**Abb. 5.7**). Verantwortlich für die verstärkte Expression des Insulinrezeptors ist dabei die erhöhte Aktivität von Nrf2 in HBV-exprimierenden Zellen und die Anwesenheit eines sog. *antioxidant response elements* (ARE) in der Promoterregion des Insulinrezeptor-Gens, welches für die Nrf2-abhängige Genexpression erforderlich ist (**Abb. 5.9**, **5.10** und **5.11**). Trotz der erhöhten Mengen des Insulinrezeptors wurde beobachtet, dass stabil HBV-exprimierende Zellen wie auch primäre Maushepatozyten aus HBV-transgenen Mäusen weniger Insulin binden als entsprechende HBV-negative Kontrollzellen (**Abb. 5.12**). Ursächlich für diesen Befund ist eine verringerte Anzahl an Insulinrezeptoren auf der Zelloberfläche von HBV-exprimierenden Hepatozyten (**Abb. 5.13** und **5.14**). Es konnte in dieser Arbeit beobachtet werden, dass der Insulinrezeptor in HBV-exprimierenden Zellen intrazellulär zurückgehalten und daher nicht an die Zelloberfläche transloziert wird (**Abb. 5.16**). Weiterhin konnte beobachtet werden, dass erhöhte Mengen des Proteins α-Taxilin an der intrazellulären Retention des Insulinrezeptors beteiligt sind (**Abb. 5.17**). α-Taxilin ist ein Protein, das bei intrazellulären Transportprozessen eine Rolle spielt und einen negativen regulatorischen Effekt auf den SNARE-vermittelten Vesikeltransport zur Plasmamembran hat. Es ist zudem bekannt, dass HBV die Expression von α-Taxilin induziert. Als Folge der reduzierten Menge des Insulinrezeptors an der Zelloberfläche und der damit verbundenen verringerten

Insulinbindung ist die Insulinsensitivität HBV-exprimierender Zellen herabgesenkt, was durch eine verringerte Insulinrezeptor-Aktivierung durch Tyrosin-Phosphorylierung sowohl *in vivo* (**Abb. 5.6**) als auch *in vitro* (**Abb. 5.18**) bestätigt wird. Zusätzlich ist die Expression des insulin-abhängigen Glucokinase-Gens nach Insulin-Stimulierung in stabil-exprimierenden Zellen vermindert (**Abb. 5.19**) und die Zellen weisen eine verringerte Basal-Expression des Glucosetransporters 4 (GLUT4) auf (**Abb. 5.20**). Bei einer Langzeit-Behandlung von HBV-transgenen und Wildtyp-Mäusen mit CCl_4 zeigen HBV-transgene Mäuse eine höhere Leberschädigung anhand von signifikant erhöhten Transaminase-Werten im Serum (**Abb. 5.21**). Durch die Langzeit-Behandlung mit CCl_4 kann eine Leberfibrose induziert werden, gekennzeichnet durch die Ablagerung von extrazellulären Matrixproteinen wie z. B. Collagen und *alpha-smooth muscle actin* (α-SMA). HBV-transgene Mäuse zeigen dabei signifikant höhere Mengen an Collagen und α-SMA in der Leber im Vergleich zu Wildtyp-Mäusen nach CCl_4-Langzeitbehandlung (**Abb. 5.24** und **5.25**). Dieser Befund deutet auf eine verstärkte Fibrosierung der Leber von HBV-transgenen Mäusen aufgrund einer verminderten Regenerationsfähigkeit im Vergleich zu Wildtyp-Mäusen hin. Zusammengefasst konnte in dieser Arbeit aufgeklärt werden, dass HBV über die erhöhte Aktivität von Nrf2 die Expression des Insulinrezeptors induziert, und damit zu einer erhöhten Proteinmenge des Rezeptors führt. Der Insulinrezeptor wird jedoch durch die erhöhten Mengen an α-Taxilin in HBV-exprimierenden Zellen intrazellulär zurückgehalten, sodass dieser nicht an die Zelloberfläche gelangen kann. Dadurch ist die Bindung von Insulin vermindert, was eine verringerte Insulinrezeptor-Aktivierung und eine verringerte Expression insulin-abhängiger

Gene zur Folge hat. Durch die intrazelluläre Retention des Insulinrezeptors werden HBV-exprimierende Hepatozyten von mitogenen Signalwegen wie dem Insulinrezeptor-Signalweg abgekoppelt und weisen dadurch ein eingeschränktes Proliferationsverhalten auf. Hierdurch wird die Leberregeneration nach einer Leberschädigung inhibiert, was wiederum die Fibrosierung der Leber und dadurch die Entwicklung schwerwiegender Lebererkrankungen begünstigt. Die Ergebnisse dieser Arbeit tragen zu einem besseren Verständnis des Einflusses von HBV auf die Leberpathogenese der chronischen Hepatitis B bei.

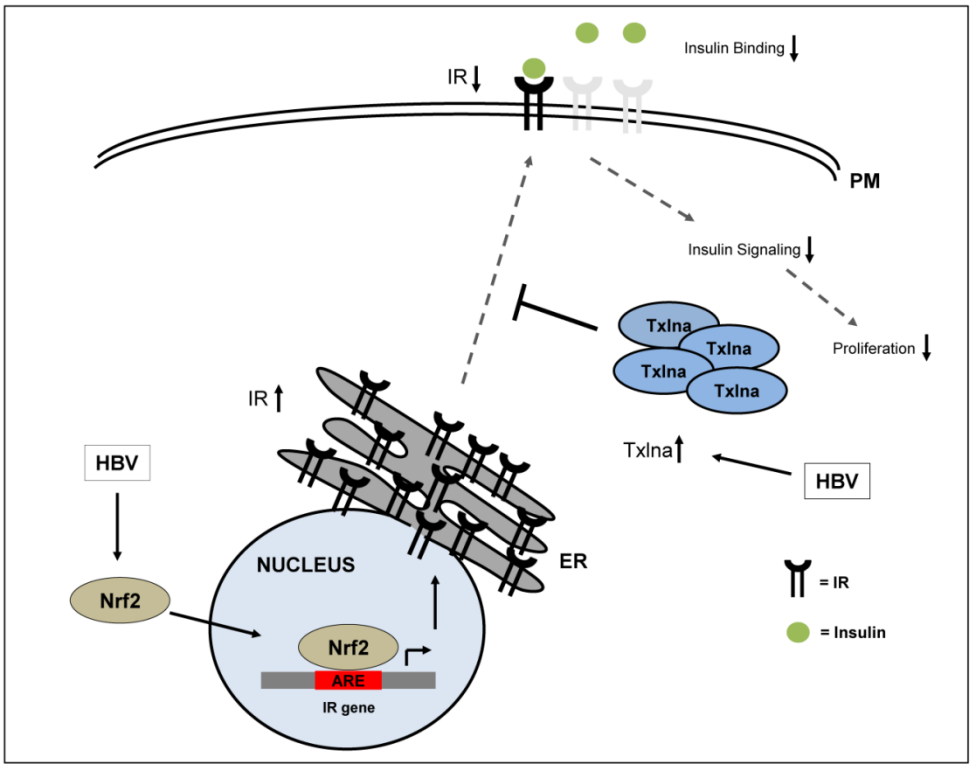

Abb.8.1. Schematische Darstellung der HBV-induzierten Insulinrezeptor-Retention. HBV induziert die Aktivierung von Nrf2, welches im Zellkern die ARE-vermittelte Expression des Insulinrezeptors (IR) aktiviert. Parallel dazu induziert HBV die verstärkte Expression von α-Taxilin (Txlna), welche die intrazellulare Retention und Akkumulation des IR vermittelt. Die verminderte Menge des IR an der Zelloberfläche führt zu einer verminderten Insulinbindung, einer Inhibition des Insulinrezeptor-Signalweges und damit einhergehend einer verringerten Zellproliferation.

9 References

Alberstein M, Zornitzki T, Zick Y, Knobler H. 2012. Hepatitis C core protein impairs insulin downstream signalling and regulatory role of IGFBP-1 expression. *J Viral Hepat.* **19**: 65–71.

Aleksunes LM, Manautou JE. 2007. Emerging role of Nrf2 in protecting against hepatic and gastrointestinal disease. *Toxicol Pathol.* **35**: 459–473.

Amaya MJ, Oliveira AG, Guimarães ES, Casteluber MCF, Carvalho SM, Andrade LM, Pinto MCX, Mennone A, Oliveira CA, Resende RR, Menezes GB, Nathanson MH, Leite MF. 2014. The insulin receptor translocates to the nucleus to regulate cell proliferation in liver. *Hepatology (Baltimore, Md.)* **59**: 274–283.

Ananthanarayanan M, Ng OC, Boyer JL, Suchy FJ. 1994. Characterization of cloned rat liver Na(+)-bile acid cotransporter using peptide and fusion protein antibodies. *Am J Physiol.* **267**: G637-643.

Anderson EJ, Lustig ME, Boyle KE, Woodlief TL, Kane DA, Lin C, Price JW, Kang L, Rabinovitch PS, Szeto HH, Houmard JA, Cortright RN, Wasserman DH, Neufer PD. 2009. Mitochondrial H2O2 emission and cellular redox state link excess fat intake to insulin resistance in both rodents and humans. *J Clin Invest.* **119**: 573–581.

Arndt T, Gressner AM. 2013. Lexikon der Medizinischen Laboratoriumsdiagnostik. *Berlin, Springer-Verlag*.

auf dem Keller U, **Huber M, Beyer TA, Kümin A, Siemes C, Braun S, Bugnon P, Mitropoulos V, Johnson DA, Johnson JA, Hohl D, Werner S.** 2006. Nrf transcription factors in keratinocytes are essential for skin tumor prevention but not for wound healing. *Mol Cell Biol.* **26**: 3773–3784.

Authier F, Rachubinski RA, Posner BI, Bergeron JJ. 1994. Endosomal proteolysis of insulin by an acidic thiol metalloprotease unrelated to insulin degrading enzyme. *J Biol Chem.* **269**: 3010–3016.

Banerjee S, Saito K, Ait-Goughoulte M, Meyer K, Ray RB, Ray R. 2008. Hepatitis C virus core protein upregulates serine phosphorylation of insulin receptor substrate-1 and impairs the downstream akt/protein kinase B signaling pathway for insulin resistance. *J Virol.* **82**: 2606–2612.

Bartenschlager R, Schaller H. 1988. The amino- terminal domain of the hepadnaviral P-gene encodes the terminal protein (genome-linked protein) believed to prime reverse transcription. *EMBO J.* **7**: 4185–4192.

Beasley RP. 1988. Hepatitis B virus. The major etiology of hepatocellular carcinoma. *Cancer* **61**: 1942–1956.

Beck J, Nassal M. 2007. Hepatitis B virus replication. *World J Gastroenterol.* **13**: 48–64.

Belfiore A, Frasca F, Pandini G, Sciacca L, Vigneri R. 2009. Insulin receptor isoforms and insulin receptor/insulin-like growth factor receptor hybrids in physiology and disease. *Endocr Rev.* **30**: 586–623.

Benn J, Schneider RJ. 1994. Hepatitis B virus HBx protein activates Ras-GTP complex formation and establishes a Ras, Raf, MAP kinase signaling cascade. *Proc Natl Acad Sci USA* **91**: 10350–10354.

Besse-Patin A, Estall JL. 2014. An Intimate Relationship between ROS and Insulin Signalling: Implications for Antioxidant Treatment of Fatty Liver Disease. *Int J Cell Biol.* **2014**: 519153.

Beyer TA, Werner S. 2008a. The cytoprotective Nrf2 transcription factor controls insulin receptor signaling in the regenerating liver. *Cell Cycle* **7**: 874–878.

Beyer TA, Xu W, Teupser D, auf dem Keller, Ulrich, **Bugnon P, Hildt E, Thiery J, Kan YW, Werner S.** 2008b. Impaired liver regeneration in Nrf2 knockout mice: role of ROS-mediated insulin/IGF-1 resistance. *EMBO J.* **27**: 212–223.

Bhatia M, Karlenius TC, Di Trapani G, Tonissen K. 2013. The Interaction Between Redox and Hypoxic Signalling Pathways in the Dynamic Oxygen Environment of Cancer Cells. *In: Carcinogenesis:* **Chapter 7**: p. 125–152.

Birnboim HC, Doly J. 1979. A rapid alkaline extraction procedure for screening recombinant plasmid DNA. *Nucleic Acids Res.* **7**: 1513–1523.

Bissig K, Wieland SF, Tran P, Isogawa M, Le TT, Chisari FV, Verma IM. 2010. Human liver chimeric mice provide a model for hepatitis B and C virus infection and treatment. *J Clin Invest.* **120**: 924–930.

Blight KJ, McKeating JA, Rice CM. 2002. Highly permissive cell lines for subgenomic and genomic hepatitis C virus RNA replication. *J Virol.* **76**: 13001–13024.

Blumberg BS. 2002. Hepatitis B: The hunt for a killer virus. *Princeton University Press*.

Blumberg BS, Alter HJ, Visnich SA. 1965. "New" antigen in Leukemia Sera. *JAMA* **191**: 242–275.

Bock C, Schwinn S, Locarnini S, Fyfe J, Manns MP, Trautwein C, Zentgraf H. 2001. Structural organization of the hepatitis B virus minichromosome. *J Mol Biol.* **307**: 183–196.

Bock CT, Schranz P, Schröder CH, Zentgraf H. 1994. Hepatitis B virus genome is organized into nucleosomes in the nucleus of the infected cell. *Virus Genes* **8**: 215–229.

Böhm F, Köhler UA, Speicher T, Werner S. 2010. Regulation of liver regeneration by growth factors and cytokines. *EMBO Mol Med.* **2**: 294–305.

Böhmer F. 1865. Zur pathologischen Anatomie der Meningitis cerebromedularis epidemica. *Aerztl Intelligenzb (Munich)* **12**: 539–550.

Bose SK, Shrivastava S, Meyer K, Ray RB, Ray R. 2012. Hepatitis C virus activates the mTOR/S6K1 signaling pathway in inhibiting IRS-1 function for insulin resistance. *J Virol.* **86**: 6315–6322.

Bouchard MJ, Schneider RJ. 2004. The enigmatic X gene of hepatitis B virus. *J Virol.* **78**: 12725–12734.

Boura-Halfon S, Zick Y. 2009. Phosphorylation of IRS proteins, insulin action, and insulin resistance. *Am J Physiol Endocrinol Metab.* **296**: E581-91.

Bouskila M, Hunter RW, Ibrahim AF, Delattre L, Peggie M, van Diepen JA, Voshol PJ, Jensen J, Sakamoto K. 2010. Allosteric regulation of glycogen synthase controls glycogen synthesis in muscle. *Cell Metab.* **12**: 456–466.

Bradford MM. 1976. A rapid and sensitive method for the quantitation of microgram quantities of protein utilizing the principle of protein-dye binding. *Anal Biochem.* **72**: 248–254.

Brady MJ, Nairn AC, Saltiel AR. 1997. The regulation of glycogen synthase by protein phosphatase 1 in 3T3-L1 adipocytes. Evidence for a potential role for DARPP-32 in insulin action. *J Biol Chem.* **272**: 29698–29703.

Brandenburg B, Stockl L, Gutzeit C, Roos M, Lupberger J, Schwartlander R, Gelderblom H, Sauer IM, Hofschneider PH, Hildt E. 2005. A novel system for efficient gene transfer into primary human hepatocytes via cell-permeable hepatitis B virus-like particle. *Hepatology* **42**: 1300–1309.

Brechot C, Pourcel C, Louise A, Rain B, Tiollais P. 1980. Presence of integrated hepatitis B virus DNA sequences in cellular DNA of human hepatocellular carcinoma. *Nature* **286**: 533–535.

Bruns M, Miska S, Chassot S, Will H. 1998. Enhancement of Hepatitis B Virus Infection by Noninfectious Subviral Particles. *J Virol.* **72**: 1462–1468.

Bruss V. 2007. Hepatitis B virus morphogenesis. *World J Gastroenterol.* **13**: 65–73.

Carpentier JL. 1994. Insulin receptor internalization: molecular mechanisms and physiopathological implications. *Diabetologia* **37**: S117-124.

Carpentier JL, Fehlmann M, van Obberghen E, Gorden P, Orci L. 1985. Insulin receptor internalization and recycling: mechanism and significance. *Biochimie* **67**: 1143–1145.

Carvajal-Yepes M, Himmelsbach K, Schaedler S, Ploen D, Krause J, Ludwig L, Weiss T, Klingel K, Hildt E. 2011. Hepatitis C virus impairs the induction of cytoprotective Nrf2 target genes by delocalization of small Maf proteins. *J Biol Chem.* **286**: 8941–8951.

Cersosimo E, Garlick P, Ferretti J. 1999. Insulin regulation of renal glucose metabolism in humans. *Am J Physiol Endocrinol Metab.* **276**: E78-E84.

Chan K, Han XD, Kan YW. 2001. An important function of Nrf2 in combating oxidative stress: detoxification of acetaminophen. *Proc Natl Acad Sci USA* **98**: 4611–4616.

Chang JJ, Lewin SR. 2007. Immunopathogenesis of hepatitis B virus infection. *Immunol Cell Biol.* **85**: 16–23.

Cheng J, Han Y, Jiang J. 2014. Establishment of drug-resistant HBV small-animal models by hydrodynamic injection. *Acta Pharm Sin B.* **4**: 270–276.

Chisari FV, Isogawa M, Wieland SF. 2010. Pathogenesis of hepatitis B virus infection. *Pathol Biol. (Paris)* **58**: 258–266.

Constandinou C, Henderson N, Iredale JP. 2005. Modeling liver fibrosis in rodents. *Methods Mol Med.* **117**: 237–250.

Cornberg M, Protzer U, Petersen J, Wedemeyer H, Berg T, Jilg W, Erhardt A, Wirth S, Sarrazin C, Dollinger MM, Schirmacher P, Dathe K, Kopp IB, Zeuzem S, Gerlich WH, Manns MP. 2011. Aktualisierung der S 3-Leitlinie zur Prophylaxe, Diagnostik und Therapie der Hepatitis-B-Virusinfektion. *Z Gastroenterol.* **49**: 871–930.

Cressman DE, Diamond RH, Taub R. 1995. Rapid activation of the stat3 transcription complex in liver regeneration. *Hepatology* **21**: 1443–1449.

Cross DA, Alessi DR, Cohen P, Andjelkovich M, Hemmings BA. 1995. Inhibition of glycogen synthase kinase-3 by insulin mediated by protein kinase B. *Nature* **378**: 785–789.

Dane DS, Cameron CH, Briggs M. 1970. Virus-like particles in serum of patients with Australia-antigen-associated hepatitis. *Lancet* **1**: 695–698.

Dayoub R, Vogel A, Schuett J, Lupke M, Spieker SM, Kettern N, Hildt E, Melter M, Weiss TS. 2013. Nrf2 activates augmenter of liver regeneration (ALR) via antioxidant response element and links oxidative stress to liver regeneration. *Mol Med.* **19**: 237–244.

Deng C, Chen RR. 2004. A pH-sensitive assay for galactosyltransferase. *Anal Biochem.* **330**: 219–226.

Devarajan T, Jeyabalan S. 2014. Biotechnology and Bioinformatics: Advances and Applications for Bioenergy, Bioremediation and Biopharmaceutical Research. *CRC Press*.

Diehl AM. 2002. Liver regeneration. *Front Biosci.* **7**: e301-314.

Döhner K, Sodeik B. 2005. The role of the cytoskeleton during viral infection. *Curr Top Microbiol Immunol.* **285**: 67–108.

Dong Z, Zhang J, Sun R, Wei H, Tian Z. 2007. Impairment of liver regeneration correlates with activated hepatic NKT cells in HBV transgenic mice. *Hepatology* **45**: 1400–1412.

Drew JS, London WT, Lustbader E, Hesse JE, Blumberg BS. 1978. Hepatitis B virus and sex ratio of offring. *Science* **201**: 687–692.

Drexler JF, Geipel A, König A, Corman VM, van Riel D, Leijten LM, Bremer CM, Rasche A, Cottontail VM, Maganga GD, Schlegel M, Müller MA, Adam A, Klose SM, Carneiro, Aroldo José

Borges, **Stöcker A, Franke CR, Gloza-Rausch F, Geyer J, Annan A et al,.** 2013. Bats carry pathogenic hepadnaviruses antigenically related to hepatitis B virus and capable of infecting human hepatocytes. *Proc Natl Acad Sci USA* **110**: 16151–16156.

Du Y, Wei T. 2014. Inputs and outputs of insulin receptor. *Protein Cell.* **5**: 203–213.

Duckworth WC, Bennett RG, Hamel FG. 1998. Insulin degradation: progress and potential. *Endocr Rev.* **19**: 608–624.

Eckhardt SG, Milich DR, McLachlan A. 1991. Hepatitis B virus core antigen has two nuclear localization sequences in the arginine-rich carboxyl terminus. *J Virol.* **65**: 575–582.

Ehrhardt C, Schmolke M, Matzke A, Knoblauch A, Will C, Wixler V, Ludwig S. 2006. Polyethylenimine, a cost-effective transfection reagent. *Signal Transduct.* **6**: 179–184.

Enomoto A, Itoh K, Nagayoshi E, Haruta J, Kimura T, O'Connor T, Harada T, Yamamoto M. 2001. High Sensitivity of Nrf2 Knockout Mice to Acetaminophen Hepatotoxicity Associated with Decreased Expression of ARE-Regulated Drug Metabolizing Enzymes and Antioxidant Genes. *Toxicol Sci.* **59**: 169–177.

Fausto N. 2000. Liver regeneration. *J Hepatol.* **32**: 19–31.

Fausto N. 2004. Liver regeneration and repair: hepatocytes, progenitor cells, and stem cells. *Hepatology* **39**: 1477–1487.

Fehlmann M, Carpentier JL, van Obberghen E, Freychet P, Thamm P, Saunders D, Brandenburg D, Orci L. 1982. Internalized insulin receptors are recycled to the cell surface in rat hepatocytes. *Proc Natl Acad Sci USA* **79**: 5921–5925.

Fischer E. 1875. Eosin als Tinctionsmittel für mikroskopische Präparate. *Arch Mikrosk Anat.* **12**: 349–352.

FitzGerald MJ, Webber EM, Donovan, JR, Fausto N. 1995. Rapid DNA binding by nuclear factor kappa B in hepatocytes at the start of liver regeneration. *Cell Growth Differ.* **6**: 417–427.

Foretz M, Pacot C, Dugail I, Lemarchand P, Guichard C, Le Lièpvre X, Berthelier-Lubrano C, Spiegelman B, Kim JB, Ferré P, Foufelle F. 1999. ADD1/SREBP-1c Is Required in the Activation of Hepatic Lipogenic Gene Expression by Glucose. *Mol Cell Biol.* **19**: 3760–3768.

Forman HJ. 2010. Reactive oxygen species and alpha,beta-unsaturated aldehydes as second messengers in signal transduction. *Ann N Y Acad Sci.* **1203**: 35–44.

Friedman SL. 2008. Mechanisms of hepatic fibrogenesis. *Gastroenterology* **134**: 1655–1669.

Friedrich B, Wollersheim M, Brandenburg B, Foerste R, Will H, Hildt E. 2005. Induction of anti-proliferative mechanisms in hepatitis B virus producing cells. *J Hepatol.* **43**: 696–703.

Fu Z, R. Gilbert E, Liu D. 2012. Regulation of Insulin Synthesis and Secretion and Pancreatic Beta-Cell Dysfunction in Diabetes. *Curr Diabetes Rev.* **9**: 25–53.

Fung J, Lai C, Seto W, Yuen M. 2011. Nucleoside/nucleotide analogues in the treatment of chronic hepatitis B. *J Antimicrob Chemother.* **66**: 2715–2725.

Furukawa S, Fujita T, Shimabukuro M, Iwaki M, Yamada Y, Nakajima Y, Nakayama O, Makishima M, Matsuda M, Shimomura I. 2004. Increased oxidative stress in obesity and its impact on metabolic syndrome. *J Clin Invest.* **114**: 1752–1761.

Ganem D. 1991. Assembly of hepadnaviral virions and subviral particles. *Curr Top Microbiol Immunol.* **168**: 61–83.

Gao Z, Hwang D, Bataille F, Lefevre M, York D, Quon MJ, Ye J. 2002. Serine phosphorylation of insulin receptor substrate 1 by inhibitor kappa B kinase complex. *J Biol Chem.* **277**: 48115–48121.

Gerlich WH. 2013. Medical virology of hepatitis B: how it began and where we are now. *Virol J.* **10**: 239–263.

Gerlich WH, Kann M. 2005. Hepatitis B, p. 1226-1268. *In B. W. J. Mahy and V. ter Meulen (ed.), Topley and Wilson's microbiology and microbial infections, vol. 2. ASM Press, Washington, DC.*

Glebe D, König A. 2014. Molecular virology of hepatitis B virus and targets for antiviral intervention. *Intervirology* **57**: 134–140.

Goh LK, Sorkin A. 2013. Endocytosis of receptor tyrosine kinases. *Cold Spring Harb Perspect Biol.* **5**: a017459.

Goldstein BJ, Mahadev K, Wu X, Zhu L, Motoshima H. 2005. Role of insulin-induced reactive oxygen species in the insulin signaling pathway. *Antioxid Redox Signal.* **7**: 1021–1031.

Goncalves L, Albarran B, Salmen S, Borges L, Fields H, Montes H, Soyano A, Diaz Y, Berrueta L. 2004. The nonresponse to hepatitis B vaccination is associated with impaired lymphocyte activation. *Virology* **326**: 20–28.

Gowda S, Desai PB, Hull VV, Math AA, Vernekar SN, Kulkarni SS. 2009. A review on laboratory liver function tests. *Pan Afr Med J.* **17**: 15.

Guidotti LG, Chisari FV. 2006. Immunobiology and pathogenesis of viral hepatitis. *Annu Rev Pathol.* **1**: 23–61.

Guidotti LG, Matzke B, Schaller H, Chisari FV. 1995. High-level hepatitis B virus replication in transgenic mice. *J Virol.* **69**: 6158–6169.

Guo H, Mason WS, Aldrich CE, Saputelli, JR, Miller DS, Jilbert AR, Newbold JE. 2005. Identification and characterization of avihepadnaviruses isolated from exotic anseriformes maintained in captivity. *J Virol.* **79**: 2729–2742.

Guo S. 2014. Insulin signaling, resistance, and the metabolic syndrome: insights from mouse models into disease mechanisms. *J Endocrinol.* **220**: T1-T23.

Hafner A, Brandenburg B, Hildt E. 2003. Reconstitution of gene expression from a regulatory-protein-deficient hepatitis B virus genome by cell-permeable HBx protein. *EMBO Rep.* **4**: 767–773.

Halegoua-De Marzio D, Hann H. 2014. Then and now: the progress in hepatitis B treatment over the past 20 years. *World J Gastroenterol.* **20**: 401–413.

He B, Fan Q, Yang F, Hu T, Qiu W, Feng Y, Li Z, Li Y, Zhang F, Guo H, Zou X, Tu C. 2013. Hepatitis virus in long-fingered bats, Myanmar. *Emerg Infect Dis.* **19**: 638–640.

He W, O'Neill TJ, Gustafson TA. 1995. Distinct Modes of Interaction of SHC and Insulin Receptor Substrate-1 with the Insulin Receptor NPEY Region via Non-SH2 Domains. *J Biol Chem.* **270**: 23258–23262.

Heim MH, Gamboni G, Beglinger C, Gyr K. 1997. Specific activation of AP-1 but not Stat3 in regenerating liver in mice. *Eur J Clin Invest.* **27**: 948–955.

Hepatitis B Foundation. 2009. Vaccine Non-Responders **Oct 2009**.

Hepatitis B Foundation. 2014. What is Hepatitis B - Transmission **Feb 2014**.

Hildt E, Munz B, Saher G, Reifenberg K, Hofschneider PH. 2002. The PreS2 activator MHBst of hepatitis B virus activates c-raf-1/Erk2 signaling in transgenic mice. *EMBO J.* **21**: 525–535.

Hintermann E, Ehser J, Christen U. 2012. The CYP2D6 animal model: how to induce autoimmune hepatitis in mice. *J Vis Exp.* **Feb 3**.

Hirosumi J, Tuncman G, Chang L, Görgün CZ, Uysal KT, Maeda K, Karin M, Hotamisligil GS. 2002. A central role for JNK in obesity and insulin resistance. *Nature* **420**: 333–336.

Hodgson AJ, Keasler VV, Slagle BL. 2008. Premature cell cycle entry induced by hepatitis B virus regulatory HBx protein during compensatory liver regeneration. *Cancer Res.* **68**: 10341–10348.

Hoffmann J. 2013. Charakterisierung der Rolle von alpha-Taxilin für den Zelleintritt und die Morphogenese von Hepatitis B. PhD thesis.

Hoffmann J, Boehm C, Himmelsbach K, Donnerhak C, Roettger H, Weiss TS, Ploen D, Hildt E. 2013. Identification of α-taxilin as an essential factor for the life cycle of hepatitis B virus. *J Hepatol.* **59**: 934–941.

Hotamisligil GS, Peraldi P, Budavari A, Ellis R, White MF, Spiegelman BM. 1996. IRS-1-mediated inhibition of insulin receptor tyrosine kinase activity in TNF-alpha- and obesity-induced insulin resistance. *Science* **271**: 665–668.

Hou J, Liu Z, G F. 2005. Epidemiology and Prevention of Hepatitis B Virus Infection. *Int J Med Sci.* **2**: 50–57.

Hubbard SR. 2013. The insulin receptor: both a prototypical and atypical receptor tyrosine kinase. *Cold Spring Harb Perspect Biol.* **5**: a008946.

Hui JM, Sud A, Farrell GC, Bandara P, Byth K, Kench JG, McCaughan GW, George J. 2003. Insulin resistance is associated with chronic hepatitis C virus infection and fibrosis progression. *Gastroenterology* **125**: 1695–1704.

Hwang EW, Cheung R. 2011. Global Epidemiology of Hepatitis B Virus (HBV) Infection. *N A J Med Sci.* **4**: 7–13.

Iannacone M, Guidotti LG. 2015. Mouse Models of Hepatitis B Virus Pathogenesis. *Cold Spring Harb Perspect Med.* **5**: a021477.

Inuzuka T, Takahashi K, Chiba T, Marusawa H. 2014. Mouse models of hepatitis B virus infection comprising host-virus immunologic interactions. *Pathogens* **3**: 377–389.

Iredale JP. 2007. Models of liver fibrosis: exploring the dynamic nature of inflammation and repair in a solid organ. *J Clin Invest.* **117**: 539–548.

Itoh K, Chiba T, Takahashi S, Ishii T, Igarashi K, Katoh Y, Oyake T, Hayashi N, Satoh K, Hatayama I, Yamamoto M, Nabeshima Y. 1997. An Nrf2/Small Maf Heterodimer Mediates the Induction of Phase II Detoxifying Enzyme Genes through Antioxidant Response Elements. *Biochem Biophys Res Commun.* **236**: 313–322.

Iynedjian PB, Jotterand D, Nouspikel T, Asfari M, Pilot PR. 1989. Transcriptional induction of glucokinase gene by insulin in cultured liver cells and its repression by the glucagon-cAMP system. *J Biol Chem.* **264**: 21824–21829.

Jaiswal AK. 2004. Nrf2 signaling in coordinated activation of antioxidant gene expression. *Free Radic Biol Med.* **36**: 1199–1207.

Jilg W, Gerlich W. 2014. Klinischer Leitfaden Virushepatitis. *Wissenschaftliche Verlagsabteilung Abbott GmbH*.

Jin Z, Sun R, Wei H, Gao X, Chen Y, Tian Z. 2011. Accelerated liver fibrosis in hepatitis B virus transgenic mice: involvement of natural killer T cells. *Hepatology* **53**: 219–229.

Junqueira L, Bignolas G, Brentani RR. 1979. Picrosirius staining plus polarization microscopy, a specific method for collagen detection in tissue sections. *Histochem J.* **11**: 447–455.

Kadowaki T, Ueki K, Yamauchi T, Kubota N. 2012. SnapShot: Insulin signaling pathways. *Cell* **148**: 624.

Kann M, Sodeik B, Vlachou A, Gerlich WH, Helenius A. 1999. Phosphorylation-dependent binding of hepatitis B virus core particles to the nuclear pore complex. *J Cell Biol.* **145**: 45–55.

Kaplan SA. 1984. The insulin receptor. *J Pediatr.* **104**: 327–336.

Kasuga M, Karlsson F, Kahn C. 1982a. Insulin stimulates the phosphorylation of the 95,000-dalton subunit of its own receptor. *Science* **215**: 185–187.

Kasuga M, Zick Y, Blith DL, Karlsson FA, Häring HU, Kahn CR. 1982b. Insulin stimulation of phosphorylation of the beta subunit of the insulin receptor. Formation of both phosphoserine and phosphotyrosine. *J Biol Chem.* **257**: 9891–9894.

Khungar V, Han S. 2010. A Systematic Review of Side Effects of Nucleoside and Nucleotide Drugs Used for Treatment of Chronic Hepatitis B. *Curr Hepat Rep.* **9**: 75–90.

Kian Chua P, Lin M, Shih C. 2006. Potent inhibition of human Hepatitis B virus replication by a host factor Vps4. *Virology* **354**: 1–6.

Kim CM, Koike K, Saito I, Miyamura T, Jay G. 1991. HBx gene of hepatitis B virus induces liver cancer in transgenic mice. *Nature* **351**: 317–320.

Kim K, Kim KH, Cheong J. 2010. Hepatitis B virus X protein impairs hepatic insulin signaling through degradation of IRS1 and induction of SOCS3. *PLoS One* **5**: e8649.

Knowles BB, Howe CC, Aden DP. 1980. Human hepatocellular carcinoma cell lines secrete the major plasma proteins and hepatitis B surface antigen. *Science* **209**: 497–499.

Kobayashi A, Kang M, Okawa H, Ohtsuji M, Zenke Y, Chiba T, Igarashi K, Yamamoto M. 2004. Oxidative stress sensor Keap1 functions as an adaptor for Cul3-based E3 ligase to regulate proteasomal degradation of Nrf2. *Mol Cell Biol.* **24**: 7130–7139.

Kobayashi M, Yamamoto M. 2005. Molecular mechanisms activating the Nrf2-Keap1 pathway of antioxidant gene regulation. *Antioxid Redox Signal.* **7**: 385–394.

Köhler UA, Kurinna S, Schwitter D, Marti A, Schäfer M, Hellerbrand C, Speicher T, Werner S. 2014. Activated Nrf2 impairs liver regeneration in mice by activation of genes involved in cell-cycle control and apoptosis. *Hepatology* **60**: 670–678.

Kramvis A, Kew M, François G. 2005. Hepatitis B virus genotypes. *Vaccine* **23**: 2409–2423.

Ladner SK, Otto MJ, Barker CS, Zaifert K, Wang GH, Guo JT, Seeger C, King RW. 1997. Inducible expression of human hepatitis B virus (HBV) in stably transfected hepatoblastoma cells: a novel system for screening potential inhibitors of HBV replication. *Antimicrob Agents Chemother.* **41**: 1715–1720.

Laemmli UK. 1970. Cleavage of structural proteins during the assembly of the head of bacteriophage T4. *Nature* **227**: 680–685.

Lambert C, Döring T, Prange R. 2007. Hepatitis B virus maturation is sensitive to functional inhibition of ESCRT-III, Vps4, and gamma 2-adaptin. *J Virol.* **81**: 9050–9060.

Lau A, Villeneuve NF, Sun Z, Wong PK, Zhang DD. 2008. Dual roles of Nrf2 in cancer. *Pharmacol Res.* **58**: 262–270.

Lawrence MC, McKern NM, Ward CW. 2007. Insulin receptor structure and its implications for the IGF-1 receptor. *Curr Opin Struct Biol.* **17**: 699–705.

Leistner CM, Gruen-Bernhard S, Glebe D. 2008. Role of glycosaminoglycans for binding and infection of hepatitis B virus. *Cell Microbiol.* **10**: 122–133.

Lepère C, Régeard M, Le Seyec J, Gripon P. 2007. The translocation motif of hepatitis B virus envelope proteins is dispensable for infectivity. *J Virol.* **81**: 7816–7818.

LeRoith D, Roberts, C. T. JR. 2003. The insulin-like growth factor system and cancer. *Cancer Lett* **195**: 127–137.

Liang TJ. 2009. Hepatitis B: the virus and disease. *Hepatology* **49**: S13-21.

London WT, Drew JS. 1977. Sex differences in response to hepatitis B infection among patients receiving chronic dialysis treatment. *Proc Natl Acad Sci USA* **74**: 2561–2563.

London WT, Sutnick AI, Blumberg BS. 1969. Australia antigen and acute viral hepatitis. *Ann Intern Med.* **70**: 55–59.

Lozano R, Naghavi M, Foreman K, Lim S, Shibuya K, Aboyans V, Abraham J, Adair T. 2012. Global and regional mortality from 235 causes of death for 20 age groups in 1990 and 2010: a systematic analysis for the Global Burden of Disease Study 2010. *Lancet* **380**: 2095–2128.

Lupberger J, Hildt E. 2007. Hepatitis B virus-induced oncogenesis. *World J Gastroenterol.* **13**: 74–81.

Lutwick LI, Robinson WS. 1977. DNA synthesized in the hepatitis B Dane particle DNA polymerase reaction. *J Virol.* **21**: 96–104.

Madden CR, Finegold MJ, Slagle BL. 2001. Hepatitis B virus X protein acts as a tumor promoter in development of diethylnitrosamine-induced preneoplastic lesions. *J Virol.* **75**: 3851–3858.

Mahoney FJ, Kane M. 1999. Hepatitis B vaccine. *Vaccines* **3**: 158–182.

Malaguarnera R, Belfiore A. 2014. The emerging role of insulin and insulin-like growth factor signaling in cancer stem cells. *Front Endocrinol* **5**: 10.

Mårin P, Rebuffé-Scrive M, Smith U, Björntorp P. 1987. Glucose uptake in human adipose tissue. *Metabolism* **36**: 1154–1160.

Marsenic O. 2009. Glucose control by the kidney: an emerging target in diabetes. *Am J Kid Dis.* **53**: 875–883.

Masoudi S, Ploen D, Kunz K, Hildt E. 2014. The adjuvant component α-tocopherol triggers via modulation of Nrf2 the expression and turnover of hypocretin in vitro and its implication to the development of narcolepsy. *Vaccine* **32**: 2980–2988.

Mauss S, Berg T, Rockstroh J, Sarrazin C, Wedemeyer H. 2015. Hepatology 2015 - A Clinical Textbook, 6th Edition. *Flying Publisher*.

McMahon M, Itoh K, Yamamoto M, Hayes JD. 2003. Keap1-dependent proteasomal degradation of transcription factor Nrf2 contributes to the negative regulation of antioxidant response element-driven gene expression. *J Biol Chem.* **278**: 21592–21600.

McManus EJ, Sakamoto K, Armit LJ, Ronaldson L, Shpiro N, Marquez R, Alessi DR. 2005. Role that phosphorylation of GSK3 plays in insulin and Wnt signalling defined by knockin analysis. *EMBO J.* **24**: 1571–1583.

Meyer C, Dostou JM, Welle SL, Gerich JE. 2002. Role of human liver, kidney, and skeletal muscle in postprandial glucose homeostasis. *Am J Physiol Endocrinol Metab.* **282**: E419-27.

Mîinea CP, Sano H, Kane S, Sano E, Fukuda M, Peränen J, Lane WS, Lienhard GE. 2005. AS160, the Akt substrate regulating GLUT4 translocation, has a functional Rab GTPase-activating protein domain. *Biochem J.* **391**: 87–93.

Mitchell C, Willenbring H. 2008. A reproducible and well-tolerated method for 2/3 partial hepatectomy in mice. *Nat Protoc.* **3**: 1167–1170.

Nakae J, Park B, Accili D. 1999. Insulin Stimulates Phosphorylation of the Forkhead Transcription Factor FKHR on Serine 253 through a Wortmannin-sensitive Pathway. *J Biol Chem.* **274**: 15982–15985.

Nassal M. 2008. Hepatitis B viruses: reverse transcription a different way. *Virus Res.* **134**: 235–249.

Nelson DL, Cox MM, Lehninger AL. 2004. Lehninger principles of biochemistry. *4. ed: W.H. Freeman*.

Nguyen VT, Law MG, Dore GJ. 2009. Hepatitis B-related hepatocellular carcinoma: epidemiological characteristics and disease burden. *J Viral Hepat.* **16**: 453–463.

Nielsen DA, Welsh M, Casadaban MJ, Steiner DF. 1985. Control of insulin gene expression in pancreatic beta-cells and in an insulin-producing cell line, RIN-5F cells. I. Effects of glucose and cyclic AMP on the transcription of insulin mRNA. *J Biol Chem.* **260**: 13585–13589.

Niture SK, Khatri R, Jaiswal AK. 2014. Regulation of Nrf2-an update. *Free Radic Biol Med.* **66**: 36–44.

Nogami S, Satoh S, Nakano M, Shimizu H, Fukushima H, Maruyama A, Terano A, Shirataki H. 2003a. Taxilin; a novel syntaxin-binding protein that is involved in Ca2+-dependent exocytosis in neuroendocrine cells. *Genes Cells* **8**: 17–28.

Nogami S, Satoh S, Nakano M, Terano A, Shirataki H. 2003b. Interaction of taxilin with syntaxin which does not form the SNARE complex. *Biochem Biophys Res Commun.* **311**: 797–802.

O'Brien RM, Streeper RS, Ayala JE, Stadelmaier BT, Hornbuckle LA. 2001. Insulin-regulated gene expression. *Biochem Soc Trans.* **29**: 552–558.

Oe S, Lemmer ER, Conner EA, Factor VM, Levéen P, Larsson J, Karlsson S, Thorgeirsson SS. 2004. Intact signaling by transforming growth factor beta is not required for termination of liver regeneration in mice. *Hepatology* **40**: 1098–1105.

Oess S, Hildt E. 2000. Novel cell permeable motif derived from the PreS2-domain of hepatitis-B virus surface antigens. *Gene Therapy* **7**: 750–758.

Offensperger WB, Offensperger S, Walter E, Blum HE, Gerok W. 1991. Inhibition of duck hepatitis B virus infection by lysosomotropic agents. *Virology* **183**: 415–418.

Oh IS, Park S. 2015. Immune-mediated Liver Injury in Hepatitis B Virus Infection. *Immune Netw.* **15**: 191–198.

Ozawa K, Ida T, Yamada T, Honjo I. 1976. Significance of glucose tolerance as prognostic sign in hepatectomized patients. *Am J Surg.* **131**: 541–546.

Ozer A, Khaoustov VI, Mearns M, Lewis DE, Genta RM, Darlington GJ, Yoffe B. 1996. Effect of hepatocyte proliferation and cellular DNA synthesis on hepatitis B virus replication. *Gastroenterology* **110**: 1519–1528.

Park E, Park YK, Shin CY, Park SH, Ahn SH, Kim DH, Lim K, Kwon SY, Kim KP, Yang S, Seong BL, Kim K. 2013. Hepatitis B virus inhibits liver regeneration via epigenetic regulation of urokinase-type plasminogen activator. *Hepatology* **58**: 762–776.

Parsa P, Decaux JF, Bossard P, Robey BR, Magnuson MA, Granner DK, Girard J. 1996. Induction of the glucokinase gene by insulin in cultured neonatal rat hepatocytes. Relationship with DNase-I hypersensitive sites and functional analysis of a putative insulin-response element. *Eur J Biochem.* **236**: 214–221.

Parvaiz F, Manzoor S, Iqbal J, Sarkar-Dutta M, Imran M, Waris G. 2015. Hepatitis C virus NS5A promotes insulin resistance through IRS-1 serine phosphorylation and increased gluconeogenesis. *World J Gastroenterol.* **21**: 12361–12369.

Patti M, Kahn CR. 1998. The Insulin Receptor - A Critical Link in Glucose Homeostasis and Insulin Action. *J Basic Clin Physiol Pharmacol.* **9**: 89–109.

Pellicoro A, Ramachandran P, Iredale JP, Fallowfield JA. 2014. Liver fibrosis and repair: immune regulation of wound healing in a solid organ. *Nat Rev Immunol.* **14**: 181–194.

Perz JF, Armstrong GL, Farrington LA, Hutin, Yvan J F, **Bell BP.** 2006. The contributions of hepatitis B virus and hepatitis C virus infections to cirrhosis and primary liver cancer worldwide. *J Hepatol.* **45**: 529–538.

Pilkis SJ, Granner DK. 1992. Molecular physiology of the regulation of hepatic gluconeogenesis and glycolysis. *Annu Rev Physiol.* **54**: 885–909.

Pirola L, Johnston AM, van Obberghen E. 2004. Modulation of insulin action. *Diabetologia* **47**: 170–184.

Pratt DS, Kaplan MM. 2000. Evaluation of abnormal liver-enzyme results in asymptomatic patients. *The New England journal of medicine* **342**: 1266–1271.

Procino G, Barbieri C, Carmosino M, Rizzo F, Valenti G, Svelto M. 2010. Lovastatin-induced cholesterol depletion affects both apical sorting and endocytosis of aquaporin-2 in renal cells. *Am J Physiol Renal Physiol.* **298**: F266-78.

Puchtler H, Waldrop FS, Valentine LS. 1973. Polarization microscopic studies of connective tissue stained with picro-sirius red FBA. *Beitr Pathol.* **150**: 174–187.

Pujol FH, Navas M, Hainaut P, Chemin I. 2009. Worldwide genetic diversity of HBV genotypes and risk of hepatocellular carcinoma. *Cancer Lett.* **286**: 80–88.

Quétier I, Brezillon N, Duriez M, Massinet H, Giang E, Ahodantin J, Lamant C, Brunelle M, Soussan P, Kremsdorf D. 2013. Hepatitis B virus HBx protein impairs liver regeneration through enhanced expression of IL-6 in transgenic mice. *J Hepatol.* **59**: 285–291.

Rabe B, Glebe D, Kann M. 2006. Lipid-Mediated Introduction of Hepatitis B Virus Capsids into Nonsusceptible Cells Allows Highly Efficient Replication and Facilitates the Study of Early Infection Events. *J Virol.* **80**: 5465–5473.

Ramadori G, Saile B. 2004. Inflammation, damage repair, immune cells, and liver fibrosis: Specific or nonspecific, this is the question. *Gastroenterology* **127**: 997–1000.

Ramos-Gomez M, Kwak MK, Dolan PM, Itoh K, Yamamoto M, Talalay P, Kensler TW. 2001. Sensitivity to carcinogenesis is increased and chemoprotective efficacy of enzyme inducers is lost in nrf2 transcription factor-deficient mice. *Proc Natl Acad Sci USA* **98**: 3410–3415.

Raney AK, Le HB, McLachlan A. 1992. Regulation of transcription from the hepatitis B virus major surface antigen promoter by the Sp1 transcription factor. *J Virol.* **66**: 6912–6921.

Ranjbar R, Davari A, Izadi M, Jonaidi N, Alavian SM. 2011. HIV/HBV Co-Infections: Epidemiology, Natural History, and Treatment: A Review Article. *Iran Red Crescent Med J.* **13**: 855–862.

Rehermann B. 2013. Pathogenesis of chronic viral hepatitis: differential roles of T cells and NK cells. *Nat Med.* **19**: 859–868.

Rehermann B, Ferrari C, Pasquinelli C, Chisari FV. 1996. The hepatitis B virus persists for decades after patients' recovery from acute viral hepatitis despite active maintenance of a cytotoxic T–lymphocyte response. *Nat Med.* **2**: 1104–1108.

Rehermann B, Nascimbeni M. 2005. Immunology of hepatitis B virus and hepatitis C virus infection. *Nat Rev Immunol.* **5**: 215–229.

Rivière L, Ducroux A, Buendia MA. 2014. The oncogenic role of hepatitis B virus. *Recent Results Cancer Res.* **193**: 59–74.

Sajan MP, Standaert ML, Nimal S, Varanasi U, Pastoor T, Mastorides S, Braun U, Leitges M, Farese RV. 2009. The critical role of atypical protein kinase C in activating hepatic SREBP-1c and NFkappaB in obesity. *J Lipid Res.* **50**: 1133–1145.

Salmeen A, Andersen, JN, Myers, MP, **Tonks NK, Barford D.** 2000. Molecular basis for the dephosphorylation of the activation segment of the insulin receptor by protein tyrosine phosphatase 1B. *Mol Cell.* **6**: 1401–1412.

Saltiel AR, Kahn CR. 2001. Insulin signalling and the regulation of glucose and lipid metabolism. *Nature* **414**: 799–806.

Sasaoka T, Kobyashi M. 2000. The Functional Significance of Shc in Insulin Signaling as a Substrate of the Insulin Receptor. *Endocr J.* **47**: 373–381.

Schädler S, Hildt E. 2009. HBV Life Cycle: Entry and Morphogenesis. *Viruses* **1**: 185–209.

Schädler S, Krause J, Himmelsbach K, Carvajal-Yepes M, Lieder F, Klingel K, Nassal M, Weiss TS, Werner S, Hildt E. 2010. Hepatitis B virus induces expression of antioxidant response element-regulated genes by activation of Nrf2. *J Biol Chem.* **285**: 41074–41086.

Schaefer S. 2007. Hepatitis B virus taxonomy and hepatitis B virus genotypes. *World J Gastroenterol.* **13**: 14–21.

Schiff ER, Lee SS, Chao Y, Kew Yoon S, Bessone F, Wu S, Kryczka W, Lurie Y, Gadano A, Kitis G, Beebe S, Xu D, Tang H, Iloeje U. 2011. Long-term treatment with entecavir induces reversal of advanced fibrosis or cirrhosis in patients with chronic hepatitis B. *Clin Gastroenterol Hepatol.* **9**: 274–276.

Schlüter V, Meyer M, Hofschneider PH, Koshy R, Caselmann WH. 1994. Integrated hepatitis B virus X and 3' truncated preS/S sequences derived from human hepatomas encode functionally active transactivators. *Oncogene* **9**: 3335–3344.

Schmitz A, Schwarz A, Foss M, Zhou L, Rabe B, Hoellenriegel J, Stoeber M, Panté N, Kann M, Taylor J. 2010. Nucleoporin 153 Arrests the Nuclear Import of Hepatitis B Virus Capsids in the Nuclear Basket. *PLoS Pathogens* **6**: e1000741.

Schulze A, Gripon P, Urban S. 2007. Hepatitis B virus infection initiates with a large surface protein-dependent binding to heparan sulfate proteoglycans. *Hepatology* **46**: 1759–1768.

Schwarz E. 1867. Über eine Methode doppelter Färbung mikroskopischer Objecte, und ihre Anwendung zur Untersuchung der Musculatur des Milz, Lymphdrüsen und anderer Organe. *Sitz Akad W Math Naturw Cl.* **55**: 671–691.

Scott RM, Snitbhan R, Bancroft WH, Alter HJ, Tingpalapong M. 1980. Experimental transmission of hepatitis B virus by semen and saliva. *J Infect Dis.* **142**: 67–71.

Seeger C, Mason WS. 2000. Hepatitis B Virus Biology. *Microbiol Mol Biol Rev.* **64**: 51–68.

Seely BL, Staubs PA, Reichart, **Berhanu P, Milarski KL, Saltiel AR, Kusari J, Olefsky JM.** 1996. Protein tyrosine phosphatase 1B interacts with the activated insulin receptor. *Diabetes* **45**: 1379–1385.

Seino S, Seino M, Nishi S, Bell GI. 1989. Structure of the human insulin receptor gene and characterization of its promoter. *Proc Natl Acad Sci USA* **86**: 114–118.

Sells MA, Chen ML, Acs G. 1987. Production of hepatitis B virus particles in Hep G2 cells transfected with cloned hepatitis B virus DNA. *Proc Natl Acad Sci USA* **84**: 1005–1009.

Sharma SK, Saini N, Chwla Y. 2005. Hepatitis B virus: inactive carriers. *Virol J.* **2**: 82.

Shen Y, Zhang J, Cai H, Shao J, Zhang Y, Liu Y, Qin G, Qin Y. 2015. Identifying patients with chronic hepatitis B at high risk of type 2 diabetes mellitus: a cross-sectional study with pair-matched controls. *BMC Gastroenterol.* **15**: 32–39.

Shimomura I, Bashmakov Y, Ikemoto S, Horton JD, Brown MS, Goldstein JL. 1999. Insulin selectively increases SREBP-1c mRNA in the livers of rats with streptozotocin-induced diabetes. *Proc Natl Acad Sci USA* **96**: 13656–13661.

Shulman GI. 2000. Cellular mechanisms of insulin resistance. *J Clin Invest.* **106**: 171–176.

Siddle K. 2011. Signalling by insulin and IGF receptors: supporting acts and new players. *J Mol Endocrinol.* **47**: R1-10.

Siegler VD, Bruss V. 2013. Role of transmembrane domains of hepatitis B virus small surface proteins in subviral-particle biogenesis. *J Virol.* **87**: 1491–1496.

Singh P, Alex JM, Bast F. 2014. Insulin receptor (IR) and insulin-like growth factor receptor 1 (IGF-1R) signaling systems: novel treatment strategies for cancer. *Med Oncol.* **31**: 805.

Slagle BL, Lee TH, Medina D, Finegold MJ, Butel JS. 1996. Increased sensitivity to the hepatocarcinogen diethylnitrosamine in transgenic mice carrying the hepatitis B virus X gene. *Mol Carcinog.* **15**: 261–269.

Steiner DF, Park S, Støy J, Philipson LH, Bell GI. 2009. A brief perspective on insulin production. *Diabetes Obes Metab.* **11 Suppl 4**: 189–196.

Stevens CE, Szmuness W, Goodman AI, Weseley SA, Fotino M. 1980. Hepatitis B vaccine: immune responses in haemodialysis patients. *Lancet* **2**: 1211–1213.

Stoeckl L, Funk A, Kopitzki A, Brandenburg B, Oess S, Will H, Sirma H, Hildt E. 2006. Identification of a structural motif crucial for infectivity of hepatitis B viruses. *Proc Natl Acad Sci USA* **103**: 6730–6734.

Suk-Fong Lok A. 2015. Hepatitis B: 50 years after the discovery of Australia antigen. *J Viral Hepat.* **Aug 17**.

Summers J. 1988. The replication cycle of hepatitis B viruses. *Cancer* **61**: 1957–1962.

Sun XJ, Crimmins DL, Myers MG, Miralpeix M, White MF. 1993. Pleiotropic insulin signals are engaged by multisite phosphorylation of IRS-1. *Mol Cell Biol.* **13**: 7418–7428.

Sunbul M. 2014. Hepatitis B virus genotypes: global distribution and clinical importance. *World J Gastroenterol.* **20**: 5427–5434.

Sutherland C, O'Brien RM, Granner DK. 1996. New connections in the regulation of PEPCK gene expression by insulin. *Philos Trans R Soc Lond B Biol Sci.* **351**: 191–199.

Suzuki K, Kono T. 1980. Evidence that insulin causes translocation of glucose transport activity to the plasma membrane from an intracellular storage site. *Proc Natl Acad Sci USA* **77**: 2542–2545.

Szmuness W, Stevens CE, Harley EJ, Zang EA, Oleszko WR, William DC, Sadovsky R, Morrison JM, Kellner A. 1980. Hepatitis B vaccine: demonstration of efficacy in a controlled clinical trial in a high-risk population in the United States. *N Engl J Med.* **303**: 833–841.

Tachtatzis PM, Marshall A, Aravinthan A, Verma S, Penrhyn-Lowe S, Mela M, Scarpini C, Davies SE, Coleman N, Alexander, Graeme J M. 2015. Chronic Hepatitis B Virus Infection: The Relation between Hepatitis B Antigen Expression, Telomere Length, Senescence, Inflammation and Fibrosis. *PLoS One* **10**: e0127511.

Taniguchi CM, Emanuelli B, Kahn CR. 2006. Critical nodes in signalling pathways: insights into insulin action. *Nat Rev Mol Cell Biol.* **7**: 85–96.

Tatematsu K, Tanaka Y, Kurbanov F, Sugauchi F, Mano S, Maeshiro T, Nakayoshi T, Wakuta M, Miyakawa Y, Mizokami M. 2009. A genetic variant of hepatitis B virus divergent from known human and ape genotypes isolated from a Japanese patient and provisionally assigned to new genotype J. *J Virol.* **83**: 10538–10547.

Taub R. 2004. Liver regeneration: from myth to mechanism. *Nat Rev Mol Cell Biol.* **5**: 836–847.

Terradillos O, Billet O, Renard CA, Levy R, Molina T, Briand P, Buendia MA. 1997. The hepatitis B virus X gene potentiates c-myc-induced liver oncogenesis in transgenic mice. *Oncogene* **14**: 395–404.

Thimme R, Wieland S, Steiger C, Ghrayeb J, Reimann KA, Purcell RH, Chisari FV. 2003. CD8+ T Cells Mediate Viral Clearance and Disease Pathogenesis during Acute Hepatitis B Virus Infection. *J Virol.* **77**: 68–76.

Thio CL. 2009. Hepatitis B and human immunodeficiency virus coinfection. *Hepatology* **49**: S138-45.

Tian Y, Chen W, Kuo C, Ou JJ. 2012. Viral-load-dependent effects of liver injury and regeneration on hepatitis B virus replication in mice. *J Virol.* **86**: 9599–9605.

Tong MJ, Trieu J. 2013. Hepatitis B inactive carriers: clinical course and outcomes. *J Dig Dis.* **14**: 311–317.

Towbin H, Staehelin T, Gordon J. 1979. Electrophoretic transfer of proteins from polyacrylamide gels to nitrocellulose sheets: procedure and some applications. *Proc Natl Acad Sci USA* **76**: 4350–4354.

Tralhao JG, Roudier J, Morosan S, Giannini C, Tu H, Goulenok C, Carnot F, Zavala F, Joulin V, Kremsdorf D, Bréchot C. 2002. Paracrine in vivo inhibitory effects of hepatitis B virus X protein (HBx) on liver cell proliferation: an alternative mechanism of HBx-related pathogenesis. *Proc Natl Acad Sci USA* **99**: 6991–6996.

Tran TT, Trinh TH, Abe K. 2008. New complex recombinant genotype of hepatitis B virus identified in Vietnam. *J Virol.* **82**: 5657–5663.

Tsuge M, Hiraga N, Takaishi H, Noguchi C, Oga H, Imamura M, Takahashi S, Iwao E, Fujimoto Y, Ochi H, Chayama K, Tateno C, Yoshizato K. 2005. Infection of human hepatocyte chimeric mouse with genetically engineered hepatitis B virus. *Hepatology* **42**: 1046–1054.

Tugendheim S. 2015. http://www.tugendheim.de/impfen/impfungen/hep_b/hepatitis_b.html.

Urakawa H, Katsuki A, Sumida Y, Gabazza EC, Murashima S, Morioka K, Maruyama N, Kitagawa N, Tanaka T, Hori Y, Nakatani K, Yano Y, Adachi Y. 2003. Oxidative stress is associated with adiposity and insulin resistance in men. *J Clin Endocrinol Metab.* **88**: 4673–4676.

Virkamäki A, Ueki K, Kahn CR. 1999. Protein-protein interaction in insulin signaling and the molecular mechanisms of insulin resistance. *J Clin Invest.* **103**: 931–943.

Wasserman WW, Fahl WE. 1997. Functional antioxidant responsive elements. *Proc Natl Acad Sci USA* **94**: 5361–5366.

Watanabe T, Sorensen EM, Naito A, Schott M, Kim S, Ahlquist P. 2007. Involvement of host cellular multivesicular body functions in hepatitis B virus budding. *Proc Natl Acad Sci USA* **104**: 10205–10210.

Weber LW, Boll M, Stampfl A. 2003. Hepatotoxicity and Mechanism of Action of Haloalkanes: Carbon Tetrachloride as a Toxicological Model. *Crit Rev Toxicol.* **33**: 105–136.

Webster GJ, Reignat S, Maini MK, Whalley SA, Ogg GS, King A, Brown D, Amlot PL, Williams R, Vergani D, Dusheiko GM, Bertoletti A. 2000. Incubation phase of acute hepatitis B in man: dynamic of cellular immune mechanisms. *Hepatology* **32**: 1117–1124.

Werle–Lapostolle B, Bowden S, Locarnini S, Wursthorn K, Petersen J, Lau G, Trepo C, Marcellin P, Goodman Z, Delaney IV, William E. 2004. Persistence of cccDNA during the natural history of chronic hepatitis B and decline during adefovir dipivoxil therapy. *Gastroenterology* **126**: 1750–1758.

WHO. 2015a. Fact Sheet No 204 - Hepatitis B **Jul 2015**.

WHO. 2015b. Fact Sheet No 297 - Cancer **Feb 2015**.

Wieland S, Thimme R, Purcell RH, Chisari FV. 2004. Genomic analysis of the host response to hepatitis B virus infection. *Proc Natl Acad Sci USA* **101**: 6669–6674.

Wieland SF, Chisari FV. 2005. Stealth and cunning: hepatitis B and hepatitis C viruses. *J Virol.* **79**: 9369–9380.

Wiemann SU, Satyanarayana A, Tsahuridu M, Tillmann HL, Zender L, Klempnauer J, Flemming P, Franco S, Blasco MA, Manns MP, Rudolph KL. 2002. Hepatocyte telomere shortening and senescence are general markers of human liver cirrhosis. *FASEB J.* **16**: 935–942.

Wissowzky A. 1876. Ueber das Eosin als reagenz auf Hämoglobin und die Bildung von Blutgefässen und Blutkörperchen bei Säugetier und Hühnerembryonen. *Arch Mikrosk Anat.* **13**: 479–496.

Wolf G, Trüb T, Ottinger E, Groninga L, Lynch A, White MF, Miyazaki M, Lee J, Shoelson SE. 1995. PTB Domains of IRS-1 and Shc Have Distinct but Overlapping Binding Specificities. *J Biol Chem.* **270**: 27407–27410.

Wollersheim M, Debelka U, Hofschneider PH. 1988. A transactivating function encoded in the hepatitis B virus X gene is conserved in the integrated state. *Oncogene* **3**: 545–552.

Wu B, Li C, Chen H, Chang J, Jeng K, Chou C, Hsu M, Tsai T. 2006. Blocking of G1/S transition and cell death in the regenerating liver of Hepatitis B virus X protein transgenic mice. *Biochem Biophys Res Commun.* **340**: 916–928.

Wursthorn K, Lutgehetmann M, Dandri M, Volz T, Buggisch P, Zollner B, Longerich T, Schirmacher P, Metzler F, Zankel M, Fischer C, Currie G, Brosgart C, Petersen J. 2006. Peginterferon alpha-2b plus adefovir induce strong cccDNA decline and HBsAg reduction in patients with chronic hepatitis B. *Hepatology* **44**: 675–684.

Xu G, Marshall CA, Lin TA, Kwon G, Munivenkatappa RB, Hill, JR, Lawrence, J. C. Jr, **McDaniel ML.** 1998. Insulin mediates glucose-stimulated phosphorylation of PHAS-I by pancreatic beta cells. An insulin-receptor mechanism for autoregulation of protein synthesis by translation. *J Biol Chem.* **273**: 4485–4491.

Xu R, Zhang Z, Wang F. 2012. Liver fibrosis: mechanisms of immune-mediated liver injury. *Cell Mol Immunol.* **9**: 296–301.

Xu W, Hellerbrand C, Köhler UA, Bugnon P, Kan Y, Werner S, Beyer TA. 2008. The Nrf2 transcription factor protects from toxin-induced liver injury and fibrosis. *Lab Invest.* **88**: 1068–1078.

Yamada T, Yamamoto M, Ozawa K, Honjo I. 1977. Insulin requirements for hepatic regeneration following hepatectomy. *Ann Surg.* **185**: 35–42.

Yan H, Zhong G, Xu G, He W, Jing Z, Gao Z, Huang Y, Qi Y, Peng B, Wang H, Fu L, Song M, Chen P, Gao W, Ren B, Sun Y, Cai T, Feng X, Sui J, Li W. 2012. Sodium taurocholate

cotransporting polypeptide is a functional receptor for human hepatitis B and D virus. *eLife* **1**: e00049.

Yang H, Kao J. 2014. Persistence of hepatitis B virus covalently closed circular DNA in hepatocytes: molecular mechanisms and clinical significance. *Emerg Microbes Infect.* **3**: e64.

Yoon JC, Puigserver P, Chen G, Donovan J, Wu Z, Rhee J, Adelmant G, Stafford J, Kahn CR, Granner DK, Newgard CB, Spiegelman BM. 2001. Control of hepatic gluconeogenesis through the transcriptional coactivator PGC-1. *Nature* **413**: 131–138.

You CR, Lee SW, Jang JW, Yoon SK. 2014. Update on hepatitis B virus infection. *World J Gastroenterol.* **20**: 13293–13305.

Zhang J, Shen Y, Cai H, Liu Y, Qin G. 2015. Hepatitis B virus infection status and risk of type 2 diabetes mellitus: A meta-analysis. *Hepatol Res.* **Jan 19**.

11 Publications

Personal publications

Sebastian Robert Barthel, Thekla Heinrich, Sarah Büchner, Regina Medvedev, Nadja Kettern, Eberhard Hildt. 2016. Hepatitis B Virus Inactivates Insulin Receptor Signaling and Impairs Liver Regeneration *via* Intracellular Retention of the Insulin Receptor. *Cell Mol Life Sci 2016 May 7 [Epub ahead of print].*

Tonya M. Colpitts, Sebastian Barthel, Penghua Wang, Erol Fikrig. 2011. Dengue Virus Capsid Protein Binds Core Histones and Inhibits Nucleosome Formation in Human Liver Cells. *PLoS One* 6 (9): e24365.

Presentations

- 23rd Annual Meeting of the Society for Virology, March 2013, Kiel, Germany.

  "Interference of Hepatitis B Virus with insulin-dependent signaling pathways and effects on liver regeneration and virus-associated pathogenesis"

- 8th Annual Meeting, Retreat on Biomedical Research, January 2014, Heidelberg, Germany.

  "Action of Hepatitis B Virus On Insulin Signaling and Liver Regeneration"

  (**2nd price for an outstanding oral presentation**)

- 24th Annual Meeting of the Society for Virology, March 2014, Alpbach, Austria

  "Action of Hepatitis B Virus On Insulin Signaling and Liver Regeneration"

- 8th Annual Meeting, Retreat on Biomedical Research, January 2015, Heidelberg, Germany.

  "HBV doesn't like it sweet,… how hepatitis B virus interferes with insulin receptor signaling and liver regeneration"

  (**1st price for an outstanding oral presentation**)

Posters

- 7th Annual Meeting, Retreat on Biomedical Research, January 2013, Löwenstein, Germany.

  "Interference of Hepatitis B Virus with insulin-dependent signaling pathways"

- 25th Annual Meeting, Retreat on Biomedical Research, März 2015, Bochum, Germany.

  "HBV doesn't like it sweet – Hepatitis B virus impairs liver regeneration by interference with insulin receptor signaling"

- International Meeting on the Molecular Biology of Hepatitis B Viruses, October 2015, Bad Nauheim, Germany.

  "Hepatitis B virus impairs liver regeneration by interference with insulin receptor signaling"

Eidesstattliche Erklärung

Hiermit erkläre ich an Eides statt, dass ich die vorliegende Dissertation selbstständig und ohne unerlaubte Hilfe angefertigt und andere als die in der Arbeit angegebenen Hilfsmittel nicht benutzt habe. Alle Stellen, die wörtlich oder sinngemäß aus anderen Schriften entnommen sind, habe ich als solche kenntlich gemacht. Diese Arbeit hat in gleicher oder ähnlicher Form noch keiner Prüfungsbehörde vorgelegen. Des Weiteren bin ich mit der späteren Ausleihe meiner Doktorarbeit an die Fachbereichsbibliothek einverstanden.

Frankfurt am Main, den 18. Dezember 2015

_____

Sebastian Robert Barthel